

# Photocatalyzed tandem oxidation reactions and their application in the synthesis of quinoxalines

Dissertation Submitted to the  
University of KwaZulu-Natal  
for the Degree of  
Master of Science  
(In Chemistry)

By

Vineet Jeena



School of Chemistry  
University of KwaZulu-Natal  
January 2009

## **Thesis Declaration**

The experimental work described in this dissertation was carried out in the School of Chemistry, University of KwaZulu-Natal, Pietermaritzburg, under the supervision of Dr Ross S. Robinson.

The studies represent original work by the author and have not otherwise been submitted in candidature for any other degree.

Signed.....V. Jeena (Candidate)

Signed.....Dr R.S. Robinson (Supervisor)

School of Chemistry  
University of KwaZulu-Natal  
Pietermaritzburg  
South Africa

## **Publication Declaration**

My research publication titled “Green oxidations: The Application of Titanium Dioxide as a Versatile Oxidant in Synthetic Organic Chemistry” has been included in the Appendix. See Appendix B.

The experimental work discussed in the publication as well as the writing of the publication was performed by myself and was carried out within the School of Chemistry, University of KwaZulu-Natal, Pietermaritzburg, under the supervision of Dr Ross S. Robinson. I was the primary author for the publication and minor grammatical changes were performed by me under the suggestion of my research supervisor.

These studies represent original work by the author and have not otherwise been submitted in candidature for any other degree.

Signed.....V. Jeena (Candidate)

Signed.....Dr R.S. Robinson (Supervisor)

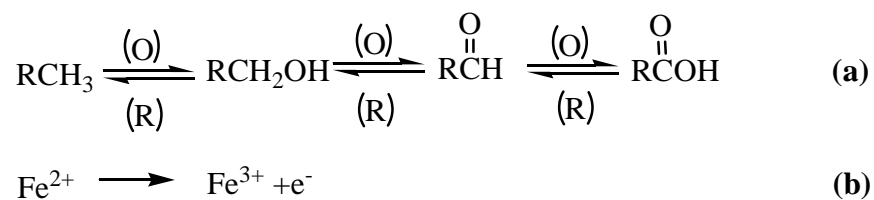
School of Chemistry  
University of KwaZulu-Natal  
Pietermaritzburg  
South Africa

# Chapter 1

## Introduction

### 1.1 BRIEF INTRODUCTION TO OXIDATIONS

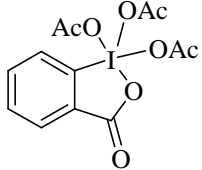
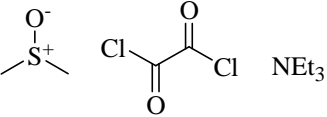
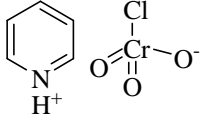
Oxidation reactions play an integral role within chemistry. In organic synthesis oxidation refers to the gaining of oxygen atoms or the replacement of hydrogen with a more electronegative element (**Scheme 1**), while in the realm of inorganic chemistry oxidation refers to the loss of one or more electrons from a metal ion (**Scheme 1**).<sup>1</sup>



**Scheme 1: Oxidation in (a) organic and (b) inorganic chemistry**

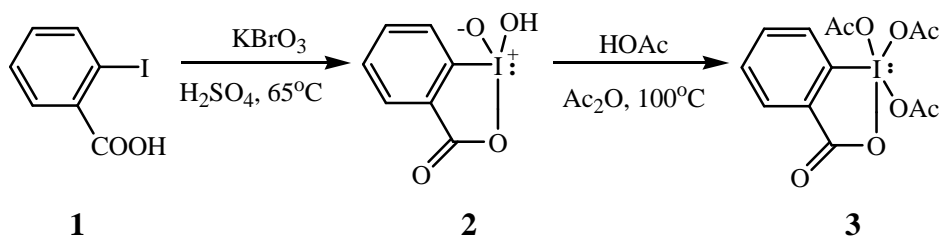
Oxidation of alcohols to aldehydes and ketones, in particular, play an important role in organic synthesis.<sup>2</sup> In 1997, the world wide annual production of carbonyl compounds was over  $10^7$  tonnes with a large portion produced by the oxidation of alcohols.<sup>3</sup> There are a number of processes available to effect this transformation, the most common being the use of the Dess-Martin Periodinane (DMP) reagent, Swern oxidation, or the use of Pyridinium chlorochromate (PCC) (**Table 1**).

**Table 1: Common oxidizing agents**

|                                 |  |
|---------------------------------|--|
| Dess-Martin periodinane reagent |  |
| Swern reagents                  |  |
| Pyridinium Chlorochromate       |  |

### 1.1.1 Dess-Martin periodinane oxidation

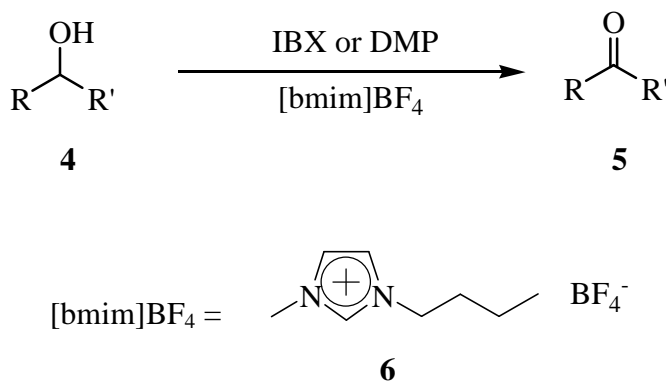
The Dess-Martin periodinane oxidation, named after chemists Daniel Benjamin Dess and James Cullen Martin, is commonly employed for the oxidation of alcohols to aldehydes and ketones.<sup>4,5</sup> The Dess-Martin periodinane reagent is synthesized by reacting 2-iodo benzoic acid **1** with potassium bromate and sulfuric acid to generate its cyclic tautomer 2-iodo benzoic acid **2** (*o*-iodobenzoic acid (IBX)) which is treated with acetic acid and acetic anhydride to produce the periodinane **3**.<sup>4</sup>



**Scheme 2: Synthesis of the Dess-Martin periodinane reagent**

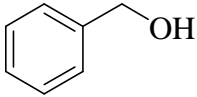
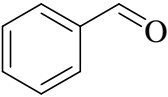
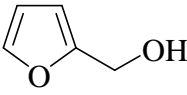
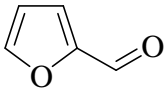
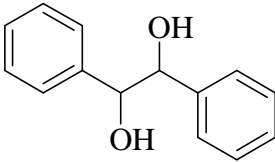
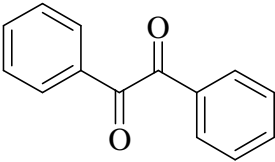
The Dess-Martin periodinane oxidation has gained immense popularity due to the ease of work up and avoiding the use of excess oxidizing agent. One disadvantage is its hazardous preparation as the cyclic tautomer **2** and the Dess-Martin periodinane reagent **3** are heat and shock sensitive exploding violently at temperatures greater than 130°C.<sup>6</sup>

Yadav and co-workers compared IBX **2** with the Dess-Martin periodinane reagent **3** as an oxidant (**Scheme 3**).<sup>7</sup> They reported that the Dess-Martin periodinane reagent was superior to IBX even though the compared reaction times are not consistent (**Table 2**). It is interesting that they report that the reaction proceeds faster in an ionic solvent ([bmim]BF<sub>4</sub>) rather than the traditional organic solvent although no explanation for this observation is provided.

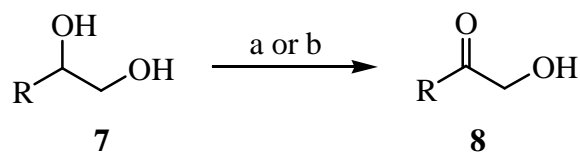


**Scheme 3: Comparison of IBX and DMP as an oxidant in an ionic solvent**

**Table 2: Comparison of DMP and IBX on selected alcohols**

| Alcohol  | Aldehyde   | DMP      |           | IBX      |           |
|--|--|----------|-----------|----------|-----------|
|  |  | Time (h) | Yield (%) | Time (h) | Yield (%) |
|   |   | 3        | 82        | 4        | 91        |
|   |   | 2.5      | 89        | 3.5      | 95        |
|  |  | 4        | 85        | 6        | 95        |

IBX has gained widespread acclaim due to mild reaction conditions, efficiency and stability against moisture.<sup>7</sup> IBX has also been used in combination with  $\beta$ -cyclodextrin<sup>8</sup> and  $\text{Bu}_4\text{NBr}$ <sup>9</sup> for chemoselective oxidation reactions with the secondary alcohol preferentially oxidized over the primary alcohol (**Scheme 4**). When  $\beta$ -cyclodextrin is used with IBX, the authors provide no explanation for the observed chemoselectivity whilst in the case of  $\text{Bu}_4\text{NBr}$ , it was proposed that the solvents in the bi-phasic solvent system led to the observed chemoselectivity.



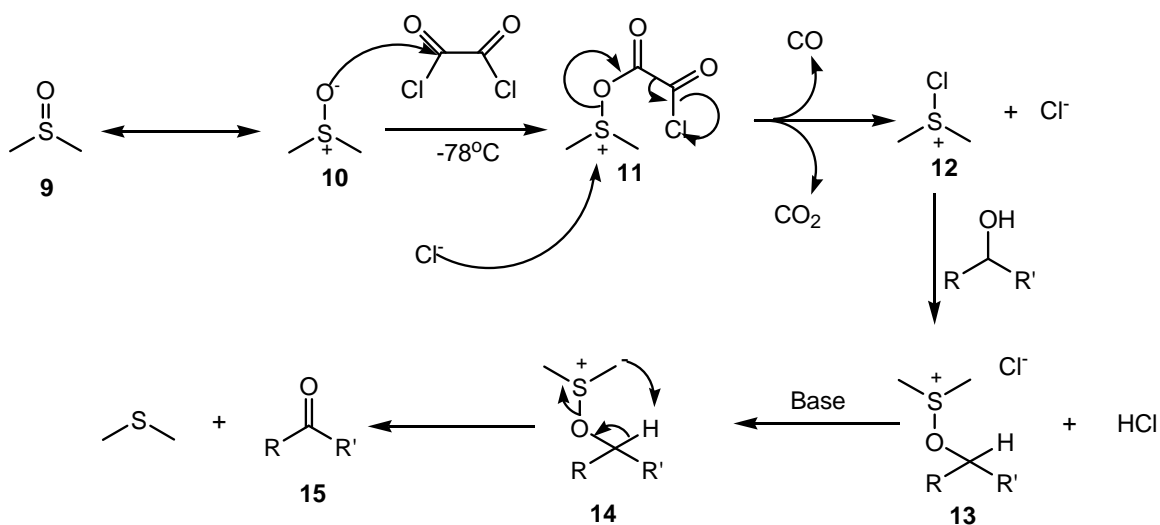
a = IBX,  $\beta$ -cyclodextrin, H<sub>2</sub>O/Acetone

b = IBX, Bu<sub>4</sub>NBr, CH<sub>2</sub>Cl<sub>2</sub>/H<sub>2</sub>O

**Scheme 4: The use of IBX with an additive for chemoselective oxidation reactions**

### 1.1.2 Swern Oxidation

The Swern oxidation, used for the oxidation of alcohols to aldehydes and ketones,<sup>10</sup> is named after American chemist Daniel Swern (**Scheme 5**). The oxidation begins with the reaction of dimethyl sulfoxide (DMSO) with oxalyl chloride producing **11** which subsequently decomposes releasing carbon dioxide, carbon monoxide and producing dimethylchlorosulfonium chloride **12**. Dimethylchlorosulfonium chloride reacts with the added alcohol to produce the alkoxy-sulfonium ion intermediate **13** which is deprotonated by base to produce the sulfur ylide **14** which decomposes *via* a 5 membered transition state, to afford the desired ketone **15** and dimethyl sulfide.



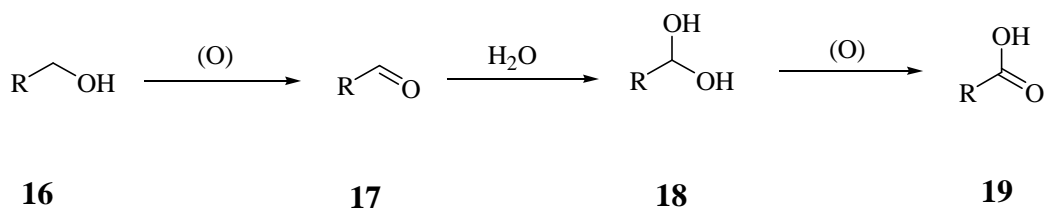
**Scheme 5: Mechanism of the Swern oxidation**



The Swern oxidation produces the desired carbonyl compounds in high yields using mild reaction conditions. However, oxalyl chloride reacts violently with dimethyl sulfoxide at room temperature so dimethyl sulfoxide activation must be conducted at low temperatures.<sup>10</sup> In addition; the formation of malodorous dimethyl sulfide detracts from this procedure.

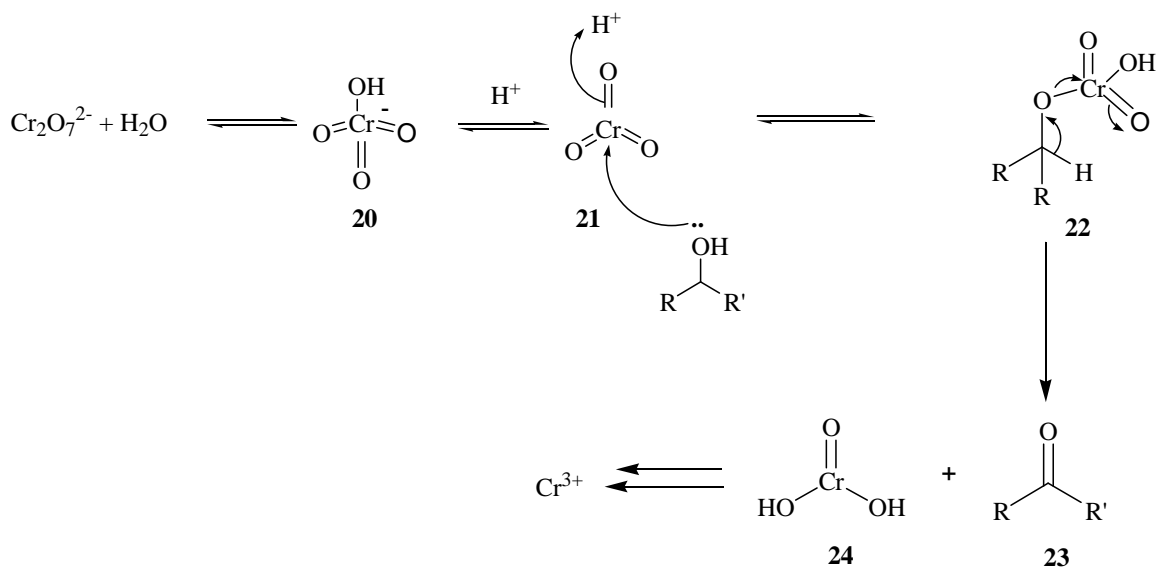
### 1.1.3 Jones Oxidation

The Jones oxidation has been used predominantly for the oxidation of primary alcohols to carboxylic acids<sup>11,12</sup> (**Scheme 6**). The oxidation of the alcohol produces the aldehyde **17** which reacts with water to produce a hydrate **18**. Hydrates are also subject to oxidation and consequently form the carboxylic derivative **19**. However, allylic and benzylic alcohols do not produce stable hydrates and can thus be oxidized to the aldehyde only.<sup>13</sup>



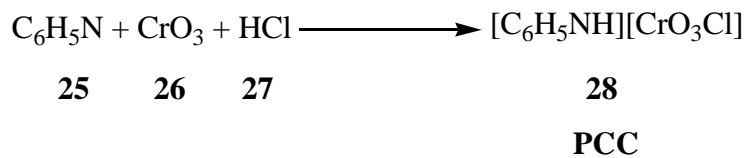
**Scheme 6: Carboxylic acid formation *via* the Jones oxidation**

The mechanism of the Jones oxidation is given below (**Scheme 7**) beginning with the formation of  $\text{HCrO}_4^-$  ions **20**. Under acidic conditions, these compounds form chromate esters **22** which subsequently decompose to form Cr(IV). Cr(IV) undergoes further oxidations to produce Cr(III). The reaction is easy to follow by the colour change of Cr(VI) (orange) to Cr(III) (green). Chromium based oxidations however, are unsuitable for large scale production owing to chromium's toxicity.



**Scheme 7: Mechanism of the Jones oxidation**

An alternative to the Jones oxidation is the use of Pyridinium chlorochromate (PCC) **28** as it oxidizes primary and secondary alcohols to aldehydes and ketones respectively with no further oxidation of the aldehyde to the acid. PCC is easily prepared by the addition of pyridine **25** to chromium(VI) oxide **26** and hydrochloric acid **27** (**Scheme 8**) followed by filtration to obtain PCC.<sup>14</sup>

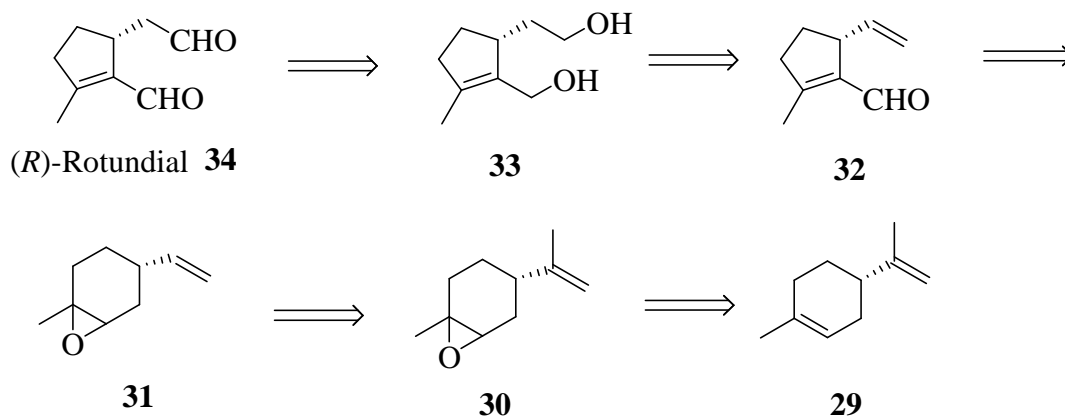


**Scheme 8: Preparation of Pyridinium chlorochromate**

## 1.2 OXIDATIONS IN NATURAL PRODUCT SYNTHESIS

### 1.2.1 Synthesis of Rotundial

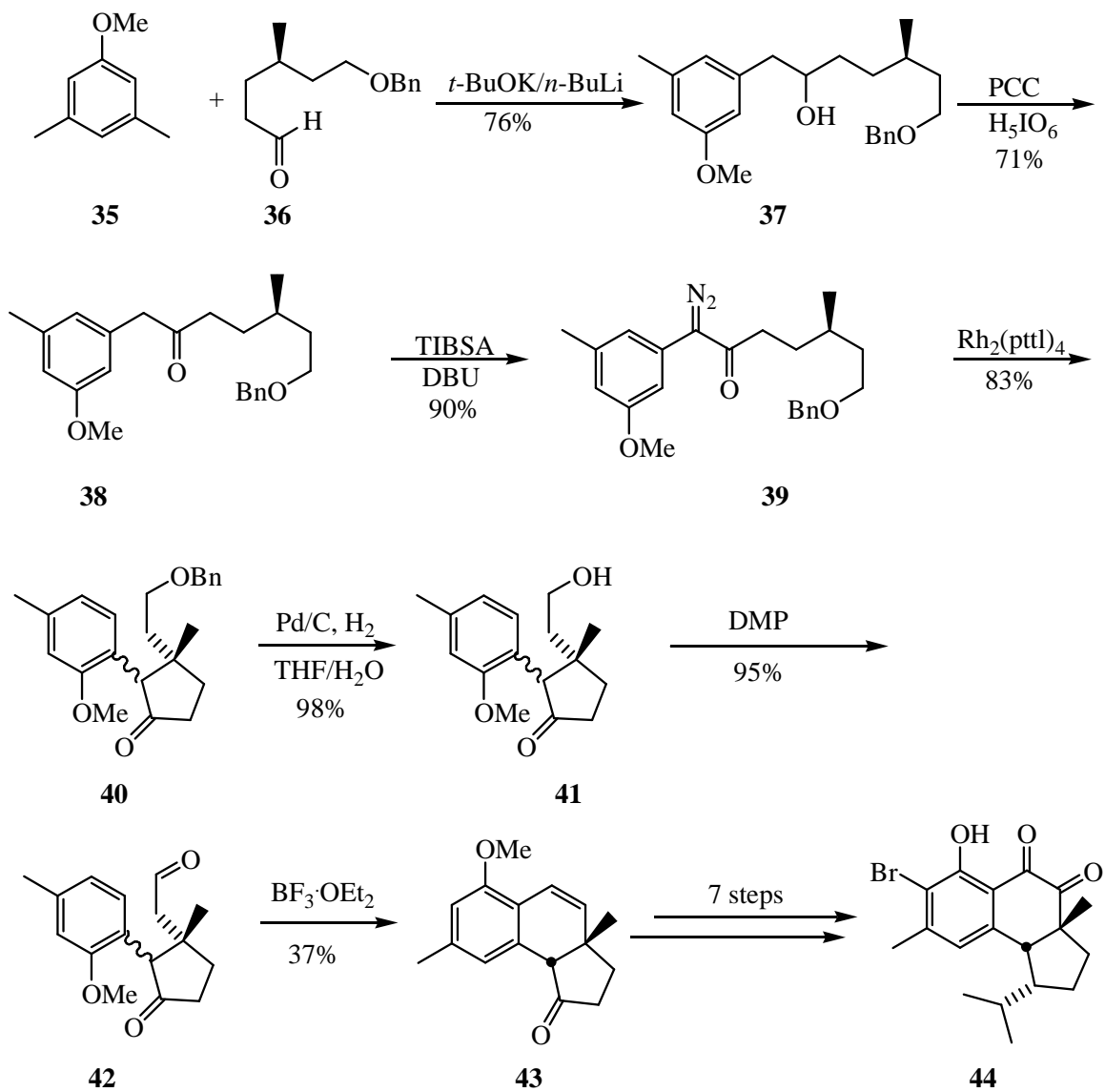
The oxidations of alcohols are extremely important, as evidenced by their numerous applications within natural product synthesis. Rotundial **34** is a monoterpene dialdehyde, isolated from the leaves of *Vitex Rotundifolia* by Watanabe *et al.*<sup>15</sup> Rotundial has been reported to have mosquito repelling activity superior to that of *N,N*-diethyl-*m*-toluamide (Deet<sup>®</sup>) – the active ingredient in many mosquito repellents. Since malaria is transmitted by the *Anopheles* mosquito,<sup>16</sup> Rotundial could potentially play an instrumental role in the fight against this disease. Mori *et al.*<sup>17</sup> undertook the task of synthesizing Rotundial and confirming its natural configuration. The retrosynthetic steps are given below (**Scheme 9**). Mori and co-workers used a 10 step synthesis which ultimately produced Rotundial in a yield of 9 and 10% for the (*R*) and (*S*) enantiomer. The last of step of the synthesis, which required the oxidation of the diol **33** to rotundial **34**, was achieved using the Swern oxidation with a yield of 57% and 64% for the (*R*) and (*S*) enantiomer respectively.



**Scheme 9: Retrosynthetic analysis of Rotundial**

### 1.2.2 Synthesis of (-)-Hamigeran B

(-)-Hamigeran B **44** is a brominated phenolic compound, isolated from *Hamigera tarangaensis*, a poecilosclerid sponge collected from the Hen and Chicken islands east of New Zealand in 2000. (-)-Hamigeran B was shown to exhibit antiviral activity against herpes and polio with minimal side effects.<sup>18</sup> In 2008, Taber and Tian reported the synthesis of (-)-Hamigeran B *via* a 14 step procedure (**Scheme 10**).<sup>19</sup> The second step of the synthetic procedure uses PCC to convert the alcohol **37** to the ketone **38** with a yield of 71%. The sixth step of the synthesis uses the Dess-Martin periodinane reagent to convert the primary alcohol **41** to the aldehyde **42** with a yield of 95%. It is important to note that without oxidation reactions both Rotundial **34** and (-)-Hamigeran B **44** would be difficult, if not impossible, to access.

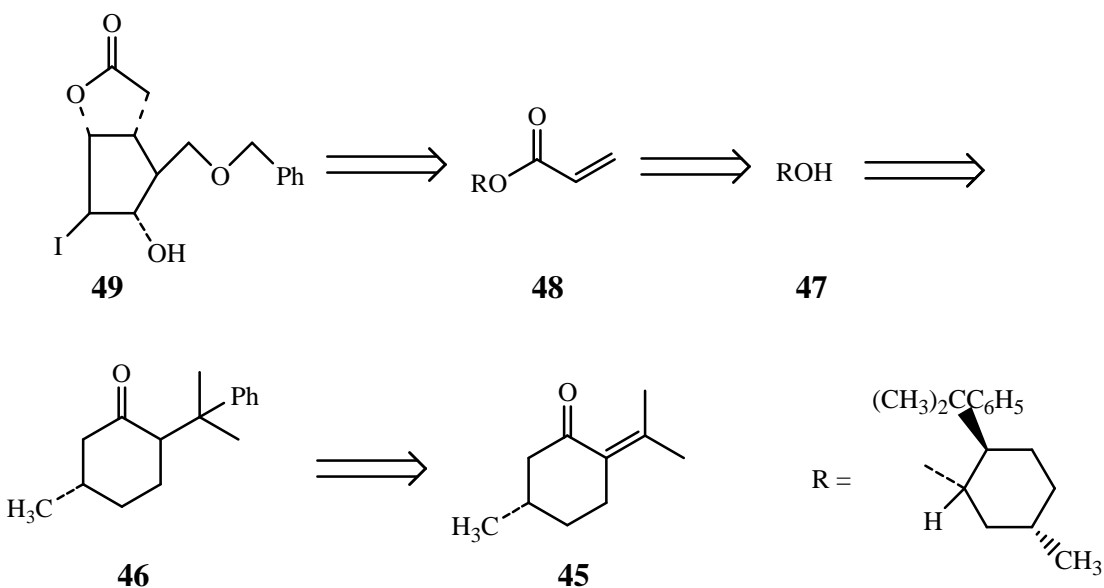


**Scheme 10: Synthesis of (-)-Hamigeran B**

## 1.3 THE TANDEM OXIDATION PROCESS

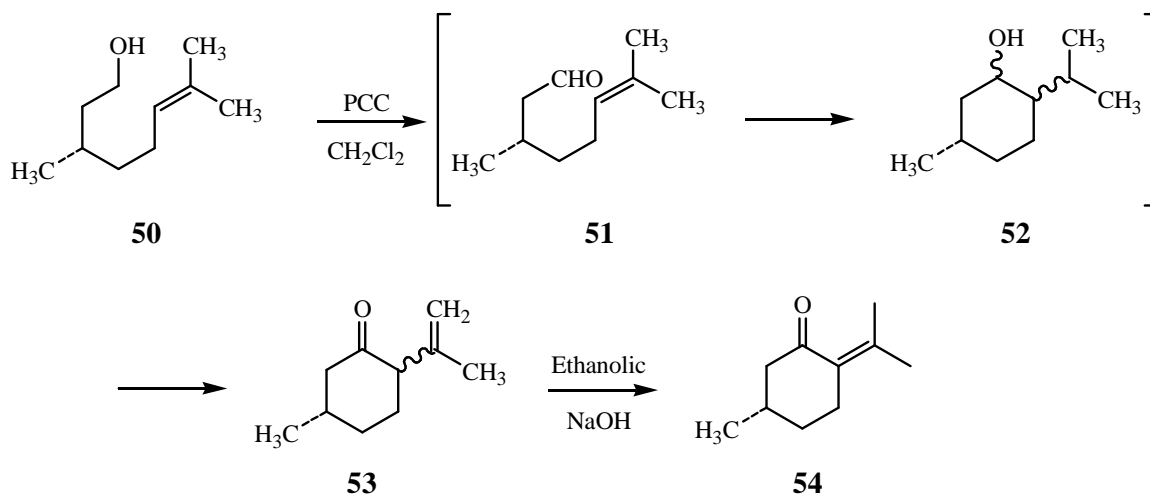
### 1.3.1 A brief history of tandem reactions-The use of PCC

In 1975, Corey and Suggs described a procedure for the preparation of a key prostaglandin intermediate **49** from (*S*)-(-)-pugelone **45** for which the retrosynthetic steps are given below (**Scheme 11**).<sup>20</sup>



**Scheme 11: Retrosynthetic analysis of prostaglandin intermediate**

Thus, a convenient source of (*S*)-(-)-pugelone was essential for the synthesis of the prostaglandin intermediate. The overall synthetic procedure depicting the route to access (*S*)-(-)-pugelone **45** is presented below in **Scheme 12**.<sup>21</sup>



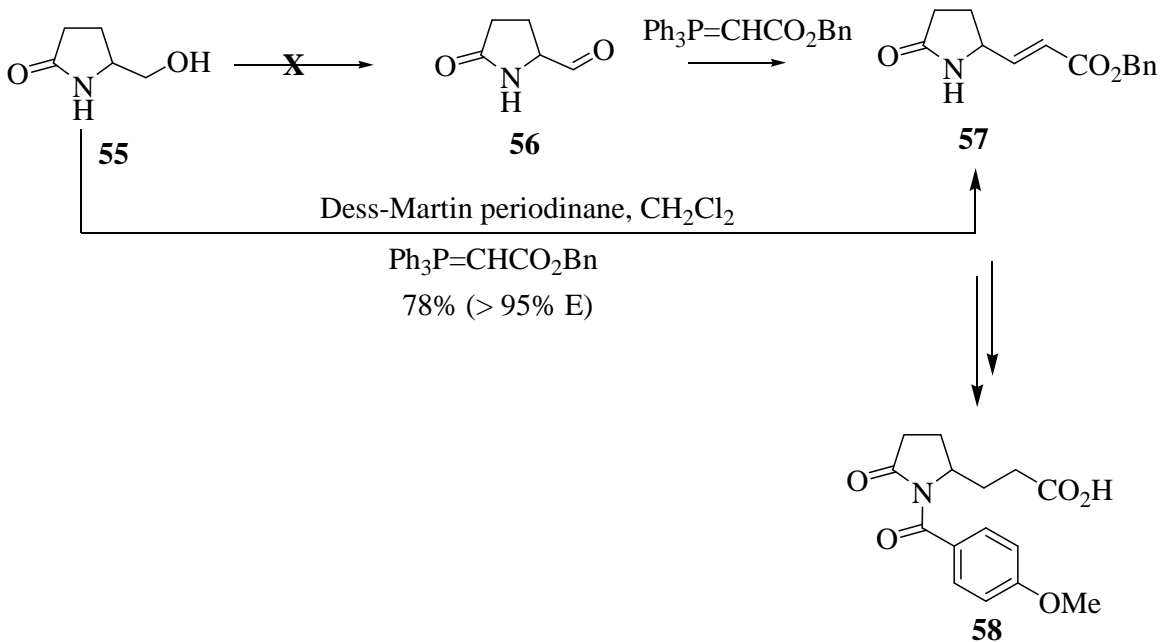
**Scheme 12: Synthesis of (*S*)-(-)-pugelone**

(-)-Citronellol **50** was treated with 2.5 equivalents of PCC in dry dichloromethane for 36 hours at room temperature. PCC oxidizes the primary alcohol to the aldehyde **51** and was sufficiently acidic to effect the cyclization of **51** to **52**, which was further oxidized by PCC to produce the ketone **53**. The ketone was treated with ethanolic sodium hydroxide to produce (-)-pugelone in a 70% overall yield. Optically pure (-)-pugelone was prepared by recrystallization of its semicarbazone from ethanol. The semicarbazone was treated with pyruvic acid and excess glacial acetic acid to produce optically pure *S*-(-)-pugelone. This process was remarkable as the first three steps were conducted *in situ* without the addition of further reagents or purification between subsequent steps.

### 1.3.2 A brief history of tandem reactions-The use of the DMP reagent

In 1987, Huang<sup>22</sup> was attempting to synthesize carbon-14-labelled CI-933 **58**. An important step involved the oxidation of alcohol **55** to aldehyde **56** which was subsequently treated with a Wittig reagent. In this case several attempts at oxidizing the aldehyde proved unsuccessful until Huang mixed the alcohol, the Dess-Martin periodinane reagent and the Wittig reagent in one pot at 0°C to room temperature

overnight (**Scheme 13**). The desired unsaturated ester **57** was obtained in a satisfactory isolated yield of 78%. It is interesting that the original synthesis to obtain the unsaturated ester **57** from the alcohol **55** was eight steps with an overall yield of 20%. Therefore, the significant improvement in yield and operational simplicity is certainly noteworthy.

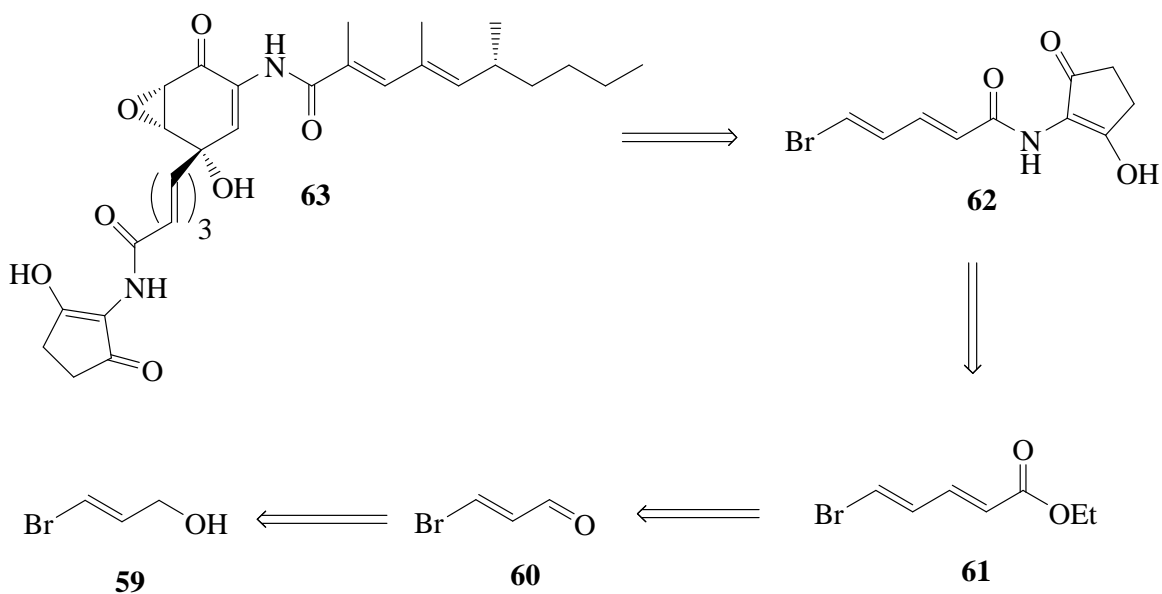


**Scheme 13: Dess-Martin periodinane mediated synthesis of CI-933**

### 1.3.3 The tandem oxidation process

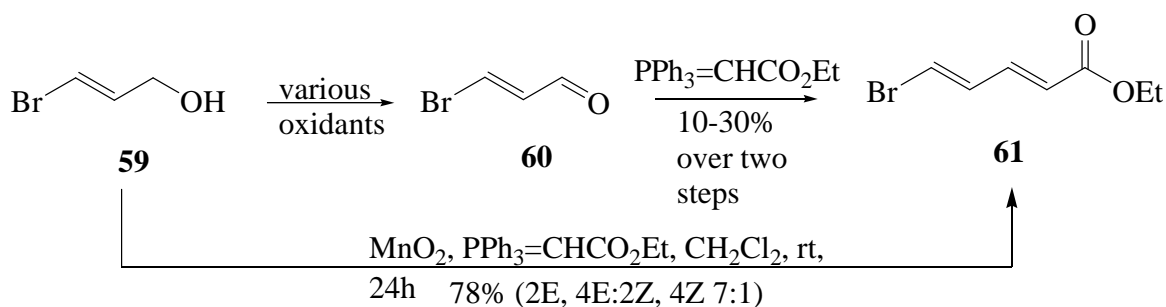
In 1998, Taylor *et al.* were investigating synthetic routes towards the manumycin class of antibiotics.<sup>23-26</sup> A key step involved the oxidation of 3-bromopropen-1-ol **59** to the aldehyde **60** which was subsequently treated with a stabilized Wittig reagent to yield the dienoate **61** (**Scheme 14**).





#### Scheme 14: Retrosynthetic analysis of the manumycin class of antibiotics

Despite all efforts, the overall yield of the dienoate **61** was 10-30% over the two steps. In addition, the aldehyde's lachrymatory nature and propensity to isomerize/polymerize<sup>27</sup> further complicated the situation. Attempts were made to add the Wittig reagent directly to the preformed aldehyde *via* a 'one pot Swern oxidation', popularly used by Ireland<sup>28</sup> *et al.*, however this proved unsuccessful, indicative of the labile nature of aldehyde **60**. Finally, Xudong Wei (a member of the Taylor research group) mixed the alcohol **59**, stabilized Wittig reagent and manganese dioxide in one pot<sup>24,25</sup> (**Scheme 15**). He reasoned that manganese dioxide would oxidize the alcohol to the aldehyde, which would be trapped by the stabilized Wittig reagent and immediately elaborated further thus avoiding the need to isolate the problematic aldehyde. Taylor and co-workers were delighted to obtain the dienoate **61** in an isolated yield of 78%<sup>25</sup> and dubbed the one pot process the 'tandem oxidation process' (TOP) in order to differentiate it from the procedure used by Ireland.

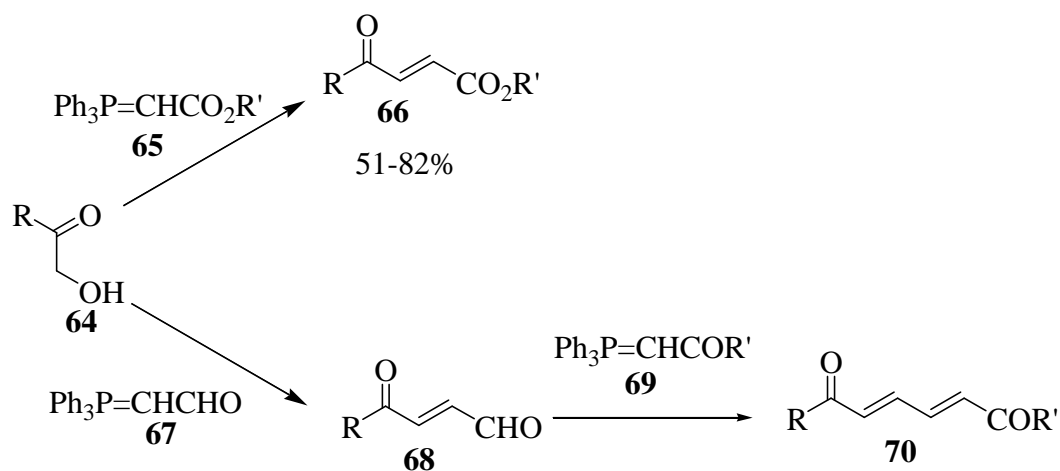


**Scheme 15: Manganese dioxide mediated TOP synthesis of dienoate**

The tandem oxidation process was a ground breaking discovery as it avoided the need to isolate the often volatile intermediate aldehyde resulting in shorter reaction times, improved yields and cost benefits. A brief summary of the applications of TOP methodology will now be given.

#### 1.4 APPLICATIONS OF TOP METHODOLOGY

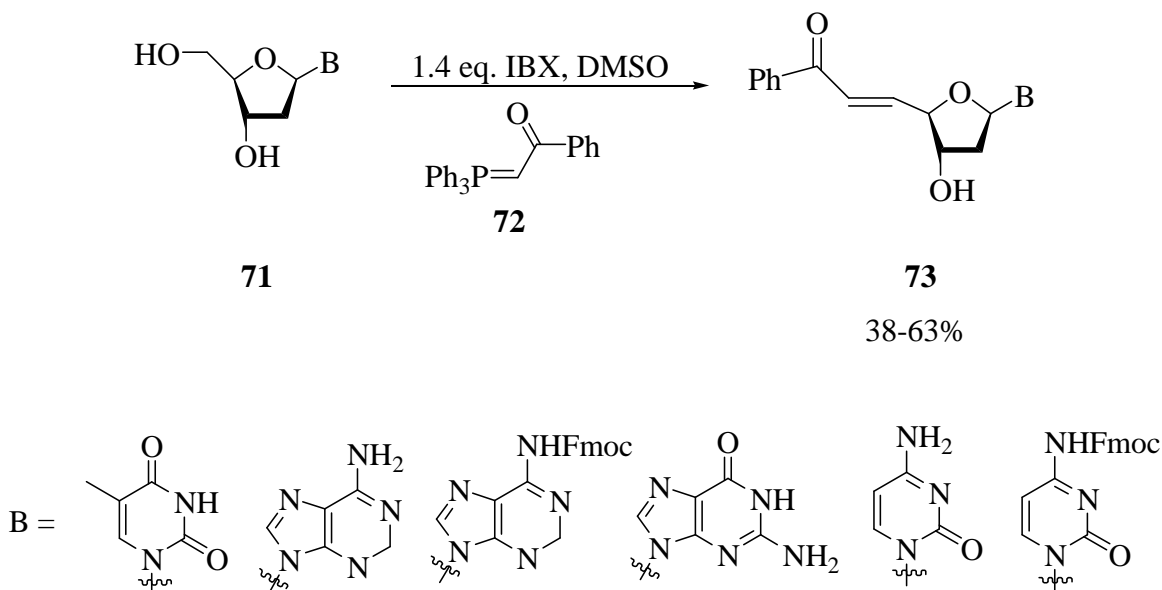
After the success of the initial tandem Wittig reaction, Taylor and co-workers then carried out a study on a series of tandem-Wittig reactions in order to explore the scope and viability of TOP on a variety of substrates. The Taylor research team applied the Tandem-Wittig methodology to other problematic aldehydes,<sup>29</sup> semi and unactivated alcohols<sup>30</sup> and tandem Wittig-Wittig<sup>31</sup> reactions in which the aldehyde was attacked by two Wittig reagents *in situ* to produce the desired dienoate (**Scheme 16**).



**Scheme 16: Expansion of manganese dioxide mediated tandem Wittig reactions**

#### 1.4.1 Synthesis of C5' homologated nucleosides

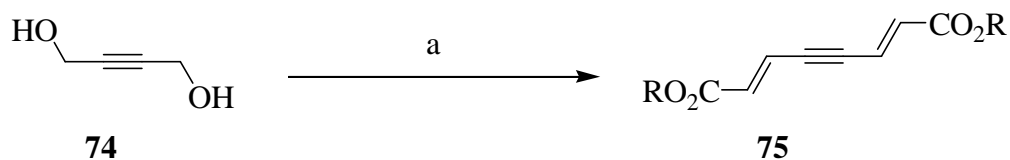
During this time, other research groups have used various oxidants to carry out one-pot Wittig reactions. Crich<sup>32</sup> and co-workers reported the synthesis of C5' homologated nucleosides using IBX as an oxidant in a one pot Wittig reaction although in modest yields (38-63%) (**Scheme 17**).



**Scheme 17: IBX mediated tandem Wittig reactions**

### 1.4.2 Synthesis of dienynes

Barrett<sup>33</sup> and co-workers applied the Dess-Martin periodinane catalyzed oxidation to diols **74** which were trapped *in situ* to produce the desired dienyne **75** (**Scheme 18**) without the need to isolate the dialdehyde which is often prone to decomposition. Benzoic acid was added to accelerate the reaction and enhance the *E:Z* selectivity of the reaction.<sup>34</sup>

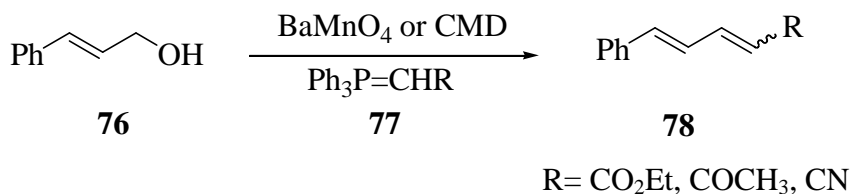


(a) PhCO<sub>2</sub>H (4 eq.), Ph<sub>3</sub>P=CHCO<sub>2</sub>R (4 eq.), Dess-Martin Periodinane reagent (2.4 eq.),  
DMSO, CH<sub>2</sub>Cl<sub>2</sub>; NaHCO<sub>3</sub>, H<sub>2</sub>O, Et<sub>2</sub>O

**Scheme 18: Dess-Martin periodinane mediated synthesis of dienynes**

### 1.4.3 Synthesis of dienes

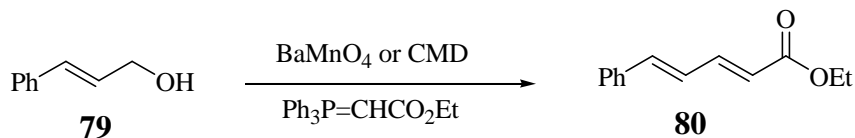
Matsuda<sup>35</sup> and co-workers reported the use of barium permanganate ( $\text{BaMnO}_4$ ) and chemical manganese dioxide (CMD)<sup>†</sup> catalyzed oxidation of  $\alpha,\beta$ -unsaturated alcohols **76** to generate the corresponding diene derivatives **78** (Scheme 19).



**Scheme 19: Barium permanganate mediated synthesis of dienes**

CMD has been reported to be superior to manganese dioxide<sup>36</sup> since the reported results for activated manganese dioxide are sometimes non-reproducible as the reactivity of activated manganese dioxide depends on the method of preparation.<sup>‡</sup> It was found that  $\text{BaMnO}_4$  produced the desired products in shorter times when compared with CMD. Also  $\text{BaMnO}_4$  oxidations are usually carried out with a large excess of the oxidant but in these tandem reactions the oxidant was used in a slight stoichiometric excess.

**Table 3: Comparison of results using  $\text{BaMnO}_4$  and CMD<sup>35</sup>**



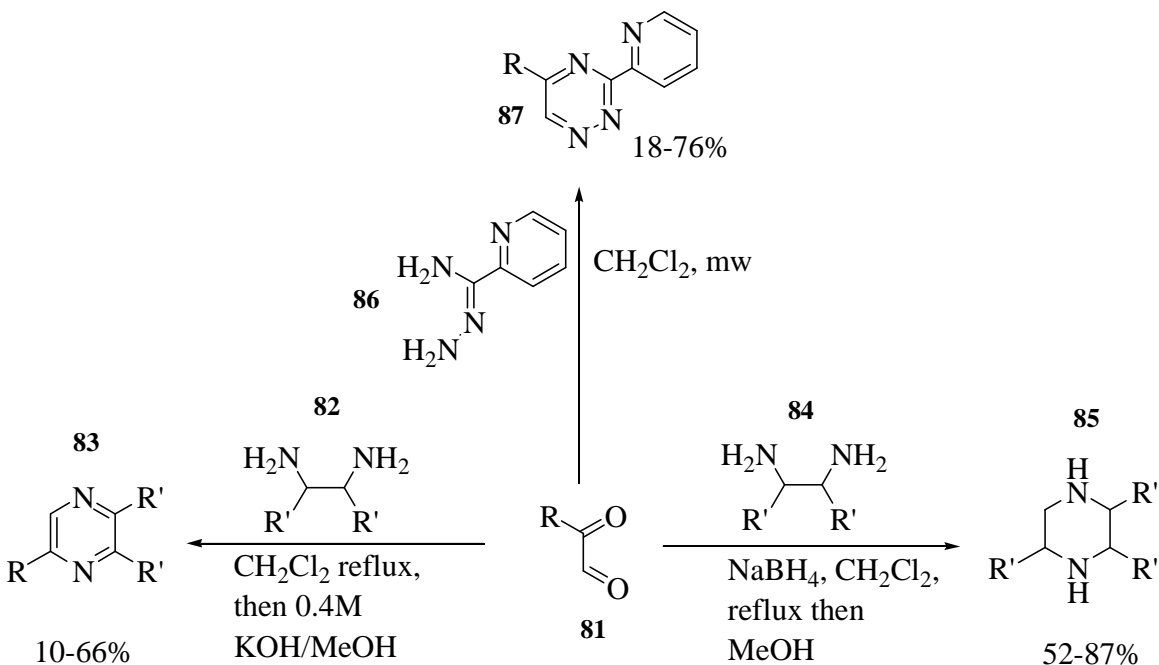
| Oxidant          | Reaction conditions                 | Yields (%) |
|------------------|-------------------------------------|------------|
| $\text{BaMnO}_4$ | $\text{CH}_2\text{Cl}_2$ , rt, 24 h | 99         |
| CMD              | $\text{CH}_2\text{Cl}_2$ , rt, 24 h | 38         |
| $\text{BaMnO}_4$ | PhMe, reflux, 1 h                   | 93         |
| CMD              | PhMe, reflux, 24 h                  | 94         |

<sup>†</sup> CMD is an industrial product used in the production of batteries and is a more efficient oxidizing agent than activated manganese dioxide.

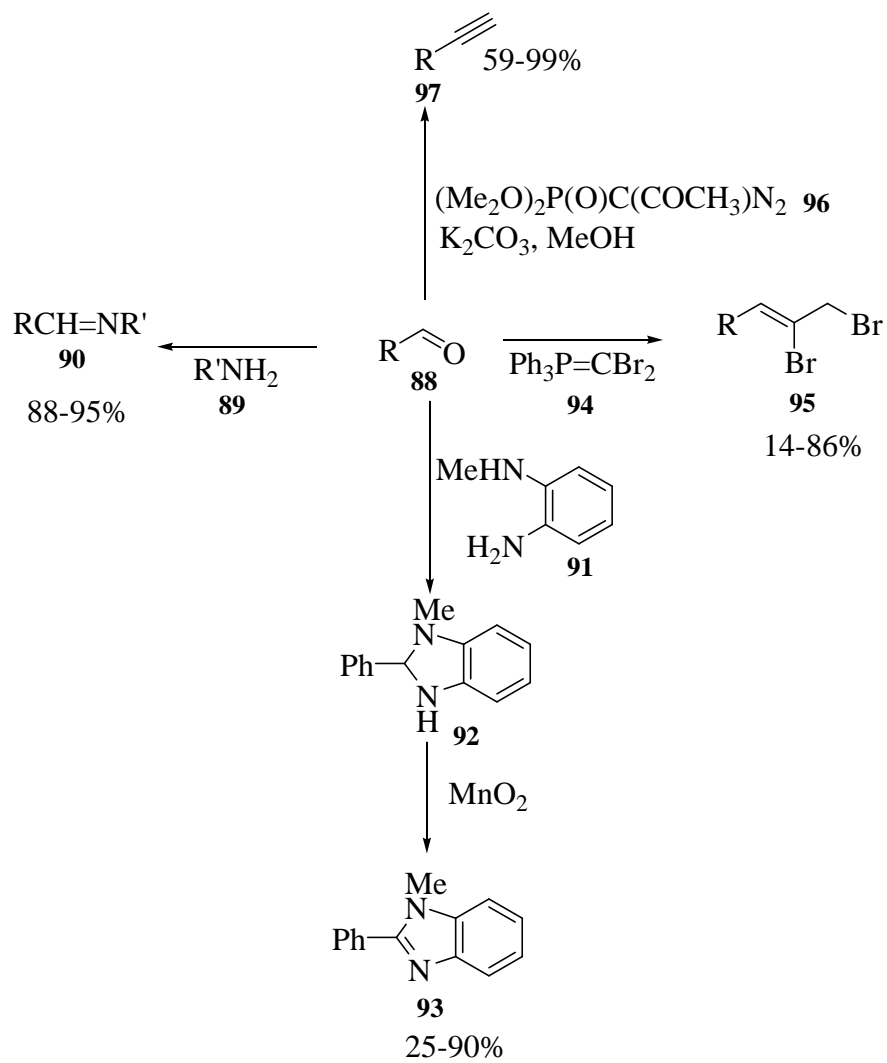
<sup>‡</sup> 'Manganese dioxide' referred to throughout this dissertation refers to the activated form.

### 1.4.4 Expansion of TOP methodology

TOP methodology is not only limited to Wittig reactions and has been expanded to the synthesis of imines,<sup>37</sup> piperazines and pyrazines,<sup>38</sup> 1,1-dibromo-alkenes and terminal alkynes,<sup>39</sup> triazines<sup>40</sup> and benzimidazoles<sup>41</sup> (**Schemes 20 and 21**) and a wide array of useful compounds<sup>42</sup> have been accessed using this methodology.



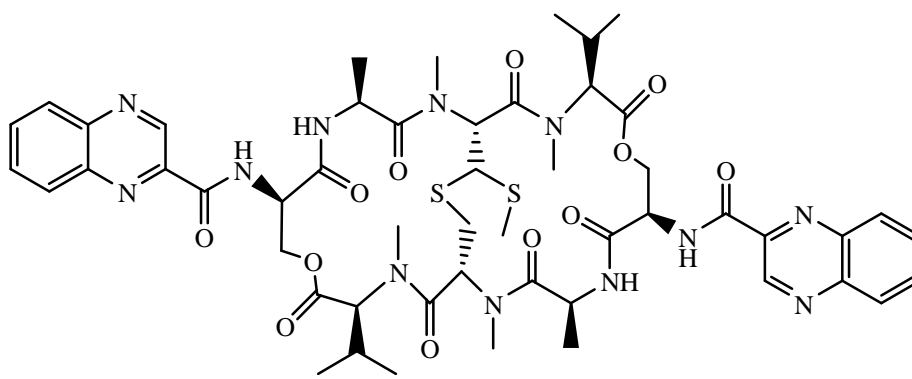
**Scheme 20: Expansion of manganese dioxide mediated tandem coupling reactions**



**Scheme 21: Expansion of manganese dioxide mediated tandem coupling reactions**

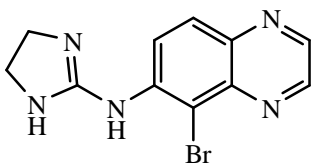
## 1.5 SYNTHESIS OF QUINOXALINES

Quinoxaline derivatives display a wide array of biological properties (**Figure 1**) ranging from DNA cleaving drugs,<sup>43</sup> antimicrobial and cancer drugs,<sup>44</sup> to antibiotic<sup>45</sup> and antitumor activity.<sup>46</sup> Therefore, there are constantly new and innovative ideas being developed to access this important moiety. There are a number of processes available to synthesize quinoxalines but for the purposes of this dissertation, attention will be focused on the most common methods.



98

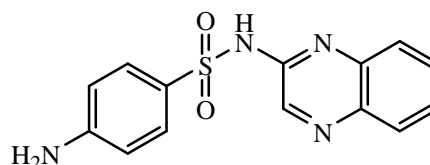
Echinomycin (antitumor/antibacterial activity)



99

Alphagan

(treatment of glaucoma and hypertension)



100

Sulfaquinoxaline

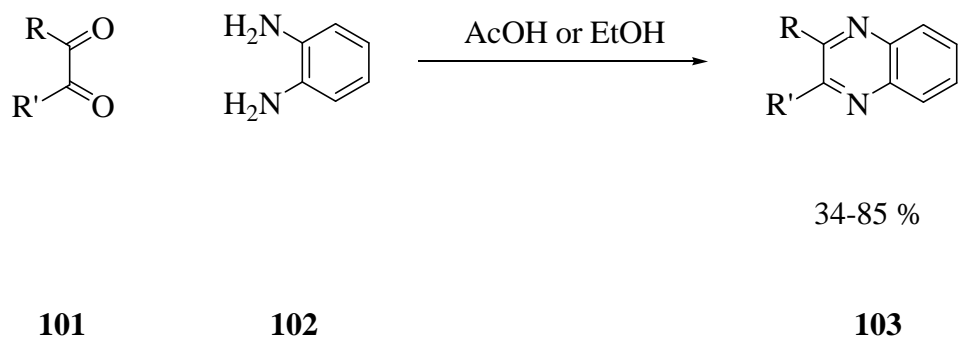
(treatment of coccidial  
infection of veterinary animals)

**Figure 1: Structures of some important quinoxaline derivatives**



### 1.5.1 General method for quinoxaline synthesis

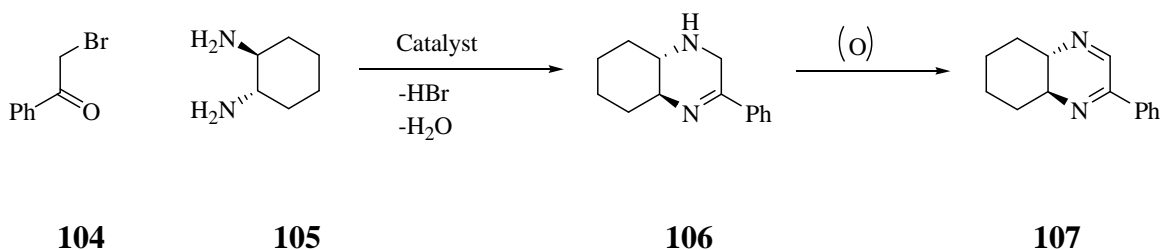
There are a number of processes available to generate quinoxalines<sup>47,48</sup> but generally, they are synthesized by the condensation of 1,2-dicarbonyls **101** with 1,2 diamines **102** in refluxing acetic acid or ethanol for 2-12 hours with yields ranging from 34-85% (Scheme 22).<sup>49</sup>



**Scheme 22: General procedure for the synthesis of quinoxalines**

### 1.5.2 Silica Supported Perchloric acid

Quinoxalines have also been synthesized by the coupling of  $\alpha$ -bromoketones and 1,2- diamines in the presence of silica supported perchloric acid ( $\text{HClO}_4 \cdot \text{SiO}_2$ )<sup>50</sup> (Scheme 23) with the desired products obtained in 15 minutes at room temperature with yields ranging from 70-95%. In the absence of  $\text{HClO}_4 \cdot \text{SiO}_2$  the reaction did not proceed even after 5 hours. The essential role of  $\text{HClO}_4 \cdot \text{SiO}_2$  was confirmed by reacting phenylacetyl bromide **104** with ( $\pm$ )-*trans*-1,2-diaminocyclohexane **105** in the presence of various other catalysts such as Amberlyst-15,  $\text{NaHSO}_4 \cdot \text{SiO}_2$  and Silica chloride. These reactions resulted in incomplete oxidation and the intermediate **106** was obtained. The authors state that the final product **107** was presumably obtained by aerobic oxidation in the presence of  $\text{HClO}_4 \cdot \text{SiO}_2$ .

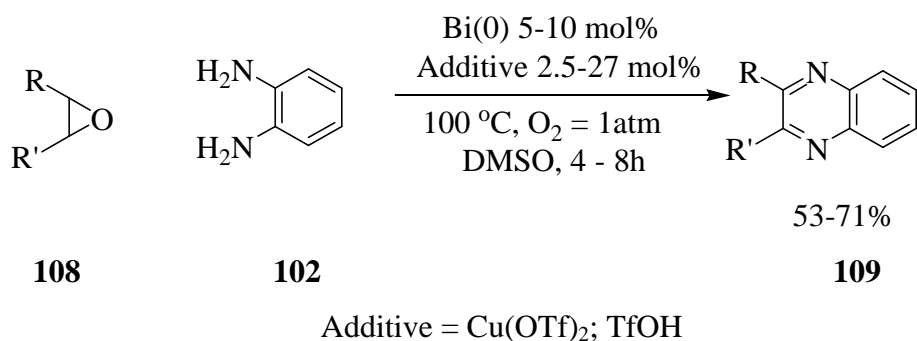


### Scheme 23: Silica supported perchloric acid mediated synthesis of quinoxalines

The use of  $\text{HClO}_4 \cdot \text{SiO}_2$  resulted in obtaining the products in high yields in short reaction times with the catalyst being used up to three times without any significant loss in activity. One disadvantage is that the catalyst requires three days preparation time.<sup>51</sup>

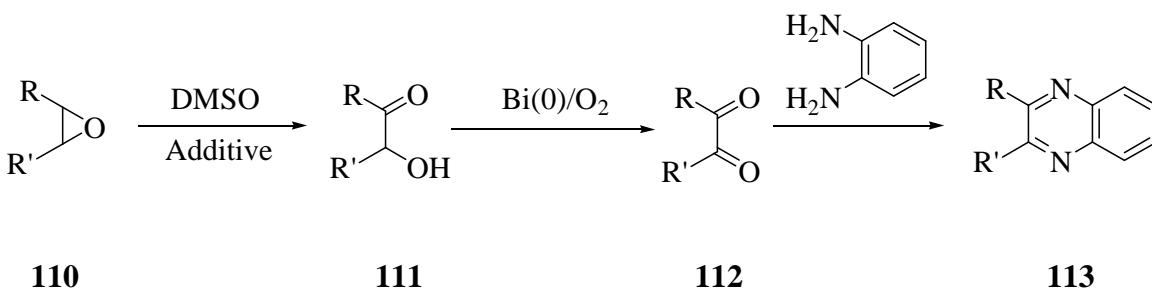
### 1.5.3 Coupling of epoxides and ene-1,2 diamines

The oxidative coupling of epoxides **108** and ene-1,2 diamines **102** in the presence of  $\text{Bi}(0)$  and acid derivatives<sup>52</sup> is an alternate procedure to access quinoxalines **109** (Scheme 24). The reaction is fascinating since epoxides are generally not used to access quinoxalines although one method using cyano and sulfonyl epoxides has been reported.<sup>53</sup>



### Scheme 24: Synthesis of quinoxalines *via* the coupling of epoxides and ene-1,2 diamines

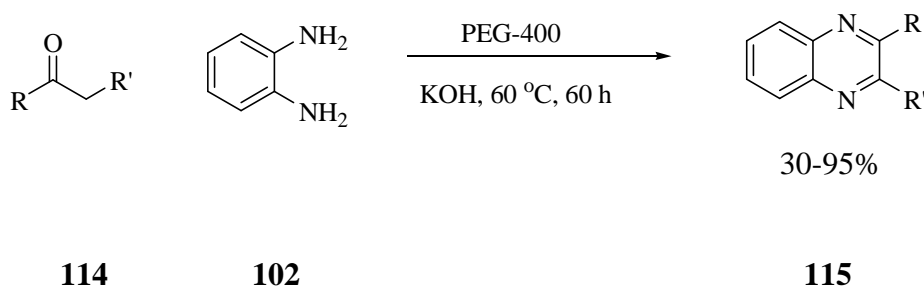
The choice of additive is interesting with  $\text{Cu}(\text{OTf})_2$  used for monosubstituted epoxides and a stronger acid  $\text{TfOH}$  required for disubstituted epoxides. The mechanism proposed suggests a DMSO/acid additive catalyzed ring opening<sup>54</sup> of the epoxide to generate the  $\alpha$ -hydroxyketone **111** which undergoes Bi(0)/ $\text{O}_2$  catalyzed oxidation, in a Bi(III)/Bi(0)<sup>55</sup> redox process to produce the diketone **112**, which is attacked by *o*-phenylene diamine to yield the quinoxaline **113**(Scheme 25).



**Scheme 25: Proposed mechanism for quinoxaline synthesis in the presence of Bi(0) and acid additives**

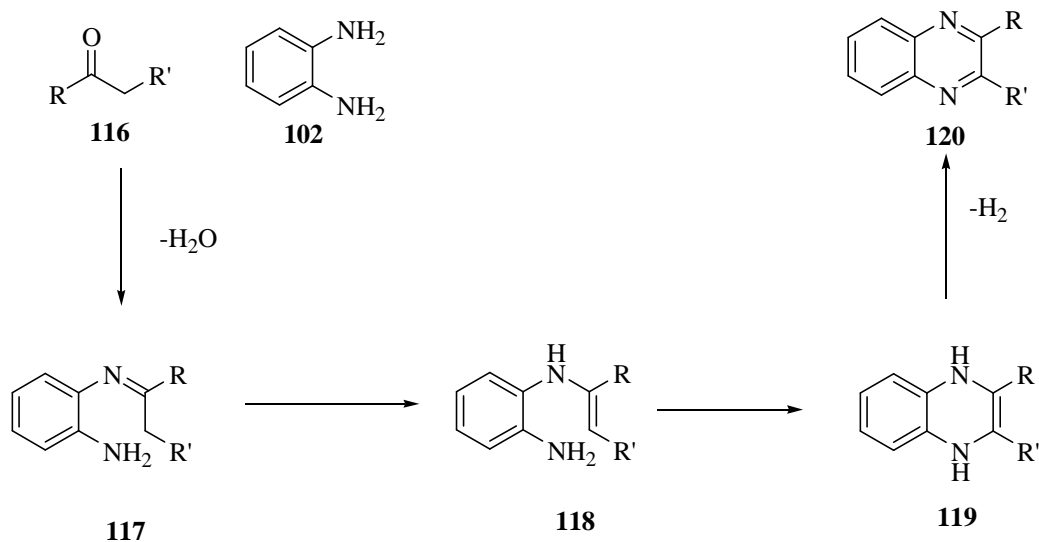
#### 1.5.4 Coupling of ketones and 1,2-diamines

Cho and co-workers<sup>56</sup> have reported the synthesis of quinoxalines using ketones and *o*-phenylenediamine in yields ranging from 30-95% (Scheme 26).



**Scheme 26: Synthesis of quinoxalines using ketones and *o*-phenylenediamine**

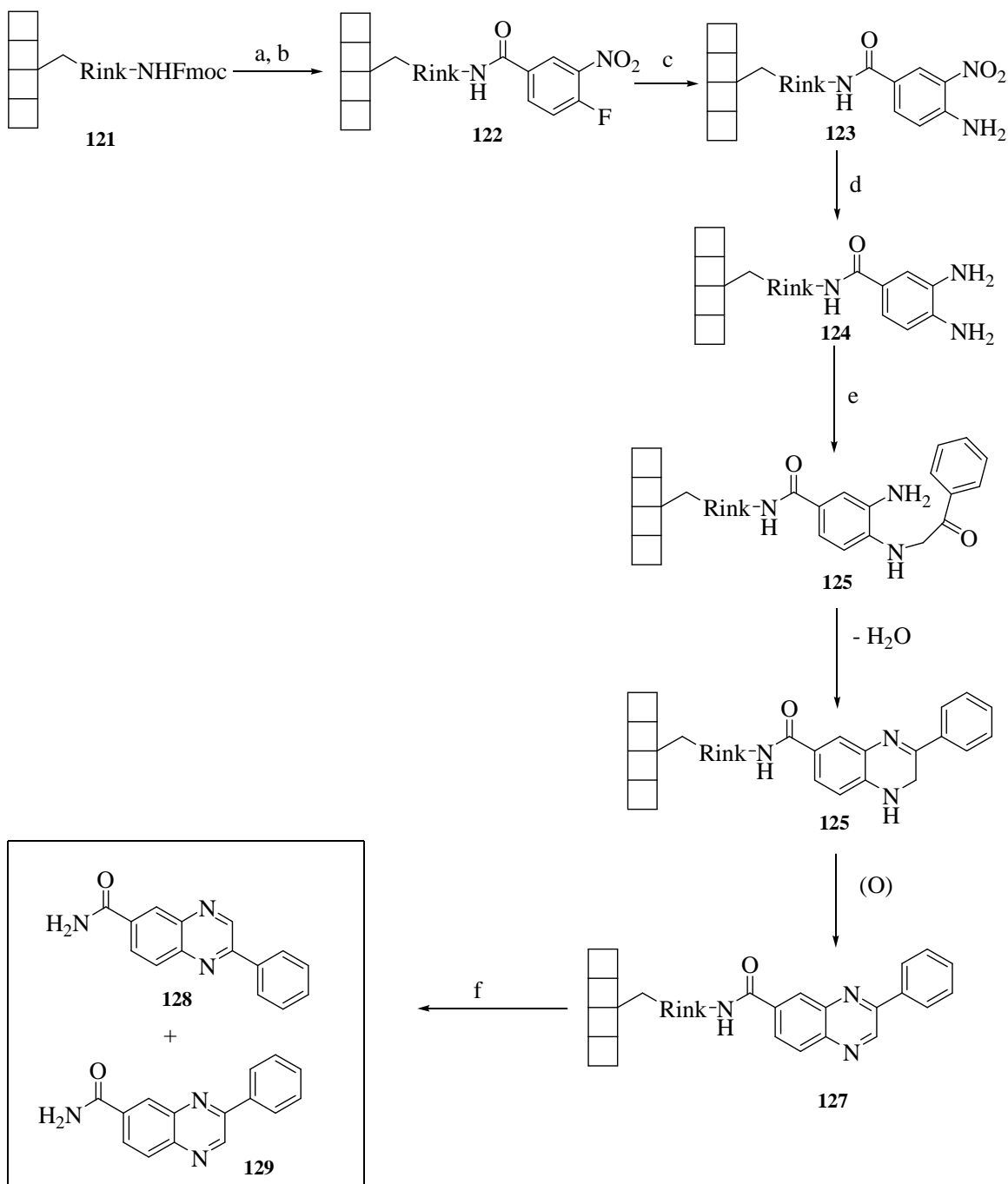
The following mechanism (**Scheme 27**) for the reaction was proposed with the ketone and 1,2-diamine forming the ketimine **117** which underwent tautomerism, facilitated by KOH to produce **118**, followed by intramolecular hydroamination and dehydrogenation to produce the desired quinoxaline. A two-fold excess of the ketone was added, as this was favourable from an atom economy point of view, since equimolar amounts of reactants resulted in lower yields. It was found that PEG-400 was the ideal solvent for these reactions compared to toluene, dioxane, dimethyl sulfoxide, tetrahydrofuran and 1,2-dimethoxyethane. Reactions carried out in the absence of KOH resulted in no product formation.



**Scheme 27: Proposed mechanism for quinoxaline synthesis using ketones and 1,2-diamines**

### 1.5.5 Solid phase synthesis

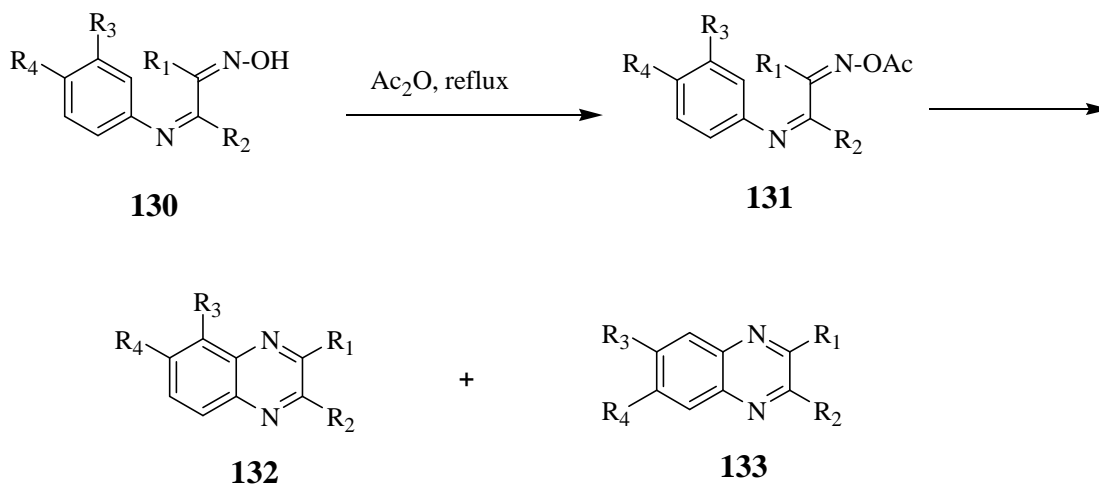
Another method that has been used to synthesize quinoxalines makes use of a solid phase.<sup>57</sup> In this procedure, 4-fluoro-3-nitro-benzoic acid is attached to a solid phase support system using peptide coupling. Substitution of the fluorobenzene by DIEA in aqueous ammonia gave the *o*-nitro aniline **123** which underwent tin chloride mediated reduction to produce the 1,2-diamine compound. The diamine **124** was treated with two equivalents of  $\alpha$ -bromoketone followed by dehydration and oxidation to generate the quinoxaline derivative **127** in a mixture of isomers which was freed from the solid support using TFA/DCM (**Scheme 28**).



**Scheme 28:** Reagents and conditions: (a) 20% piperidine in DMF, rt, 40 min; (b) 4-fluoro-3-nitrobenzoic acid, DIC, HOBt, DMF, rt, 16 h; (c) 1.0 M  $\text{NH}_3$  aqueous solution, 5% DIEA/DMF, 60 °C, 5 h; (d)  $\text{SnCl}_2 \cdot 2\text{H}_2\text{O}$ , NMP, rt, 24 h; (e) 2 eq.  $\alpha$ -bromoketone, DMF, 60 °C, 4 h; (f) 20% TFA/DCM, rt, 1 h;

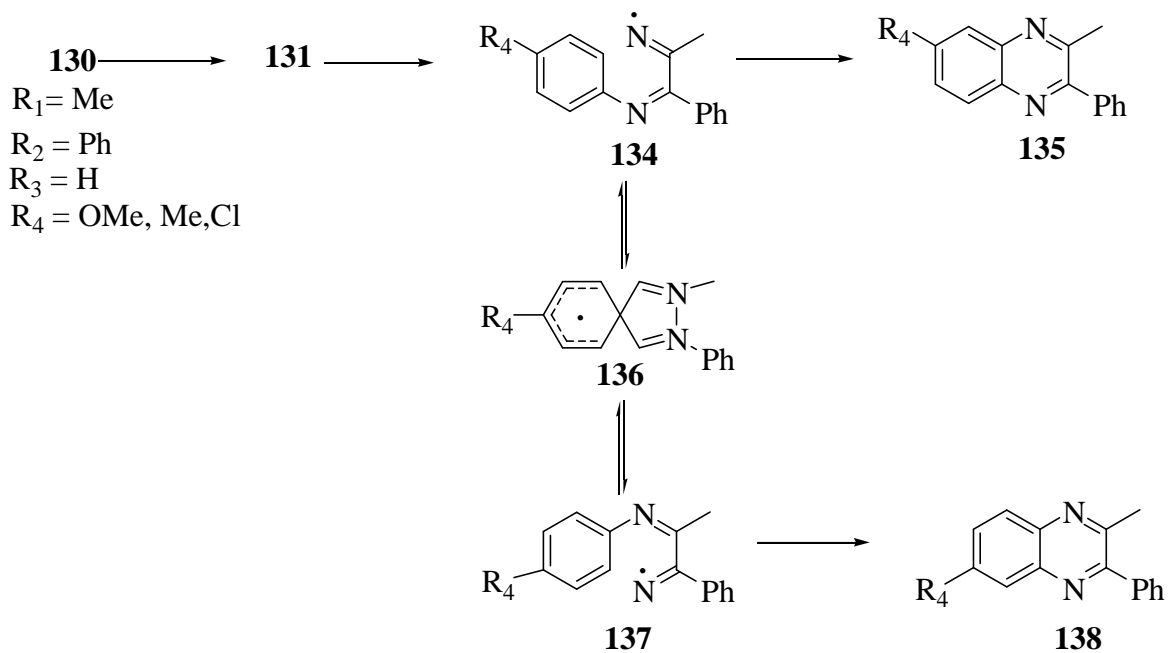
### 1.5.6 Cyclization of diaza-dienes

Maroulis and co-workers<sup>58</sup> have reported the synthesis of quinoxalines *via* the cyclization of diaza-dienes in refluxing acetic anhydride. They focused their attention on determining the mechanism for the formation of **133** (**Scheme 29**). They varied the substituents and found that attack was preferential from the *ortho* position to R<sub>3</sub> over regioisomers originating from the *para* position (R<sub>1</sub> = R<sub>2</sub> in these cases) and found that the ratio of **132/133** was only slightly dependent on the substituent. When R<sub>1</sub> and R<sub>2</sub> were varied they found that both products formed even though substitution was exclusively at the *para* position of the arylimino group (R<sub>3</sub> = H, R<sub>4</sub> = OMe, Me, Cl). They explained the preference for the *ortho* position and negligible effect of the substituent was due to homolytic aromatic substitution of iminyl radicals in which the *ortho* position is favoured.



**Scheme 29:** Synthesis of quinoxalines *via* the cyclization of diaza-dienes

The mechanism shown in **Scheme 30** was proposed in which the reaction proceeds *via* the iminyl radicals **134/137**, following rearrangement to the spirodienyl radical **136** which is in agreement with the report by McNab *et al.*<sup>59</sup>



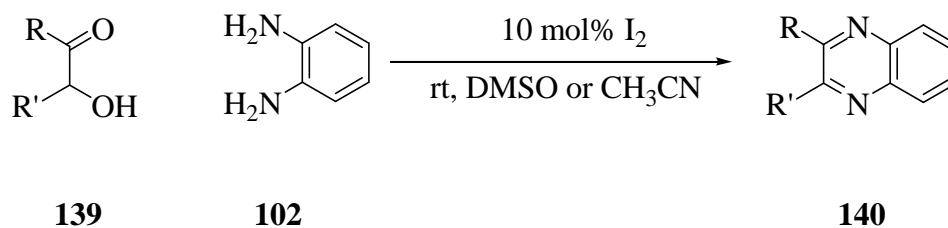
**Scheme 30: Mechanism of synthesis of quinoxalines *via* the cyclization of diaza-dienes**



## 1.6 THE USE OF CATALYSTS IN QUINOXALINE SYNTHESIS

### 1.6.1 Use of Iodine

Various catalysts have been employed to produce quinoxalines in a more efficient manner. The use of Iodine catalyzed quinoxaline synthesis (**Scheme 31**) was reported by Pawar's group<sup>60</sup> and Yao's group<sup>61</sup> at almost the same time in Tetrahedron Letters. The similarity between the papers is striking as both use 10 mol% Iodine, conduct the reaction at room temperature and report high yields. Pawar's group conducts the reaction in DMSO for 35-75 min (86-95%) while Yao's group uses acetonitrile for 3-20 min (90-98%). The role of iodine is unclear but Yao's group has suggested that it can act as a mild Lewis acid and dehydrating agent which will favour the formation of the quinoxaline products.



**Scheme 31: Iodine catalyzed synthesis of quinoxalines**

### 1.6.2 Sulfamic acid/methanol

Sulfamic acid/methanol is another catalytic system for the synthesis of quinoxalines.<sup>62</sup> The diketone and *o*-phenylenediamine are stirred in the presence of 5 mol% sulfamic acid in methanol for 5 minutes at room temperature to produce the quinoxaline in isolated yields of 67-100%. In addition, the product precipitates out of solution and can be collected by filtration (**Figure 2**).

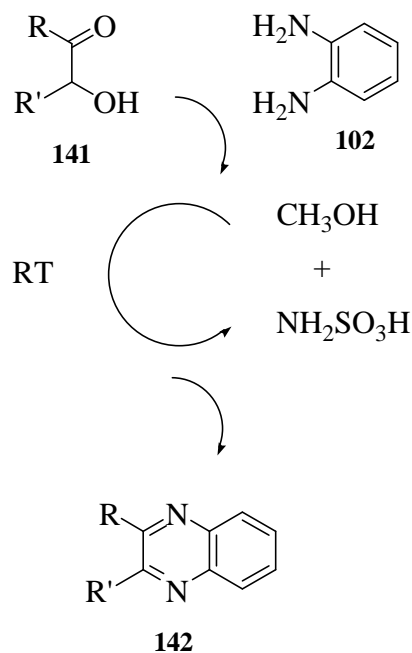


**Figure 2: Collection of quinoxaline by precipitation**

### 1.6.3 Nickel nano-particles

The use of Ni-nanoparticles as a catalyst for the synthesis of quinoxalines has recently been reported<sup>63</sup> as they are cheap, environmentally friendly and easily recyclable resulting the formation of the quinoxaline derivative in 10-50 minutes in yields ranging from 62-98%. The nanoparticles can be reused up to six times with only a slight decrease in activity. Ni-nanoparticles also exhibit dehydrating properties but have to be synthesized by a long and tedious procedure involving the reduction of Ni(II) to Ni(0) using a reverse micellar system.<sup>64</sup>

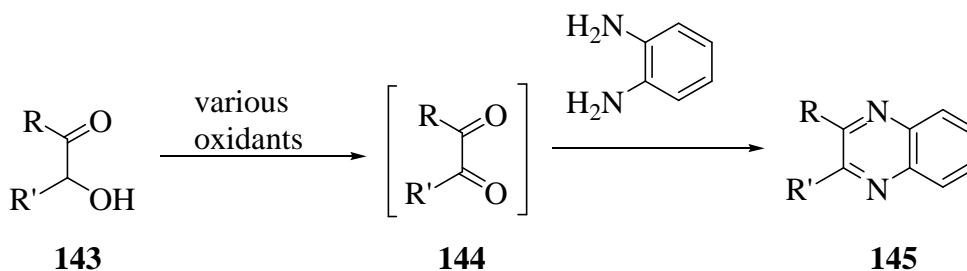
### 1.6.4 Ceric ammonium nitrate/tap water

One major concern of industry is the vast amount of toxic solvents used to carry out chemical reactions as subsequent disposal is problematic. Water is an ideal solvent from an industrial point of view due to its non-toxic properties. The use of water as a solvent

has been applied to the synthesis of quinoxaline in combination with ceric ammonium nitrate (CAN). The reaction couples the diketone and 1,2-diamine in the presence of 5 mol% CAN/tap water<sup>65</sup> at room temperature for 10-50 minutes with yields ranging from 82 – 98%.

## 1.7 SYNTHESIS OF QUINOXALINES BY THE TANDEM OXIDATION PROCESS

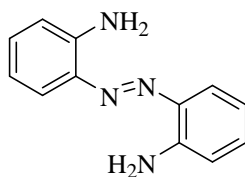
An alternate method is to start with  $\alpha$ -hydroxyketones **143** which would undergo oxidation to the diketone **144** and is trapped *in situ* by the diamine to produce the quinoxaline derivative **145** (Scheme 32).



**Scheme 32: One pot synthesis of quinoxalines**

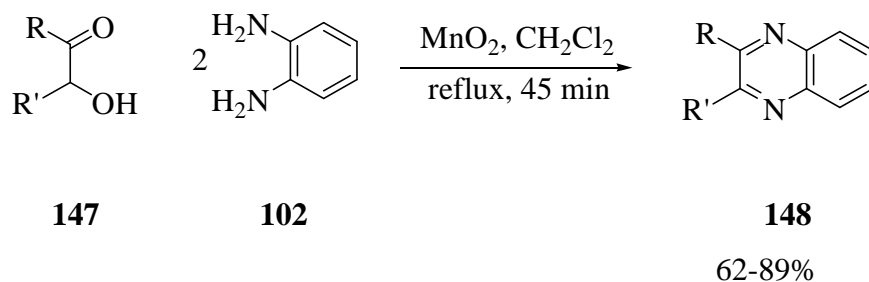
### 1.7.1 Manganese dioxide

Initial attempts at a manganese dioxide catalyzed quinoxaline synthesis resulted in consistently low yields. The major by-product was isolated and identified as the diazobenzene **146** resulting from the oxidative coupling of the diamine.<sup>66</sup>



**146**

Thus, two equivalents of amine were used and the reaction proceeded smoothly with the products obtained in good yields in 45 minutes. The oxidant can be removed by simple filtration but purification is required in order to separate the quinoxaline from the polymeric by-product.



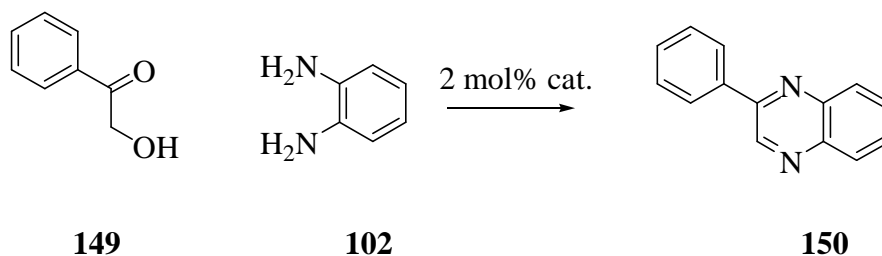
### Scheme 33: Manganese dioxide mediated synthesis

#### 1.7.2 Palladium acetate/triethylamine

The effect of various catalysts under aerobic oxidation was also used for the synthesis of quinoxalines. The effect of three catalysts on the rate of tandem quinoxaline synthesis was examined (**Table 4**) using 2-hydroxyacetophenone **149** and *o*-phenylenediamine **102** to produce the desired quinoxaline. As can be seen, the Pd(OAc)/Et<sub>3</sub>N and RuCl<sub>2</sub>(PPh<sub>3</sub>)<sub>3</sub>/TEMPO gave satisfactory results on completion. The authors<sup>67</sup> however, chose the Pd(OAc)/Et<sub>3</sub>N system due to its operational simplicity and ease of work-up.

They conducted a brief optimization study and found that the reaction could be conducted under reflux in an atmosphere of air to produce the quinoxaline product in a yield of 83% in 3 hours. This system, developed by Sigman *et al.*<sup>68</sup>, was used to synthesize a number of quinoxaline derivatives in yields ranging from 57-91%. The methods did however, require a longer reaction time (24h) for the hindered secondary alcohol and needed to be conducted at room temperature in the case of volatile aldehyde intermediate.

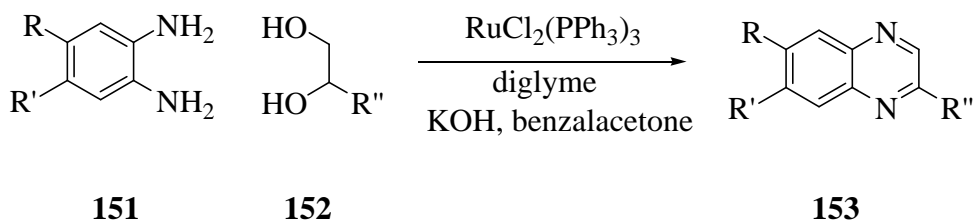
**Table 4: Evaluation of catalysts<sup>67</sup>**



| Catalyst  | Yield after 1 h (%) | Yield on completion (%) |
|---|---------------------|-------------------------|
| [( $\eta^6$ - <i>p</i> -cymene)RuCl <sub>2</sub> ] <sub>2</sub><br>Cs <sub>2</sub> CO <sub>3</sub> , PhMe, $\Delta$ | 26                  | 59 (3h)                 |
| RuCl <sub>2</sub> (PPh <sub>3</sub> ) <sub>3</sub> /TEMPO<br>PhMe, $\Delta$   | 59                  | 73 (3h)                 |
| Pd(OAc)/Et <sub>3</sub> N/O <sub>2</sub> (1 atm.)<br>PhMe, THF, rt  | Trace               | 88 (24h)                |
| Pd(OAc)/Et <sub>3</sub> N/<br>PhMe, THF, $\Delta$   | 53                  | 83 (3h)                 |

### 1.7.3 Tris(triphenylphosphine)ruthenium(II) dichloride

After this report, Cho and co-workers used  $\text{RuCl}_2(\text{PPh}_3)_3$  as an oxidant for the synthesis of quinoxalines<sup>69</sup> (**Scheme 34**) but unlike the previous authors<sup>67</sup> did not use TEMPO as co-catalyst. The quinoxaline **150** was obtained in 82% yield after reflux in diglyme for 20 hours although they attempted the tandem reaction on a diol system as opposed to the traditional  $\alpha$ -hydroxyketone. They do not explain why TEMPO was not used even though the previous author's work is referenced. Nevertheless, the longer reaction time could be due to a double oxidation process as opposed to single oxidation as well as the absence of TEMPO in the system.

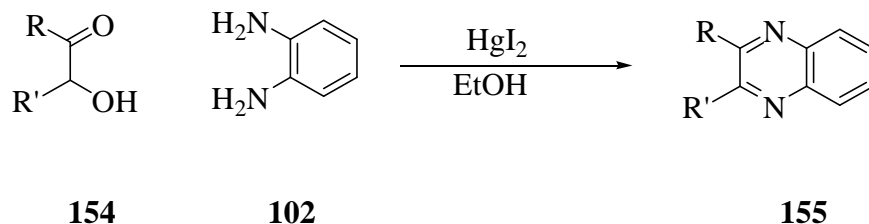


**Scheme 34: Ruthenium mediated synthesis of quinoxalines**

Nevertheless, Cho and co-workers report the yield of quinoxalines in the range 63-82%. The choice of additives is also interesting as KOH was used as a promoter for the transition metal catalyzed transfer hydrogenation reaction and benzalacetone was used as a hydrogen acceptor even though reactions carried out in its absence showed only a slight decrease in yield (75 vs. 82%).

### 1.7.4 Mercuric iodide

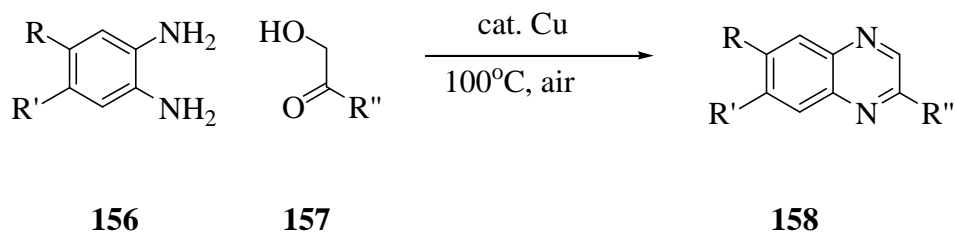
Mercuric iodide has also been used for TOP quinoxaline synthesis (**Scheme 35**).<sup>70</sup> The authors report yields ranging from 60 to 85% although the reactions were done on a larger scale (10 mmol) than the previous reported reactions (usually reactions are carried out on a 0.5 to 1 mmol scale).



**Scheme 35: Mercuric iodide mediated synthesis of quinoxalines**

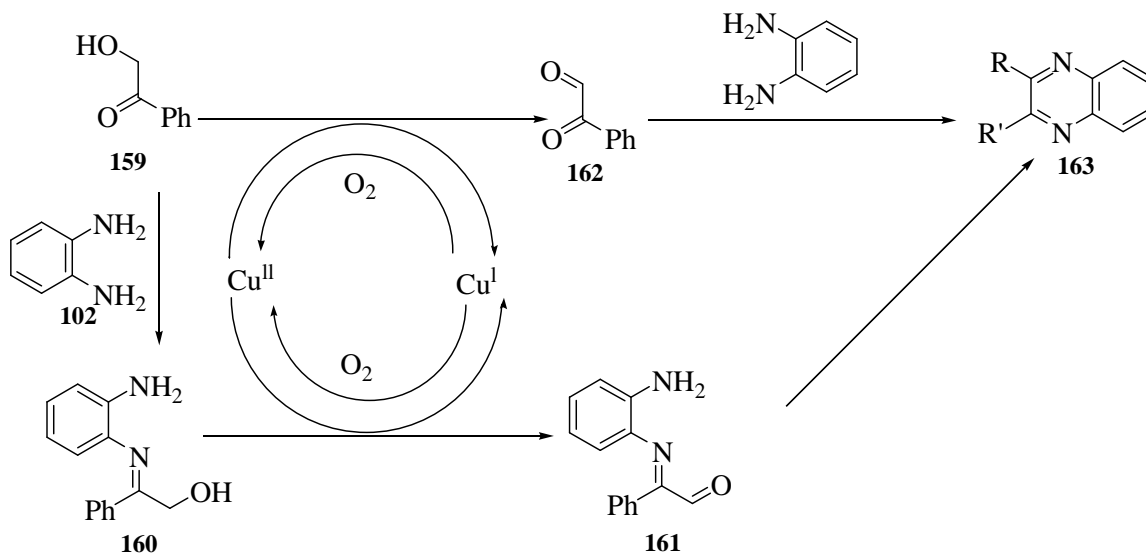
### 1.7.5 Copper(II) chloride

Another alternative, is the copper catalyzed transformation of alcohols to aldehydes and ketones and subsequent quinoxaline formation (**Scheme 36**).<sup>71</sup> Of interest, is that the authors report two methods for quinoxaline synthesis (one for a small scale reaction and the other for a large scale reaction). This is due to the formation of the impurity 1,2,3,4-tetrahydroisoquinoline when the reaction is conducted on a larger scale. When the reaction is carried out on a small scale (0.5 mmol), the alcohol, diamine, CuCl<sub>2</sub> was stirred in dry toluene for 3 hours at 100°C to provide the quinoxaline in an isolated yield of 94%. When the reaction was conducted on a larger scale (22.5 mmol) the reaction yield dropped to 70% for the same reaction.



**Scheme 36: Copper mediated synthesis of quinoxalines**

They also proposed two alternate mechanisms for the reactions (**Scheme 37**), one possibility being the oxidation of the  $\alpha$ -hydroxyketone to the diketone which subsequently undergoes attack by *o*-phenylenediamine to produce the quinoxaline. Alternatively, the  $\alpha$ -hydroxyketone may form the ketimine **160** first, followed by oxidation and subsequent attack to generate the quinoxaline.



**Scheme 37: Mechanism for copper mediated synthesis of quinoxaline**



## 1.8 THE USE OF A SEMICONDUCTOR AS AN OXIDANT

Before the unique properties of a semiconductor are introduced, the difference between a conductor, semiconductor and insulator needs to be explained. The difference between these three materials is best explained by the band model. **(Figure 3)**<sup>72</sup> When individual atoms are brought together to form a solid, electrons from neighbouring atoms that have similar values are forced to have slightly different energy levels resulting in an energy gap. Thus, electrons can be promoted from one energy level to the next by the application of an electric field. If electrons are able to 'jump' this energy gap, between the valence band (vb) and the conduction band (cb), - the crystal is a conductor (such as copper). If the electrons are unable to cross this energy gap-the crystal is an insulator (such as diamond). A semiconductor, as the name implies, can be converted into a conductor by applying a suitable energy source.

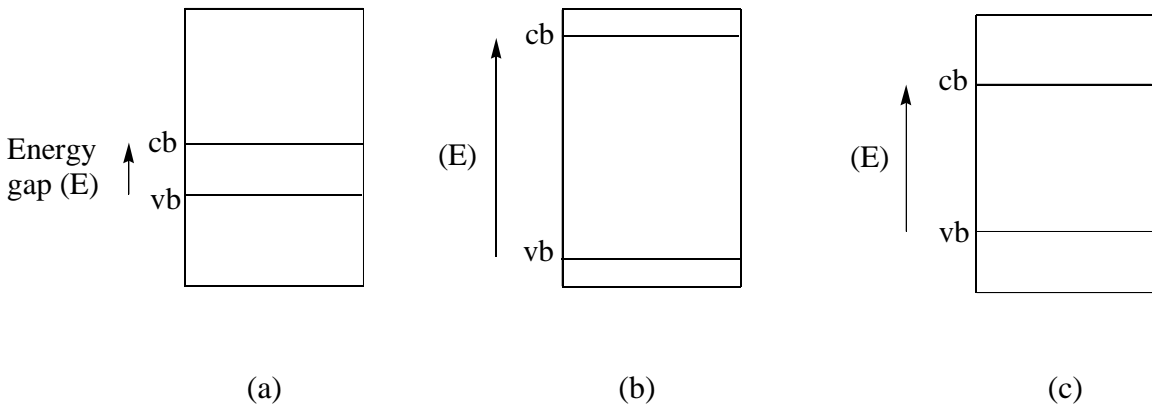


**Figure 3:** Basic description of band gap of (a) conductor, (b) insulator, (c) semiconductor

It is generally accepted that when a semiconductor is irradiated with an appropriate energy source an electron is promoted from the valence band to the conduction band leaving behind ‘positive holes’ in the valence band.<sup>§</sup> These holes are strong oxidizing agents and are able to oxidize water to generate hydroxyl radicals – which are also strong oxidizing agents (**Table 5**).

**Table 5: Oxidation potential of oxidants**<sup>73</sup>

| Oxidant           | Oxidizing potential (V) |
|-------------------|-------------------------|
| Hydroxyl radical  | 2.80                    |
| Ozone             | 2.07                    |
| Hydrogen peroxide | 1.77                    |
| Hypochlorous acid | 1.49                    |
| Chlorine          | 1.36                    |

A list of common semiconductors was examined (**Table 6**) with band gaps ranging from 318 to 886 nm and it was evident a number of semiconductors could be activated by visible light. However, a comprehensive literature review revealed that photocatalysis was not dependent on band gap only. Pelizzetti and co-workers<sup>74</sup> suggested that the ideal photocatalyst should be stable under irradiation and towards other chemicals, have a low cost and be environmentally friendly. They suggested that titanium dioxide and zinc oxide satisfied all these requirements and were the most ideal for photocatalytic reactions but also mentioned that a disadvantage of zinc oxide is its ability to dissolve in acidic solutions.

---

<sup>§</sup> A more in-depth explanation will be provided in the discussion section

**Table 6: Band gap of various semiconductors<sup>75</sup>**

| Semiconductors   | Valence Band<br>(v NHE) | Conduction<br>Band (v NHE) | Band Gap (eV) | Band gap (nm) |
|------------------|-------------------------|----------------------------|---------------|---------------|
| TiO <sub>2</sub> | + 3.1                   | -0.1                       | +3.2          | 387           |
| SnO <sub>2</sub> | +4.1                    | +0.3                       | +3.8          | 318           |
| ZnO              | +3.0                    | -0.2                       | +3.2          | 387           |
| ZnS              | +1.4                    | -2.3                       | +3.7          | 335           |
| WO <sub>3</sub>  | +3.0                    | +0.2                       | +2.8          | 443           |
| CdS              | +2.1                    | -0.4                       | +2.5          | 496           |
| CdSe             | +1.6                    | -0.1                       | +1.7          | 729           |
| GaAs             | +1.0                    | -0.4                       | +1.4          | 886           |
| GaP              | +1.3                    | -1.0                       | +2.3          | 539           |

## 1.9 TITANIUM DIOXIDE AS A PHOTOCATALYST

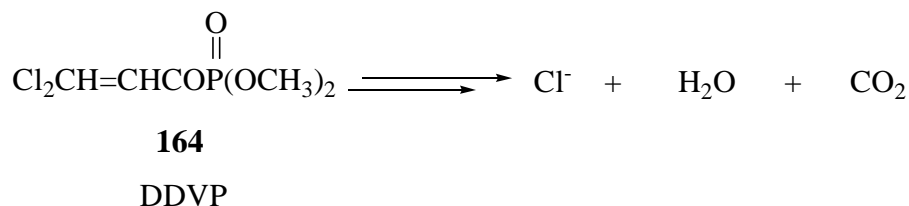
Titanium dioxide is found in three main crystalline forms namely anatase, rutile and brookite. Brookite is difficult to synthesize with most photocatalytic reactions are conducted using either anatase or rutile.<sup>76</sup> Anatase has a band gap of 387 nm while rutile has a band gap of 413 nm. Therefore, it was assumed that rutile would be the better photocatalyst as it has the smaller band gap. However, almost all photocatalytic reaction uses the anatase form of titanium dioxide. One reason could be due to the extent and nature of the surface hydroxyl groups in the anatase and rutile structure.<sup>77</sup> Also, the photocatalytic activity is related to the Fermi level which is 0.1eV higher in anatase than rutile.<sup>78</sup>

### 1.9.1 Industrial applications of titanium dioxide

Titanium dioxide has found widespread industrial application most notably in self cleaning paints.<sup>79</sup> Titanium dioxide absorbs sunlight to generate hydroxyl radicals which will degrade adsorbed dirt that can then be washed away by rain. In addition, titanium dioxide coated paints are used to neutralize pollution in the atmosphere in which gases such as nitrogen oxides are adsorbed and converted into water and carbon dioxide. Titanium dioxide has also found applications ranging from additives in food,<sup>80</sup> to UV absorbers in sunscreen lotions and cosmetics.<sup>81</sup>

### 1.9.2 Photodegradation ability of titanium dioxide

Much research has focused on the photodegradation ability of titanium dioxide, making use of titanium dioxide's strong oxidizing strength. Dichlorovos (DDVP) **164** is widely used in the agricultural industry, as a pesticide for crop protection. The LD<sub>50</sub> (Lethal dose required to kill half the number of the tested animals) for mice, rabbits and man was 87 mg/kg, 205 mg/kg and 400mg/kg respectively.<sup>82</sup> Thus, the subsequent removal of residual DDVP from accessible sources such as water is of vital importance. One method for DDVP removal is to mix it with titanium dioxide under UV light (**Scheme 38**).<sup>83</sup>



**Scheme 38: Destruction of DDVP using titanium dioxide**

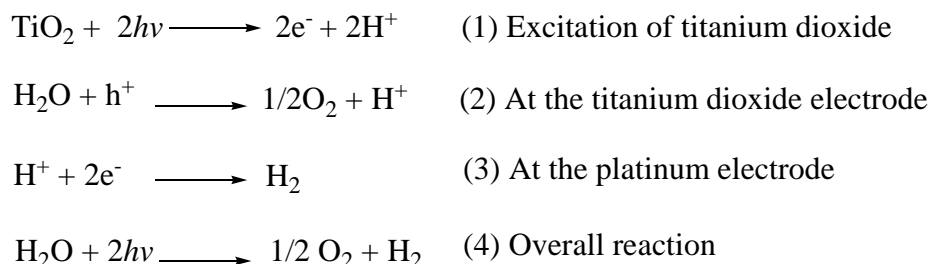
The general reaction consists of a toxic compound which is mixed with a portion of titanium dioxide and irradiated for a period of time which degrades DDVP through a

series of intermediates to ultimately produce chloride ions, water and carbon dioxide. Titanium dioxide has similarly been applied to the degradation of carcinogenic dyes,<sup>84</sup> pesticides<sup>85</sup> and the sterilization of bacteria.<sup>86</sup> This type of research reinforces the notion of titanium dioxide's oxidizing strength.

### 1.9.3 Applications in chemistry

#### 1.9.3.1 Photoelectrochemical solar cells

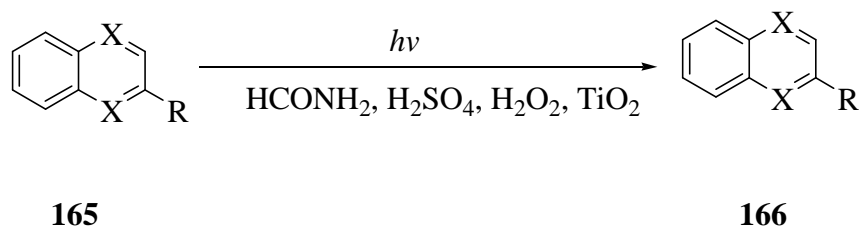
Fujishima and co-workers investigated photoelectrochemical solar cells using titanium dioxide.<sup>87</sup> A titanium dioxide electrode was connected through an electric load to a platinum-black counter electrode. When the titanium dioxide electrode was irradiated with UV light they noticed that photocurrent flowed from the platinum electrode to the titanium dioxide electrode.<sup>88</sup> The direction of the current revealed that oxidation was taking place at the titanium electrode (O<sub>2</sub> evolution) while reduction was taking place at the platinum electrode (H<sub>2</sub> evolution). This showed that water could be split into oxygen and hydrogen without applying a current through the cell according to **Scheme 39**.<sup>89</sup>



**Scheme 39: Splitting of water into hydrogen and oxygen using titanium dioxide**

### 1.9.3.2 Functionalisation of heterocyclic bases

Another reported use of titanium dioxide is the free radical functionalisation of heterocyclic bases under sunlight (**Scheme 40**).<sup>90</sup> Protonated heterocyclic bases are known to be attacked by nucleophilic radicals created *via* the reaction of hydroxyl radicals and amides, ethers, *etc.*<sup>91</sup> The authors report that in the presence of titanium dioxide the reaction proceeds with higher yields with no change in the observed products however they provide no mechanistic detail for the observed increase in yield.



X = CH, R = H

X = CH, R = CH<sub>3</sub>

X = C-CH<sub>3</sub>, R = H

X = N, R = H

X = CH, R = CONH<sub>2</sub>, 90%

X = C-CONH<sub>2</sub>, R = CH<sub>3</sub>, 100%

X = C-CH<sub>3</sub>, R = CONH<sub>2</sub>, 69%

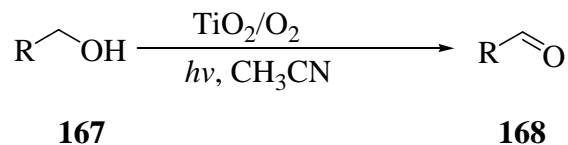
X = N, R = CONH<sub>2</sub>, 42%

**Scheme 40: Free radical functionalisation of heterocyclic bases using titanium dioxide**

### 1.9.3.3 Oxidation of alcohols

There has been immense amount of research detailing titanium dioxide's ability to carry out chemical transformations. These range from aromatic hydroxylation, alkene epoxidation, nitro-aromatic reduction and dehydrogenation.<sup>92</sup> Of interest, was titanium dioxide's ability to oxidize alcohols to aldehydes which has been reported many times.<sup>93,94</sup> The research in this field has been divided into the 'direct' and 'indirect'

oxidation. The direct reaction involved a process in which the titanium dioxide powder was dried in an oven to remove any bound water molecules and thus minimize the formation of radicals, with the positive holes carrying out the oxidation. The indirect oxidation occurs when no attempt has been made to remove the adsorbed water from the powder. The general reaction consisted of mixing the alcohol with titanium dioxide in acetonitrile which was irradiated under ultraviolet light (**Scheme 41**).

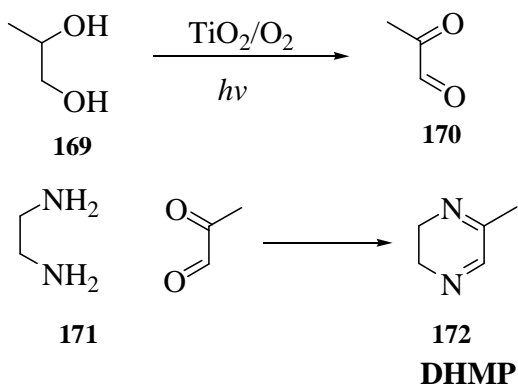


**Scheme 41: Oxidation of alcohols using titanium dioxide**

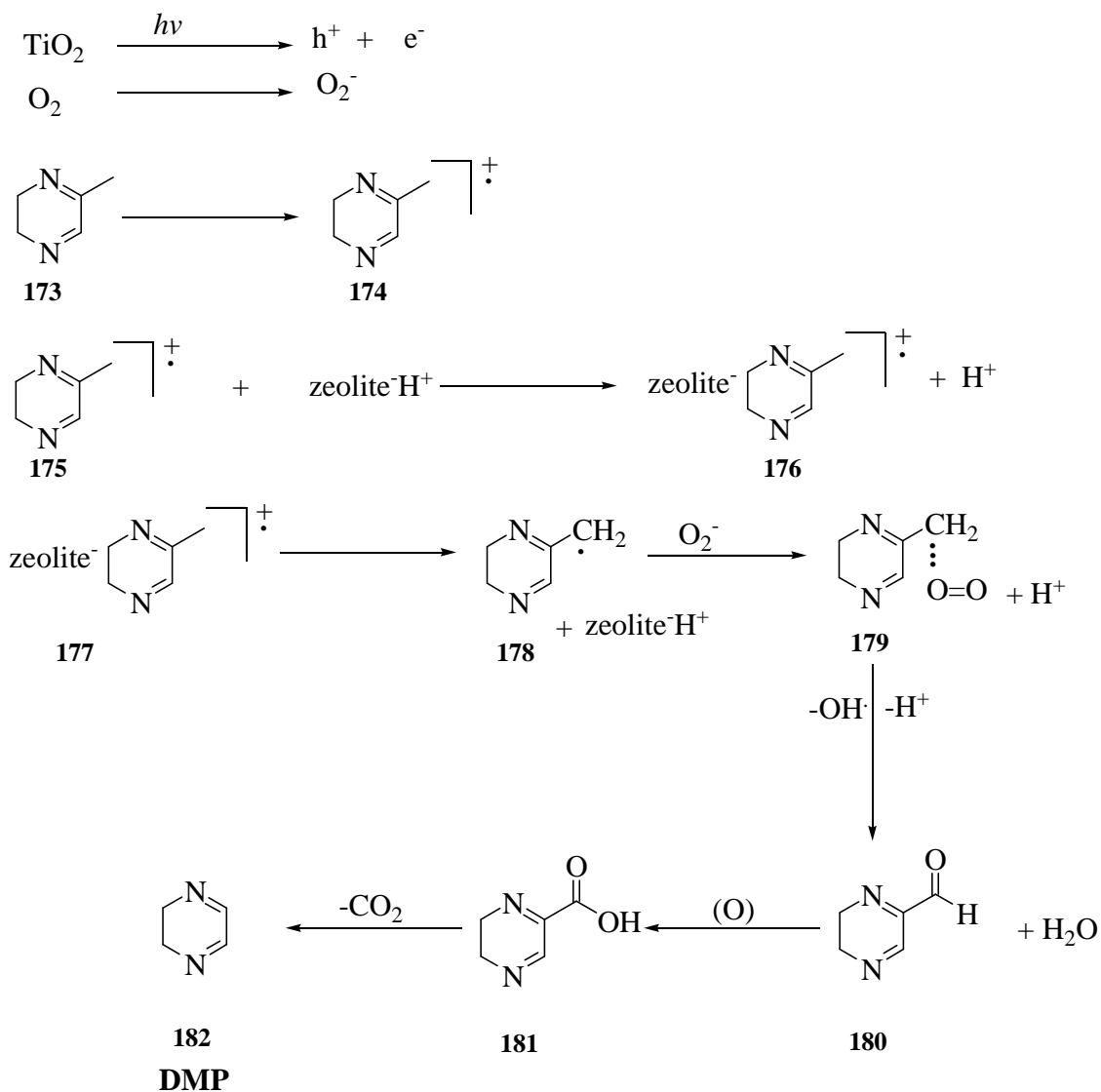
#### 1.9.3.4 Tandem oxidation type process

Dihydropyrazine (DHP) was synthesized from ethylene glycol and ethylenediamine in the presence of titanium dioxide and zeolite (**Scheme 42**).<sup>95</sup> The authors proposed that ethylene glycol would undergo titanium dioxide catalyzed oxidation to generate the diketone which would be trapped *in situ* by ethylenediamine to produce dihydromethylpyrazine (DHMP) (Step 1). DHMP is demethylated *via* a series of steps to produce dihydropyrazine (DHP) with a reported yield of 20% based on starting material recovered.

Step 1



Step 2



Scheme 42: Mechanism for the synthesis of dihydropyrazine using titanium dioxide



## **AIMS OF THE PROJECT**

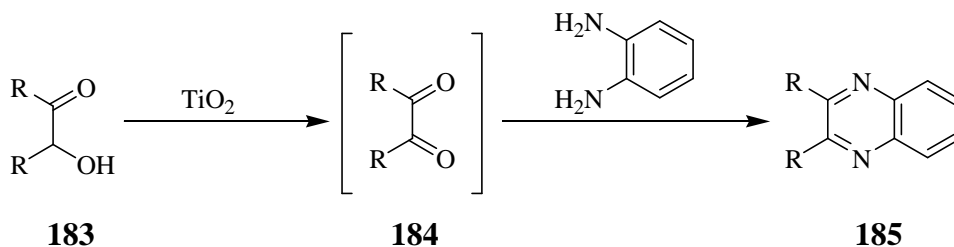
To date, an increasing number of research publications have been directed towards the utilization of the tandem oxidation type approach in the synthesis of organic molecules. The aim of this project is directed towards the study of titanium dioxide as a potential photocatalyst in organic synthesis. For this study, the class of quinoxaline type compounds will be looked at in order to evaluate titanium dioxide as an oxidant in the tandem oxidation process. The aim of this study also includes an optimization of the reaction conditions which would incorporate investigations directed towards the shifting of the titanium dioxide band gap.

## Chapter 2

### Discussion

#### 2.1 PREFEACE

The focus of this project was to develop titanium dioxide as a potential tandem oxidation type catalyst. In the discussion which follows, attention will be focused on the evaluation of titanium dioxide as an oxidant *via* the synthesis of a series of quinoxaline derivatives as illustrated in **Scheme 43**; and to evaluate potential applications on a multifunctional substrate as well as in the Wittig reaction.



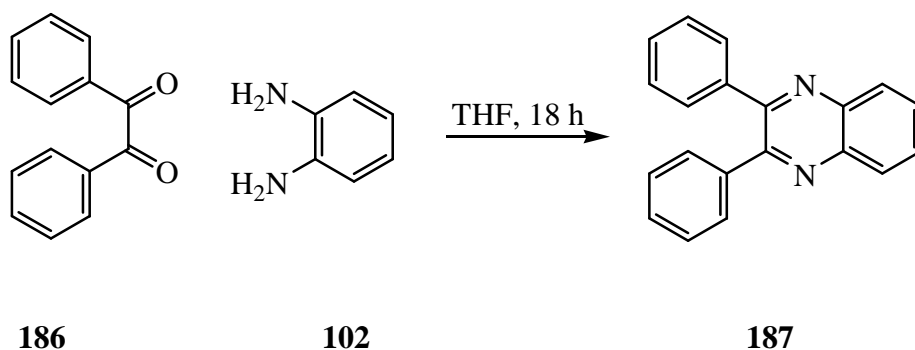
**Scheme 43: The application of titanium dioxide as an oxidant in the synthesis of quinoxalines *via* the tandem oxidation process**

Selected proton NMR and GC-MS spectra for the synthesized compounds will be discussed. Reaction times and yields of titanium dioxide catalyzed tandem oxidation processes will be compared with established TOP catalysts in order to gauge the performance of titanium dioxide.

#### 2.2 MECHANISM OF QUINOXALINE SYNTHESIS

It is relevant at this point to discuss the mechanism of quinoxaline formation before the introduction of titanium dioxide TOP methodology. The mechanism involves the attack

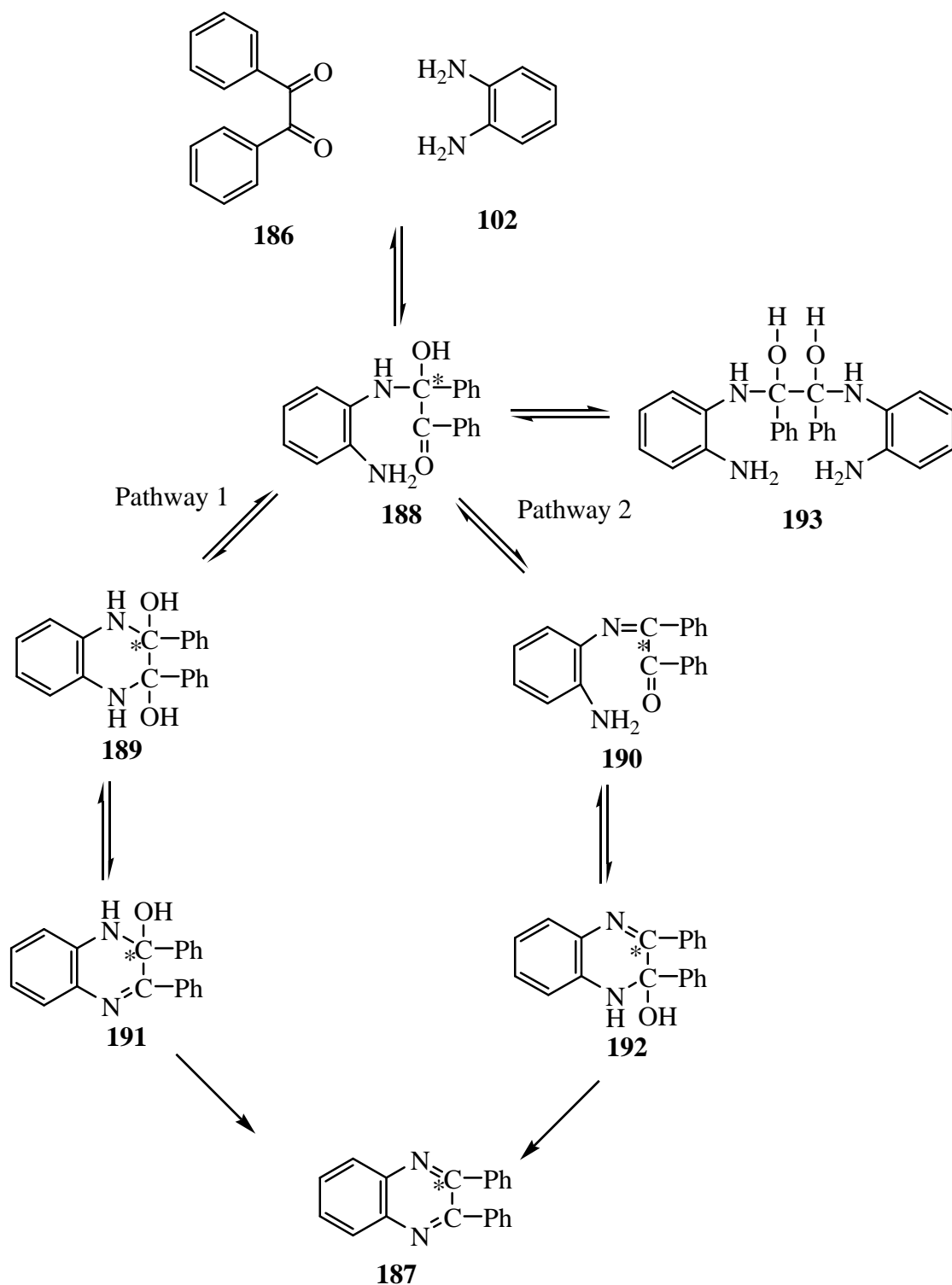
of the carbonyl groups by the diamino moieties followed by a double condensation. However, the sequence in which the reaction steps take place is relatively complex. The question arises as to whether the amino groups attack separately or simultaneously and in what order or preference? Butler and co-workers<sup>96</sup> conducted a mechanistic study on the formation of quinoxalines in an attempt to answer these essential questions. Benzil **186** and *o*-phenylenediamine **102** were reacted in tetrahydrofuran (THF) to form **187**, and as the reaction was sufficiently slow (18h), it allowed for analysis in hourly intervals by <sup>13</sup>C NMR spectroscopy (**Scheme 44**).



**Scheme 44: Coupling of benzil and *o*-phenylenediamine**

The <sup>13</sup>C abundance was enhanced in one of the carbonyl groups in order to monitor its disappearance (195.50 ppm) while the appearance of the C=N signal at 154.47 ppm was noted. After four hours the signal due to the carbonyl group had disappeared while a number of signals, which were attributed to intermediates, had appeared at approximately 84 ppm. Butler and co-workers proposed two pathways (**Scheme 45**) and attempted to correlate their experimental results. If the reaction had followed pathway 2, two signals would be expected at around 84 ppm, however this is not the case with five signals in this region. The more plausible explanation was pathway 1, with intermediates **188** and **191** each giving rise to one signal. Compound **189** has three enantiomeric forms, one *meso* (**194**) and two *rac*-forms (**195** and **196**). Compound **194** can undergo ring inversion of the half chair form, occurring at such a speed that it will result one signal (**Scheme 46a**). Compound **195** will also undergo a ring inversion of the half chair form but in this case

one of the conformations will be favoured due to hydrogen bonding (**Scheme 46b**). A similar situation occurs for **196**. The extra signal was deemed to come from **193** which results in an unisolable product.



**Scheme 45: Pathways proposed for the synthesis of the quinoxaline derivative**

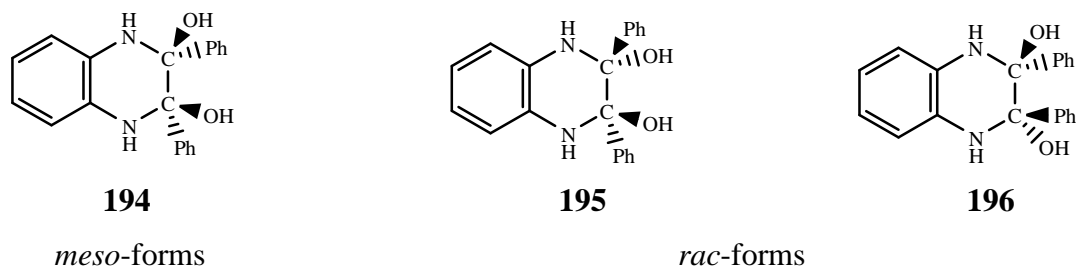
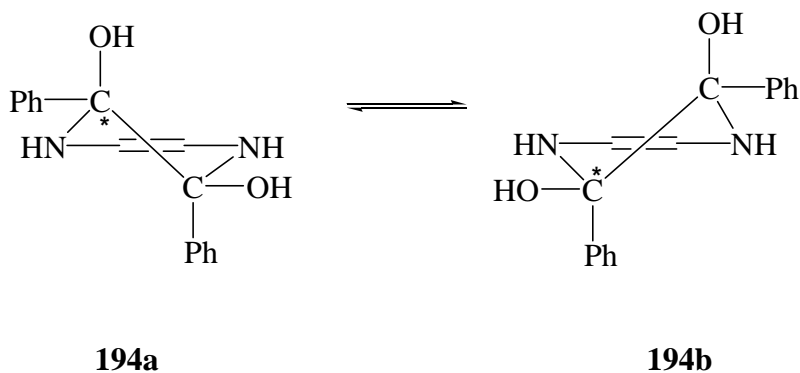
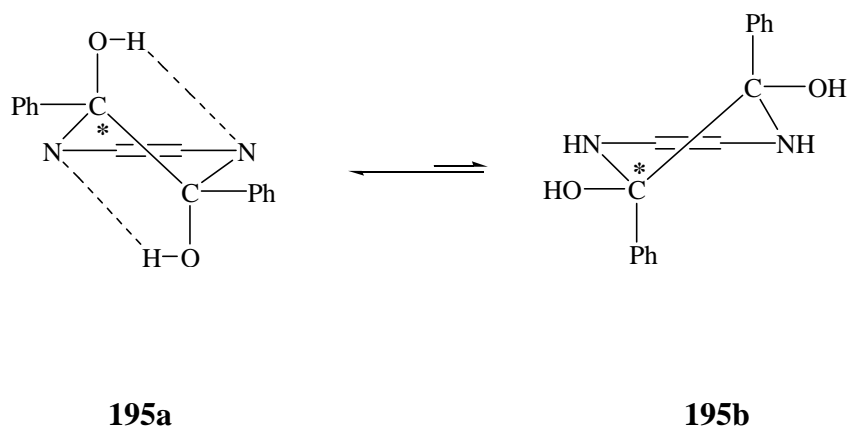


**Figure 4: *meso* and *rac* forms of target quinoxaline**

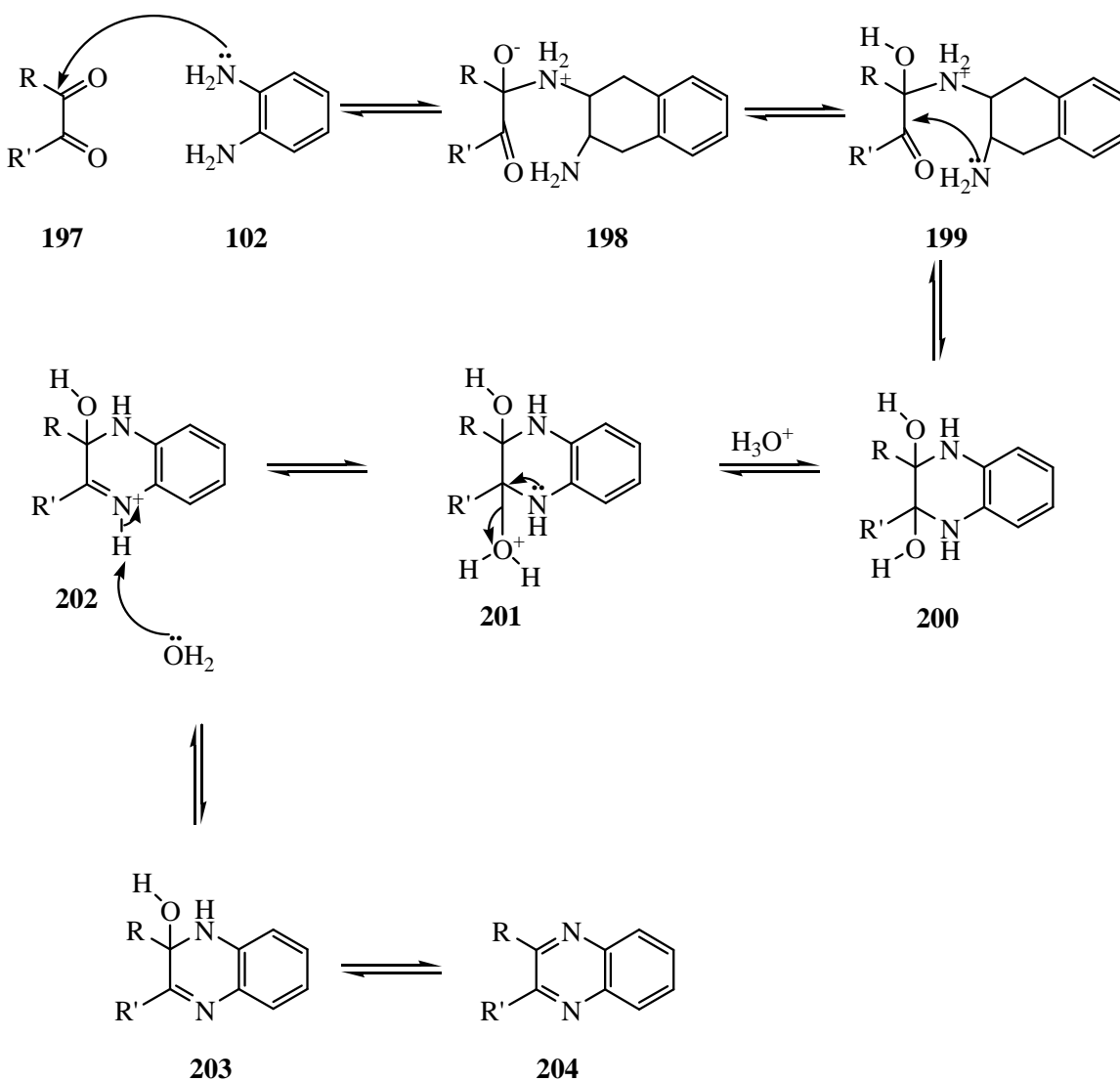


**Scheme 46a: Ring inversion of the *meso* form**



**Scheme 46b: Ring inversion of the half chair form of the *rac* form showing the favoring of conformation due to hydrogen bonding**

Based on the work of Butler and co-workers discussed above, the following mechanism (Scheme 47) is proposed.\*\* Initial attack of the carbonyl by the amine to generate the intermediate **198** which undergoes proton transfer from nitrogen to oxygen to produce **199**. This process is subsequently repeated by the second amino group to afford **200**. Under acidic conditions, the oxygen group is protonated followed by dehydration to produce **202**. Transfer of a proton to water will produce **203**. The second oxygen group is protonated, followed by dehydration and proton transfer to finally produce the product **204**.



**Scheme 47: Mechanism for the synthesis of quinoxaline**

\*\* The oxidation of the alcohol to the aldehyde will be extensively covered later.

## 2.3 APPLICATION OF TITANIUM DIOXIDE AS AN OXIDANT TOWARDS THE SYNTHESIS OF QUINOXALINES

Titanium dioxide, being a photocatalyst, must be activated using some form of irradiation in order for the oxidation to take place. In an article by Fujishima and co-workers it was claimed that placing a portion of titanium dioxide in polluted water, in the presence of sunlight results in gradual water purification.<sup>89</sup> Inspired by this result, we attempted a test reaction under conditions of natural sunlight. The coupling of 2-hydroxyacetophenone and *o*-phenylenediamine was chosen for the preliminary study as the reaction progress can be easily monitored by <sup>1</sup>H NMR spectroscopy by observing the disappearance of the methylene peak at *ca.* 4.5 ppm while noting the formation of the methine peak at *ca.* 9.3 ppm.

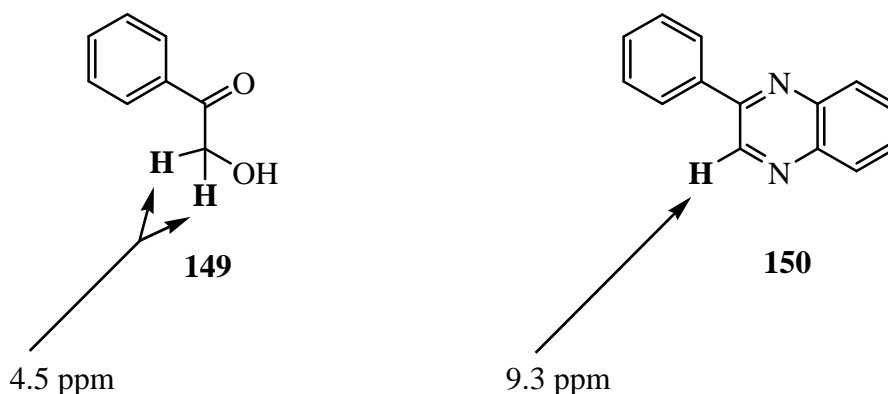
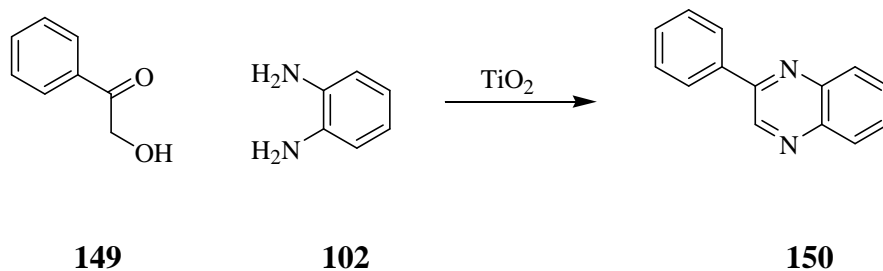


**Figure x: Chemical shifts of protons in the reactant and product used to monitor reaction progress**

2-hydroxyacetophenone, phenylenediamine and titanium dioxide was stirred under sunlight for 3 hours (**Scheme 48**). The mixture was passed through a silica plug and analyzed by <sup>1</sup>H NMR spectroscopy which revealed the absence of starting material peaks with the formation of the quinoxaline derivative evident, albeit in the presence of other unidentifiable compounds. This crude product was purified using radial chromatography to afford the title quinoxaline 2-phenylquinoxaline as an orange solid in an isolated yield of 27%.



**Scheme 48: Titanium dioxide mediated tandem coupling reaction**

$^1\text{H}$  NMR spectroscopic data was in close agreement to that obtained by Taylor and co-workers<sup>97</sup> and the peaks in the spectrum were assigned accordingly (**Figure 5**), while the GC-MS trace revealed the compound to have a molecular mass of 206 as expected for the desired quinoxaline.

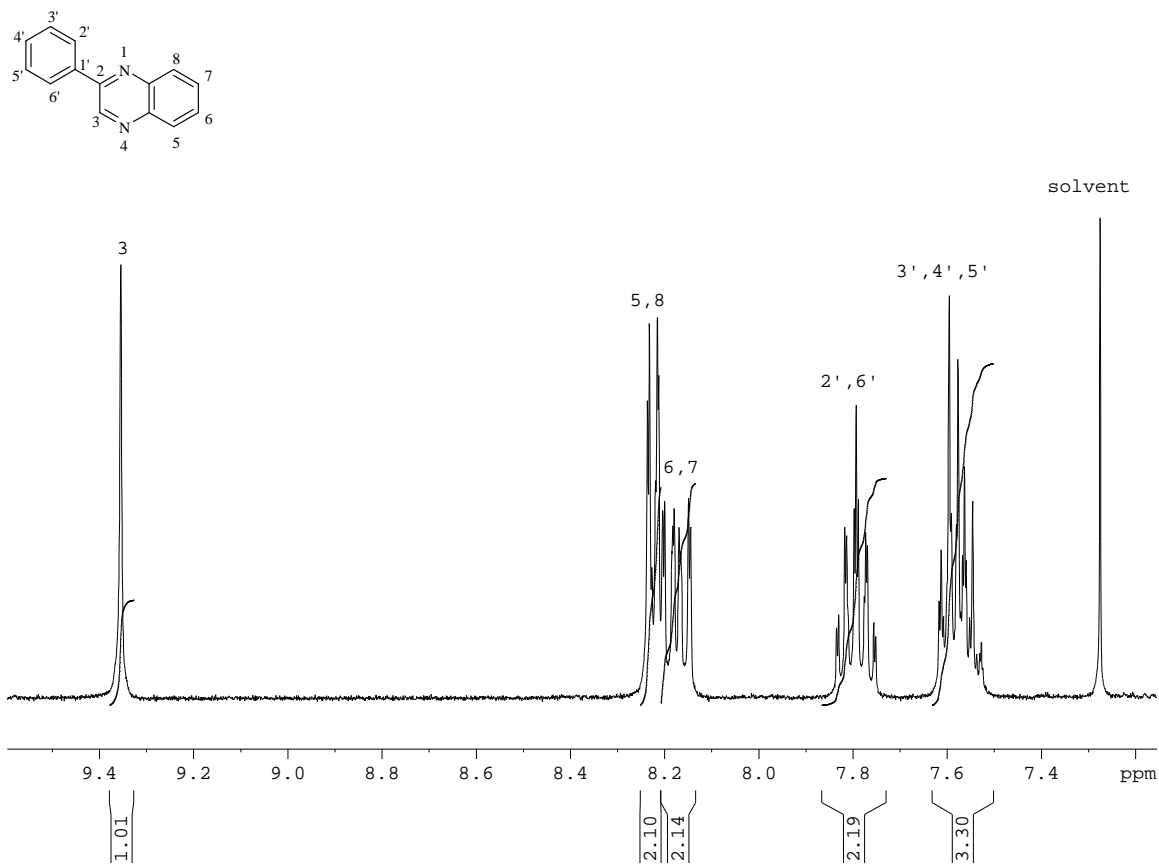


**Figure 5: Proton NMR spectrum of 2-phenylquinoxaline**



While encouraged by these preliminary results, the observed limitations of this approach were indeed evident. These included the availability and variation of natural sunlight. In addition, the tandem coupling reaction required further investigation in order to increase the yield and optimize reaction times. Thus, a better understanding of the titanium dioxide photocatalyzed process is needed.

### 2.3.1 Photocatalysis by titanium dioxide

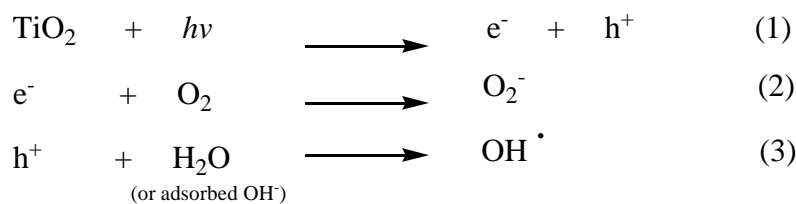
Photocatalysis by semiconductor oxides has been identified as a promising route for organic chemistry in the 21<sup>st</sup> century.<sup>92</sup> Activation of semiconductors with an appropriate energy source has led to a number of functional group transformations with the photooxidation being the most common.<sup>98</sup> Attention will now be focused specifically on a titanium dioxide mediated oxidation and the mechanistic considerations associated therewith. The most important considerations for a photocatalytic reaction are:

- the band gap of the semiconductor (E)
- the position of the lowest point in the conduction band (cb)
- the position of the highest point in the valence band (vb)

The valence band of titanium dioxide consists of 2p oxygen orbitals while the conduction band consists of 3d titanium orbitals. Titanium dioxide has a band gap of 3.2 eV corresponding to a wavelength of 387 nm.<sup>99††</sup> It is generally accepted that the following steps shown in **Scheme 49** will only occur when titanium dioxide is irradiated with photons of energy equal to or higher than 3.2 eV:<sup>92,100-102</sup>

---

†† Wavelength determined using the equation  $\lambda = 1239.8/E$  with E= band gap.



**Scheme 49: Formation of hydroxyl radicals when titanium dioxide is irradiated under UV light**

Irradiation of titanium dioxide with an appropriate energy source leads to the formation of a hole ( $h^+$ ) in the valence band and an electron ( $e^-$ ) in the conduction band. This electron reacts with oxygen to produce superoxide molecules. These positive holes, are strong oxidants and oxidize water (or adsorbed hydroxyl groups) to produce the key hydroxyl radicals. Hydroxyl radicals are known to be strong oxidants - as previously highlighted. This scheme is more adequately represented by the following diagram (Figure 6).

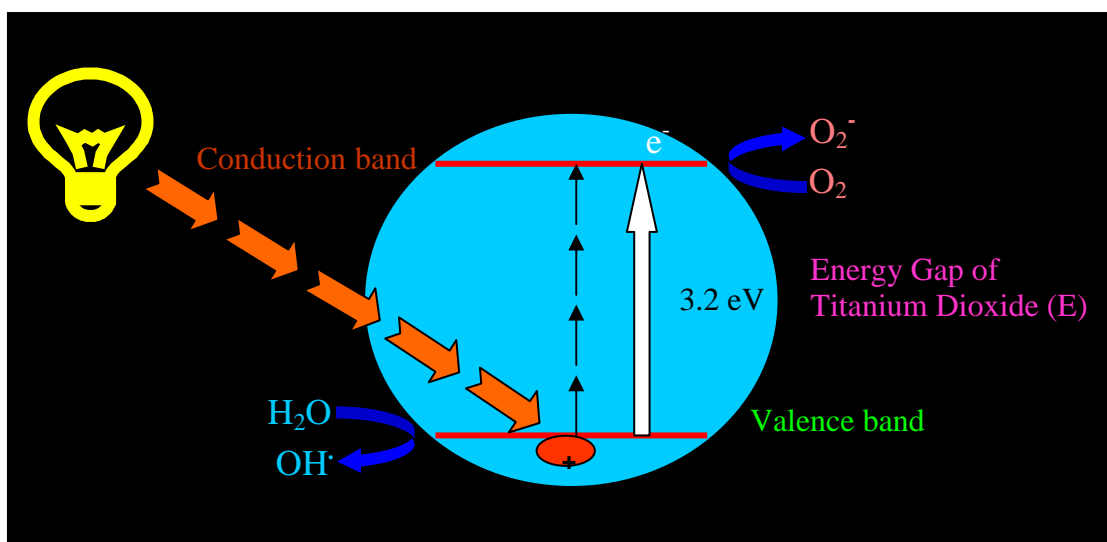


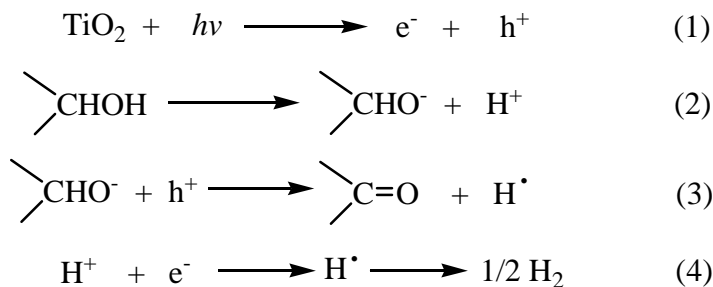
**Figure 6: Energy gap of titanium dioxide**

The hydroxyl radicals produced are capable of oxidizing alcohols to aldehydes and ketones but the mechanism is relatively complex. The first issue concerns whether oxidation of the alcohol occurs *via* the holes, hydroxyl radicals or both. The proposed mechanisms from literature have been divided into the direct (oxidation *via* the hole) and indirect (oxidation *via* the hydroxyl radicals) methods.

### 2.3.2 Evidence for the direct oxidation

Hashimoto and co-workers conducted a study to measure the quantity of hydroxyl radicals produced using a fluorescence probe when a titanium dioxide plate was irradiated with a high pressure mercury lamp.<sup>103</sup> They reported the quantum yield was much lower ( $7 \times 10^{-5}$ ) than ordinary photocatalytic reactions ( $\sim 10^{-2}$ ). The quantum yield for iodide ion oxidation was  $5.7 \times 10^{-2}$  - equivalent to that of an ordinary photocatalytic reaction. If hydroxyl radicals were the only active species then the result from the iodide oxidation is inexplicable. Based on this, the authors concluded that the photogenerated holes are more important than the hydroxyl radicals.

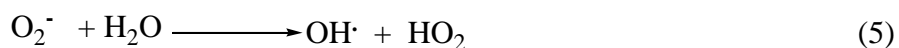
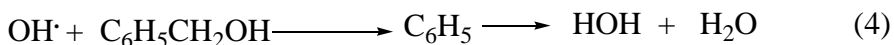
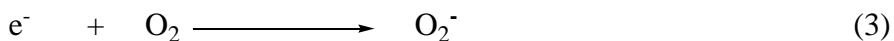
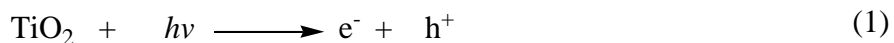
The following steps shown in **Scheme 50** have been proposed for the oxidation of alcohols *via* the direct method:<sup>104-106</sup> Titanium dioxide is first activated by an appropriate energy source to generate electrons and positive holes (step 1). This is followed by dissociative adsorption of the alcohol on the titanium dioxide basic sites (step 2), followed by a second proton abstraction from the alkoxide ion *via* reaction with the positive hole (step 3), followed by the formation and desorption of hydrogen (step 4).



**Scheme 50: Titanium dioxide mediated oxidation of alcohol *via* the indirect method**

### 2.3.3 Evidence for the indirect oxidation

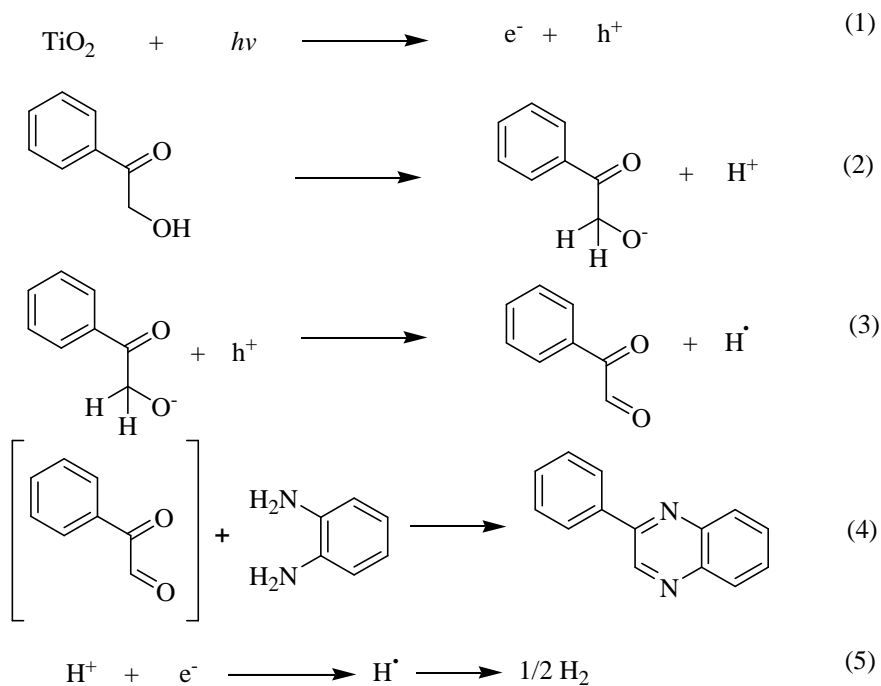
There is also an argument for an indirect mechanism, in which the holes oxidize bound hydroxyl groups or water to produce hydroxyl radicals. Hussein, *et al.* has proposed the mechanism shown in **Scheme 51** for the oxidation of benzyl alcohol to benzaldehyde *via* this method<sup>101</sup> only, neglecting the effect of the positive holes. Benzyl alcohol was mixed with a portion of titanium dioxide and stirred under UV irradiation. An electron is promoted from the valence band to the conduction band; the adsorbed hydroxyl groups (or H<sub>2</sub>O) are oxidized to hydroxyl radicals while oxygen is reduced to O<sub>2</sub><sup>-</sup> (steps 2 and 3). These hydroxyl radicals then react with benzyl alcohol (step 4) while the superoxide molecules react with water to regenerate the hydroxyl radicals (step 5). Benzaldehyde could thus be formed according to the following steps (6-8):



**Scheme 51: Proposed mechanism for benzaldehyde formation *via* the direct method**

### 2.3.4 Mechanism of titanium dioxide mediated synthesis of quinoxalines

For the tandem coupling reaction, the following mechanism (**Scheme 52**) is proposed based on the direct method proposed in section 2.3.2.



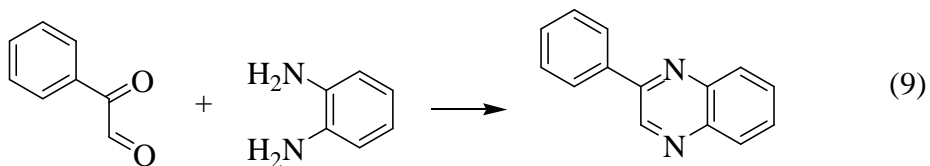
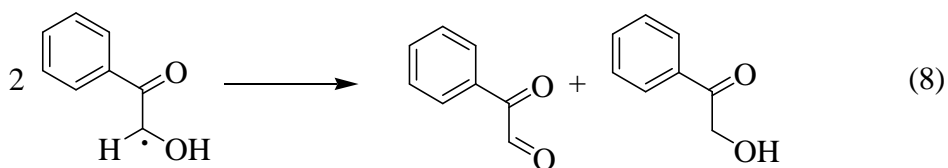
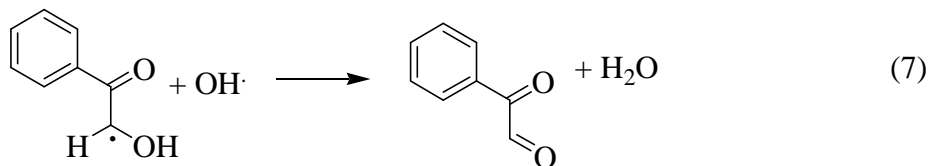
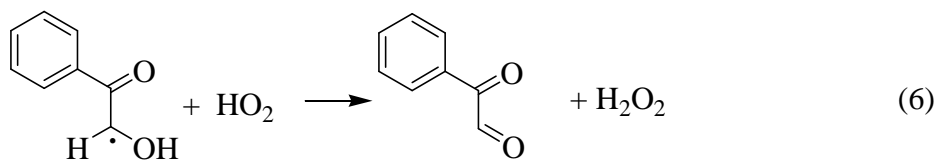
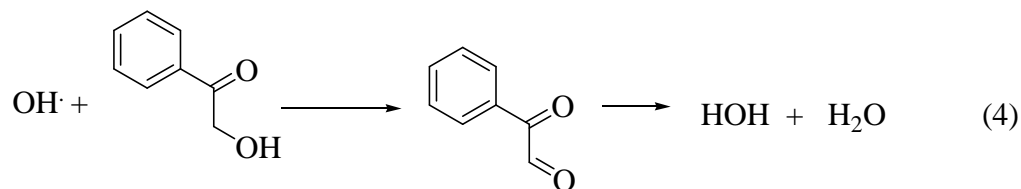
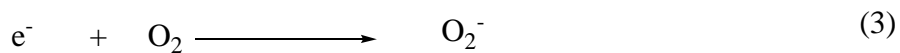
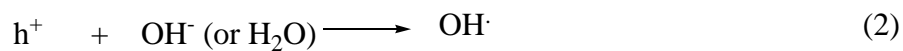
**Scheme 52: Direct titanium dioxide mediated quinoxaline synthesis**

Titanium dioxide is activated by appropriate irradiation to generate the electrons and positive holes (step 1), followed by dissociative adsorption of the alcohol on titanium dioxide's basic sites (step 2). The second proton is then abstracted to form the alkoxide ion *via* a reaction with the positive hole to produce the diketone (step 3). The diketone reacts with the diamine to produce the quinoxaline derivative<sup>‡‡</sup> (step 4) as shown by

<sup>‡‡</sup> This is a simplified step as imine formation may occur prior to oxidation.

Butler and co-workers in section 2.2. The final step is the formation and desorption of hydrogen (step 5).

Should the alcohol be oxidized by hydroxyl radicals, as in the case of the indirect mechanism, then the tandem coupling mechanism below is anticipated (**Scheme 53**). Titanium dioxide is activated by an appropriate energy source, resulting in the formation of electrons and positive holes (step 1). The positive holes and electrons react with hydroxyl radicals (or water) and oxygen respectively to produce hydroxyl radicals and superoxide molecules (steps 2 and 3). The hydroxyl radical reacts with the alcohol and superoxide molecules react with water to regenerate the hydroxyl radicals (steps 4 and 5). The diketone may be formed by one of the following steps (steps 6,7,8) and is trapped by the diamine to produce the quinoxaline (9).



**Scheme 53: Indirect titanium dioxide mediated quinoxaline synthesis**

The aldehyde used in the tandem coupling reaction may originate from either the direct or indirect method, although certain authors have attempted to favour the direct mechanism by minimizing adsorbed water on titanium dioxide.<sup>107</sup> For the purposes of the following study, no attempt was made to dry titanium dioxide and it is envisaged that the oxidation proceeds *via* simultaneous direct and indirect methods. This should result in higher yields as the alcohol can be oxidized by both the hole *and* hydroxyl radicals. An overview of the titanium dioxide catalyzed oxidation revealed that a number of factors need to be considered for a tandem coupling reaction. The most pertinent being:-

- the band gap of titanium dioxide
- choice of solvent and reaction vessel

The first point requiring attention was the large band gap of titanium dioxide which requires ultraviolet light for activation. If the band gap was decreased, titanium dioxide may be activated by light in the visible region. At this point, titanium dioxide with an unaltered band gap requires a minimum energy of 3.2 eV for activation.

An appropriate solvent and reaction vessel also needs to be selected to ensure that a maximum amount of light passed through the vessel and solvent and reached titanium dioxide, consequently generating the highest amount hydroxyl radicals and positive holes.



## 2.4 OPTIMIZING REACTION CONDITIONS USING THE SYNTHESIS OF 2-PHENYLQUINOXALINE AS A MODEL REACTION

### 2.4.1 Selection of solvent and reaction vessel

As previously noted, in choosing the reaction conditions, it needs to be ensured that a maximum amount of UV light reached titanium dioxide to catalyze the oxidation process. Certain solvents and Pyrex glass vessels absorb UV light, which would adversely affect the results, as the quantity of UV light reaching titanium dioxide would be diminished. Likewise the solvent can affect the results due to the same UV absorbing ability. A brief ultraviolet/visible spectroscopic study was conducted on various commonly employed oxidation solvents to determine the most effective. Dichloromethane, ethyl acetate, acetonitrile, toluene and methanol were examined in both Pyrex and quartz glass tubes and their absorbance in the ultraviolet/visible range monitored. All solvents showed little absorbance in the visible region in Pyrex glass and quartz tubes. Dichloromethane, ethyl acetate and acetonitrile showed absorbance in the UV region ( $< 400$  nm) in both quartz and Pyrex glass tubes and were thus unsuitable for the oxidation reaction (See Appendix A). Toluene however, showed a greater absorbance in pyrex than quartz tubes (**Figures 7 and 8**).<sup>§§</sup>

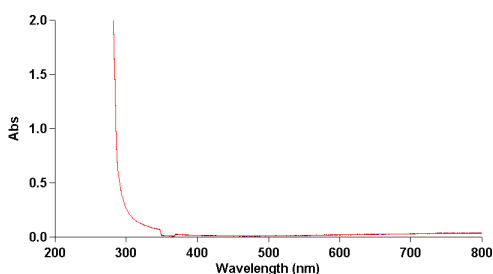


**Figure 7: Toluene in Pyrex glass**

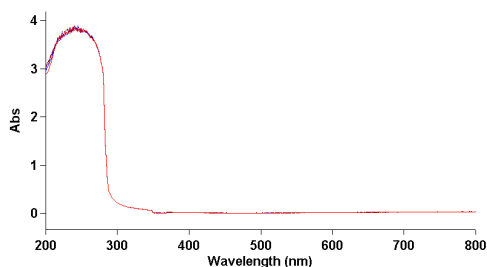


**Figure 8: Toluene in quartz**

<sup>§§</sup> Even though the y-axis, is not the same it is expected that the absorbance in the case of Pyrex glass will continue to increase beyond that of quartz.

Since the same sample of toluene was used, the ‘excess’ absorption is due to the glass cell absorbing. This point is more clearly indicated by comparing the spectra of methanol in Pyrex glass and quartz (**Figures 9 and 10**), where the absorbance is negligible in quartz but significantly higher in glass within the same region. Methanol was thus chosen as an optically clear solvent as it had a lowest absorbance over the widest spectral range.\*\*\* This study also led to the conclusion that the tandem oxidation reaction would be more effective if carried out in a quartz tube.

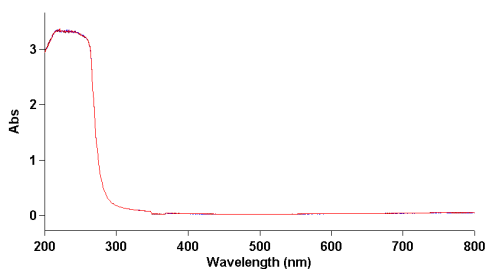


**Figure 9: Methanol in Pyrex glass**

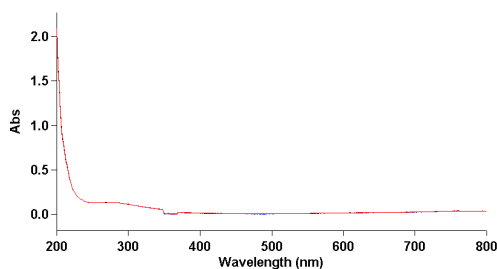


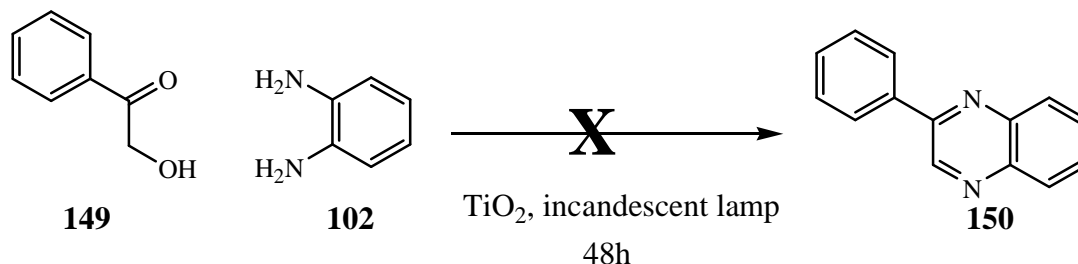
**Figure 10: Methanol in quartz**

---

\*\*\* Oxidation of methanol was not observed. For a possible explanation see page 89.

### 2.4.2 Oxygen as an electron acceptor

Having selected the appropriate solvent and reaction vessel titanium dioxide was evaluated under a range of different energy sources. Since a powerful UV light was not available in our lab, the test reaction repeated using an incandescent lamp and surprisingly, no product formation was evident even after 48 hours (**Scheme 54**).



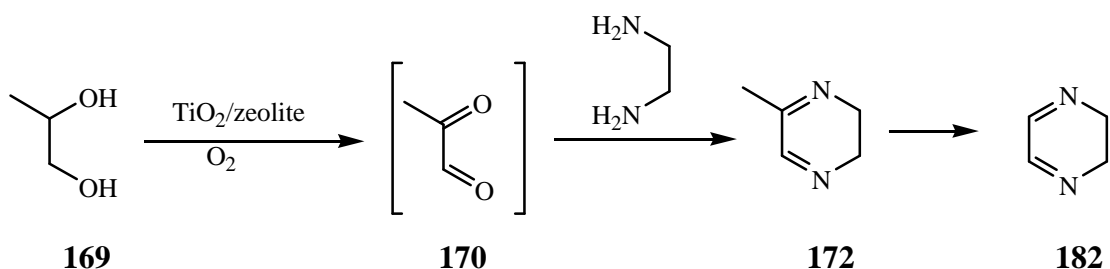
**Scheme 54: Attempted quinoxaline synthesis under an incandescent lamp using titanium dioxide as an oxidant**

The failure of this reaction is most surprising considering the success obtained for this reaction under natural sunlight. Perusal of literature revealed two publications which provided insight into these results.

Hidaka and co-workers had conducted a solar photocatalysis study in which titanium dioxide was used to degrade a commercial detergent under sunlight using a solar concentrator.<sup>100</sup> In this publication, it was claimed that oxygen was essential for this reaction, as it minimizes recombination between the photogenerated species ( $e^- + h^+$ ). The authors state that the reaction was conducted in a vessel open to the atmosphere as a means of introducing oxygen into the system. Under these conditions the reaction proceeded 'fairly rapidly'.

Subhramanyam *et al.*, using titanium dioxide for the synthesis of dihydropyrazine<sup>95</sup> (see p44) (**Scheme 55**), had also claimed that under UV light, oxygen is required as it prevents electron/hole recombination and that the rate of their photocatalytic oxidation

was high due to bubbling oxygen through the system. It is evident that the chemistry of titanium dioxide was relatively complex as under solar irradiation, oxygen bubbling is not required and conducting the reaction under atmospheric conditions was adequate for the degradation reaction to take place. This is even more remarkable since UV light constitutes only 4-5% of the solar spectrum.<sup>108</sup> In the case of the dihydropyrazine synthesis, under a high pressure mercury lamp, oxygen was needed to be bubbled through the system and after 15 hours only a 20% yield was obtained.



**Scheme 55: Titanium dioxide mediated synthesis of dihydropyrazine**

Based on the above the two reports it was proposed that the failure of the reaction, under the incandescent lamp, was due to absence of an electron acceptor consequently resulting in electron/hole recombination.

### 2.4.3 The use of TEMPO in the oxidation reaction

The use of titanium dioxide in combination with oxygen has been reported in literature, with oxygen often being used as an electron acceptor. However, titanium dioxide catalyzed reactions in the presence of oxygen are relatively slow and low yielding.<sup>†††</sup> Thus, literature was consulted for an alternative to bubbling oxygen through the reaction mixture. Rudham *et al.* described the use of platinum deposited titanium dioxide used for

<sup>†††</sup> Synthesis of a dihydropyrazine using titanium dioxide catalyzed oxidation required oxygen bubbling at a rate 20 ml/h for 15 hours with a yield of 20%(!)

the synthesis of aldehydes and ketones.<sup>109</sup> He suggested that the promoted electrons from the valence band are trapped at the platinum centers while the holes could react with surface bound hydroxyl groups to produce the hydroxyl radicals. In our opinion, it was pointless touting titanium dioxide as a cheap catalyst if it had to be used in combination with platinum. Nonetheless, the use of platinum deposited titanium dioxide may become an alternative to the use of oxygen.

It was in this search for an alternative to oxygen that our attention became focused on 2,2,6,6-tetramethyl piperidiny-1-oxyl radical (TEMPO) (**Figure 11**) as a possible co-catalyst or electron acceptor.

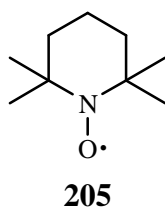
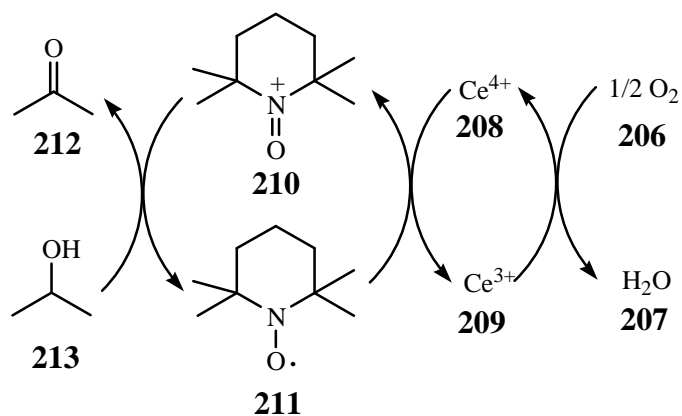


**Figure 11: Structure of TEMPO**

Chung and co-workers had reported excellent yields for the synthesis of alcohols to aldehydes and ketones using a CAN/TEMPO/O<sub>2</sub> system.<sup>110</sup> The reported yields for the synthesis of aldehydes and ketones ranged from 75-99% under varying temperature and time profiles. The CAN/TEMPO/O<sub>2</sub> systems were developed based on the following hypothesis:

- CAN is a weak oxidant and must be used in combination with a co-catalyst (TEMPO). Chung and co workers report attempting an oxidation of a secondary alcohol with CAN only, producing the ketone in a yield of 5%.
- TEMPO, in its radical form, is not the real oxidizing agent and must be converted to the *N*-ammonium salt - the active oxidizing species. Thus TEMPO must be used in combination with a stoichiometric or catalytic oxidant.
- Dioxygen is required to regenerate Ce<sup>4+</sup>

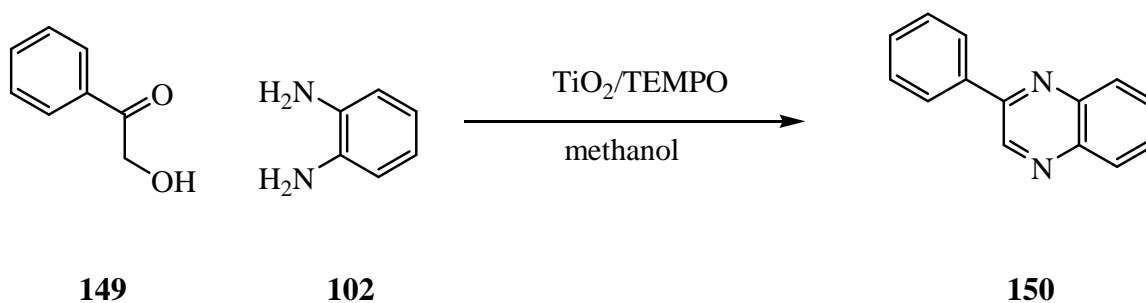
These points are better illustrated by the following mechanism proposed by the authors (**Scheme 56**):



**Scheme 56: Mechanism of alcohol oxidation using a CAN/TEMPO/O<sub>2</sub> system**

Dioxygen is reduced to water by the oxidation of Ce<sup>3+</sup> to Ce<sup>4+</sup>. TEMPO is oxidized from the radical form to the active oxidizing agent, the *N*-oxoammonium cation which oxidizes the alcohol to the aldehyde or ketone.

Since TEMPO was readily available in our laboratory at the time, titanium dioxide was used in combination with TEMPO to evaluate its effect on the tandem coupling reaction. A test reaction was attempted using 2-hydroxyacetophenone, *o*-phenylenediamine, titanium dioxide and TEMPO in methanol (**Scheme 57**).



**Scheme 57: Titanium dioxide/TEMPO mediated synthesis of quinoxaline**

The reaction mixture was purified using radial chromatography which afforded the title quinoxaline in an isolated yield of 25%. Encouraged by this result, the reaction was repeated and the reaction mixture was left stirring overnight and subsequently analyzed the following day. Thus, the mixture was filtered through a silica plug and the solvent removed *in vacuo* to produce a crude product which was analyzed by <sup>1</sup>H NMR spectroscopy. <sup>1</sup>H NMR spectra revealed the presence of only the desired product. The crude NMR spectrum obtained using the incandescent lamp was also of higher purity compared to the NMR spectrum obtained under natural sunlight. Consequently, the reaction was repeated under natural sunlight using TEMPO as co-catalyst. The mixture was purified using radial chromatography to afford the desired compound in an isolated yield of 90%.<sup>†††</sup> The use of titanium dioxide in conjunction with TEMPO had afforded excellent results under both natural sunlight and the incandescent lamp. Clearly, the use of TEMPO results in shorter reaction times and an increase in product purity. This point was clearly illustrated by comparing the crude spectra of (i) titanium dioxide mediated oxidation in the **presence** of TEMPO under the incandescent lamp and (ii) titanium dioxide mediated oxidation in the **absence** of TEMPO under natural sunlight (**Figures 12 and 13**).

---

<sup>†††</sup> For completeness, a reaction was conducted in the presence of TEMPO only, which resulted in no product formation.

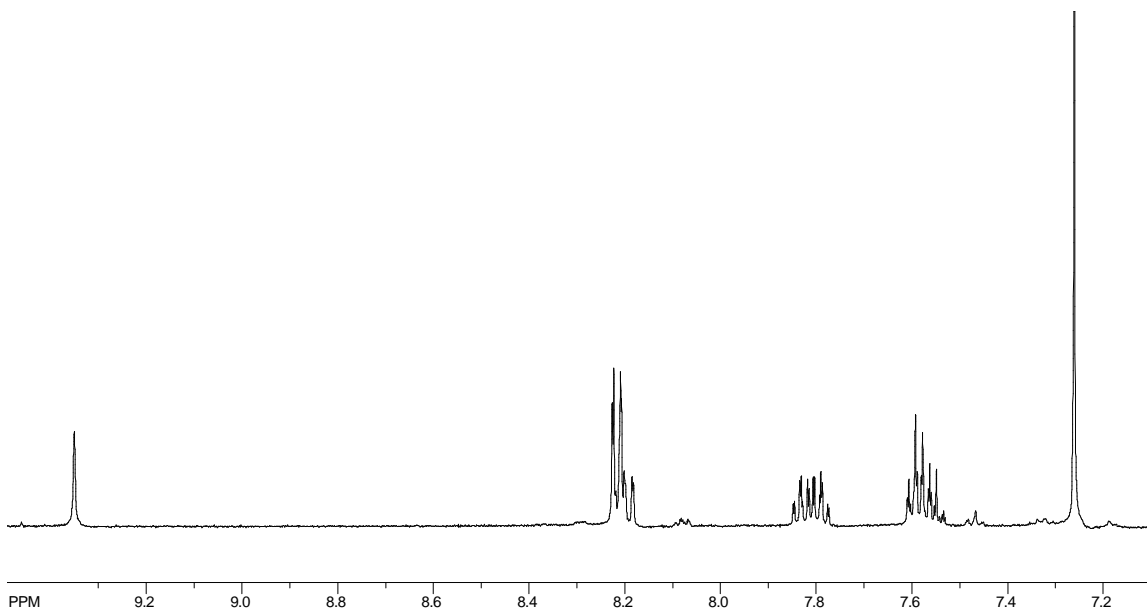


**Figure 12: Crude spectrum obtained under an incandescent lamp using TEMPO.**

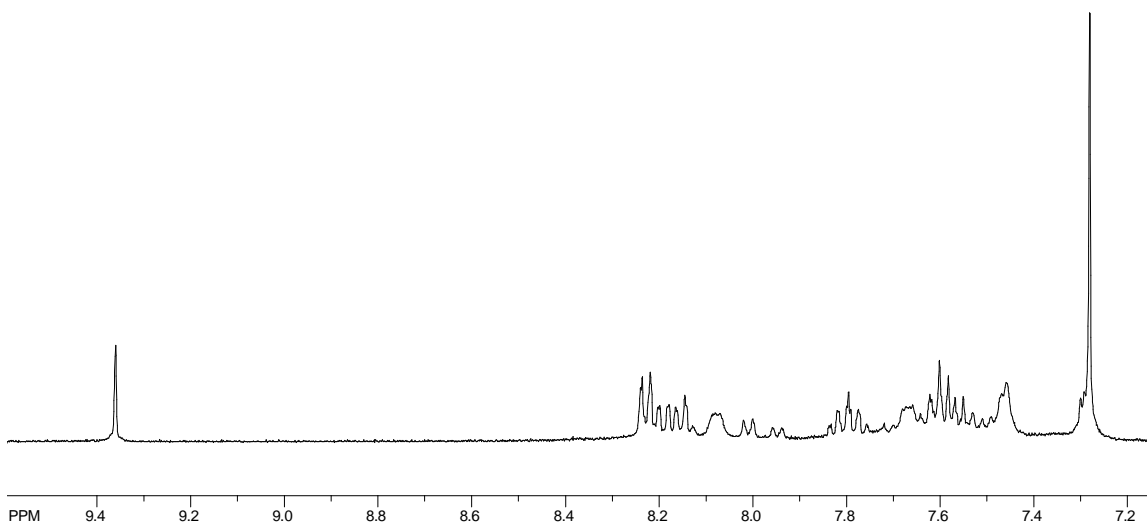


**Figure 13: Crude spectrum obtained under natural sunlight in the absence of TEMPO.**



#### 2.4.4 Use of Microwave irradiation

At this juncture, our attention was drawn to an interesting publication by Serpone and co-workers<sup>111</sup> who reported the formation of hydroxyl radicals when titanium dioxide was irradiated under microwave irradiation. This result was surprising since microwave energy is less intense than UV light. They monitored the formation of hydroxyl radicals under microwave and UV light by electron spin resonance (ESR). The highest quantity of hydroxyl radicals was observed under UV light and the lowest under microwave irradiation only. A significant increase in hydroxyl radical formation however, was observed when titanium dioxide was used in conjunction microwave irradiation. It has been suggested<sup>112</sup> that microwave energy can couple with a titanium dioxide particle generating a non-thermal distribution which leads to the diffusion of electrons and positive holes to the surface, where positive holes react with water and the electrons react with oxygen to produce the hydroxyl radical and superoxide species.

The set up, using microwave irradiation in combination with UV light, required the use of expensive equipment which was beyond the means of this project. Nevertheless, since a microwave reactor was present in our laboratory, the model reaction was attempted using microwave irradiation. A flexible fibre optic lamp was acquired which was used to direct additional light into the microwave cavity. 2-Hydroxyacetophenone, *o*-phenylene diamine, titanium dioxide and TEMPO were placed in a cylindrical tube fitted with a reflux condenser and subjected to microwave irradiation. The reaction was left refluxing under microwave irradiation for 90 minutes and the crude product submitted for <sup>1</sup>H NMR analysis. To our delight, the quinoxaline product was present in excellent yield and purity. The microwave assisted reaction had provided the quinoxaline product in a significantly shorter time than by using the incandescent lamp. Based on these results, attention was focused on optimizing reaction conditions under microwave irradiation.

At this point it was realized the tandem reaction needed to be conducted in the microwave but the reaction conditions were still to be optimized. The focal point of this study was thus, to determine the effect of the fibre optic lamp, and most importantly

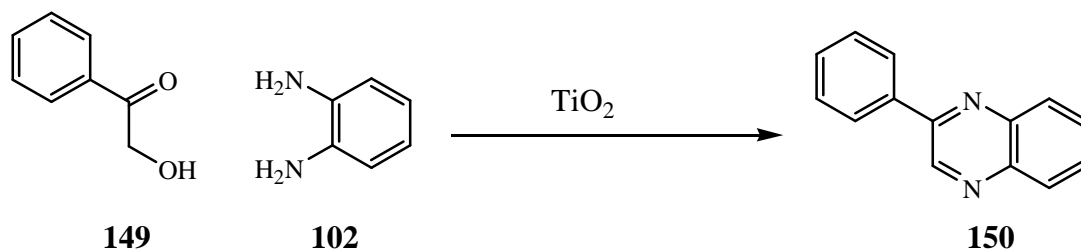
decrease reaction times. The effect of the fibre optic lamp was determined by repeating the reaction under identical microwave conditions but in the absence of the fibre optic lamp.  $^1\text{H}$  NMR spectroscopy revealed an identical spectrum to the one obtained in the presence of the fibre optic lamp. From these observations, it was determined that microwave energy was the predominant factor and the use of the fibre optic lamp was unnecessary and subsequently discontinued.

Whilst looking at optimizing the reaction conditions a significant finding to the success of this project was discovered. Chung and co-workers had reported the use of manganese dioxide for the synthesis of quinoxalines under microwave irradiation.<sup>113</sup> They reported that 1mg of manganese dioxide can be used to synthesize quinoxalines in moderate to good yields. More importantly, they state that reaction times were significantly decreased when the reaction was conducted in the absence of solvent and under a pressurized environment although they do not comment on the increased yield under a pressurized environment. Using this information, the general quinoxaline reaction was attempted in a solventless system under moderate pressure for five minutes. Crude NMR spectroscopy revealed the presence of product with the starting material still present. The reaction time was increased to 10 minutes and the crude  $^1\text{H}$  NMR spectroscopy revealed the presence of product only with minor impurities. Thus, this reaction was repeated for 10 minutes under microwave irradiation. The contents were diluted with dichloromethane and passed through a short silica plug, after which the solvent was removed *in vacuo* to produce a crude product which was subsequently purified using radial chromatography to give the desired compound 2-phenyl quinoxaline in an isolated yield of 87%.

## **2.5 SUMMARY OF RESULTS OF OPTIMIZATION STUDY**

Titanium dioxide mediated quinoxaline synthesis was evaluated under a number of energy sources such as natural sunlight, incandescent lamp and microwave energy. The best results were obtained under microwave energy using a solventless system. A summary of the results from this study is given in Table 7.

**Table 7: Summary of results for titanium dioxide test reaction**



| Energy source                                 | Time (h)  | Electron acceptor/Additive | Yield (%) <sup>a</sup> |
|---|-----------|----------------------------|------------------------|
| Sunlight                                      | 3         | -                          | 27                     |
| Sunlight                                      | 3         | TEMPO                      | 90                     |
| Incandescent lamp                             | 48        | -                          | -                      |
| Incandescent lamp                             | overnight | TEMPO                      | ≥ 99 <sup>b</sup>      |
| Incandescent lamp                             | 3         | TEMPO                      | 25                     |
| Microwave<br>(Open vessel)                    | 90 min    | TEMPO                      | ≥ 99 <sup>b</sup>      |
| Microwave<br>(Closed vessel,<br>solvent-free) | 10 min    | TEMPO                      | 87                     |

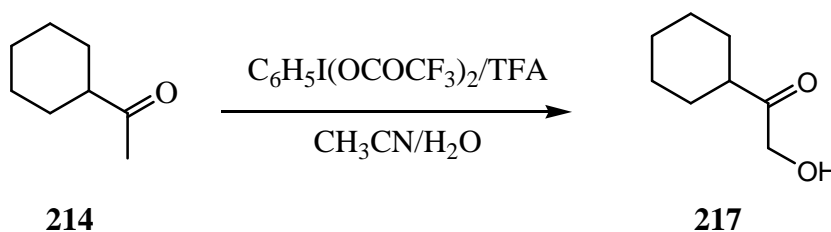
<sup>a</sup> Isolated yield. <sup>b</sup> Determined by <sup>1</sup>H NMR spectroscopy.

With this optimized procedure in hand, the scope and limitations of titanium dioxide were further evaluated using a range of alcohols and diamines.

## 2.6 SYNTHESIS OF QUINOXALINE DERIVATIVES USING A TITANIUM DIOXIDE MEDIATED TANDEM OXIDATION PROCESS

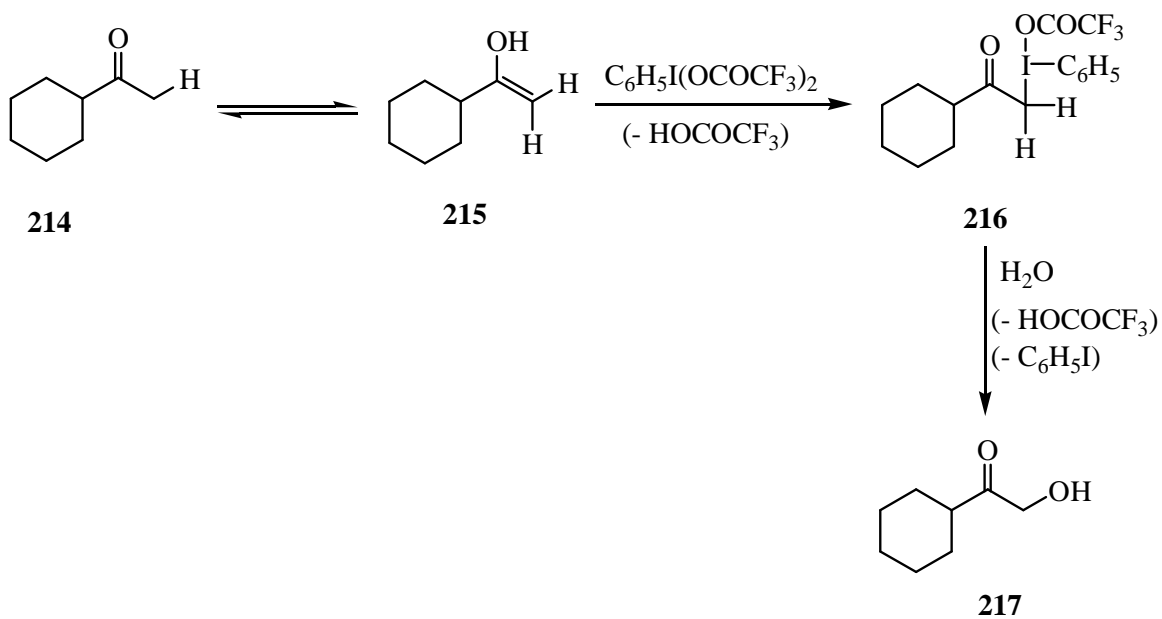
### 2.6.1 Synthesis of 1-cyclohexyl-2-hydroxyethanone

The second substrate on which a titanium dioxide catalyzed oxidation was examined was the effect of an alkyl substituent, often claimed to be problematic due to the hyper-reactivity of the intermediate keto-aldehyde.<sup>28</sup> 1-cyclohexyl-2-hydroxyethanone **217** was required for this procedure and was synthesized using the method reported by Moriarty *et al.*<sup>114</sup> This procedure involved the conversion of the methyl ketone to its corresponding  $\alpha$ -hydroxy ketone under acidic conditions using [bis(trifluoroacetoxy)]iodobenzene and trifluoroacetic acid in an acetonitrile/water mixture (**Scheme 58**) to produce **217** as a colorless oil in a yield of 90%.



**Scheme 58: Conversion of methyl ketone to the corresponding  $\alpha$ -hydroxyketone**

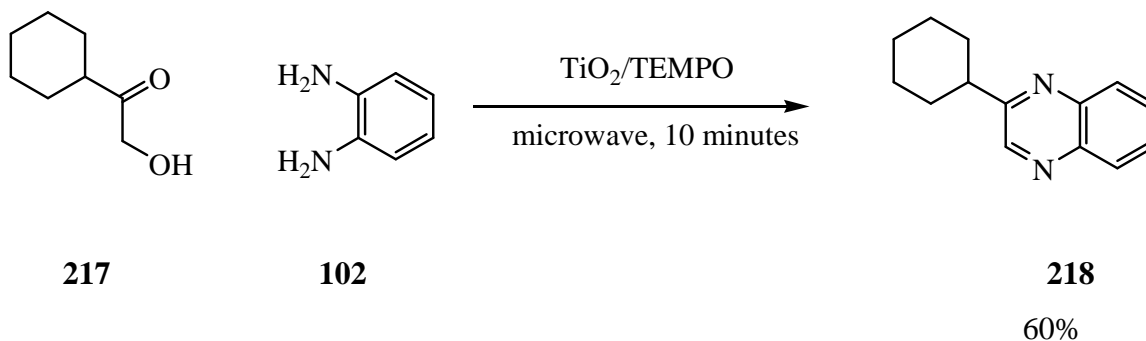
The following pathway (**Scheme 59**) was proposed by Moriarty and co-workers involving ligand exchange with the enolic form of ketone **214** to produce intermediate **216**. Replacement of the iodine moiety by water produces the  $\alpha$ -hydroxyketone **217**. Since water is a stronger nucleophile than trifluoroacetic acid,<sup>115</sup> the hydroxylated product would be expected and not the  $\alpha$ -trifluoroacetoxy ketone.



**Scheme 59: Proposed pathway for  $\alpha$ -hydroxyketone formation from the corresponding methyl ketone**

## 2.6.2 Synthesis of 2-Cyclohexylquinoxaline

With  $\alpha$ -hydroxy ketone **217** in hand, the corresponding quinoxaline could be synthesized. 1-cyclohexyl-2-hydroxyethanone was coupled with *o*-phenylene diamine in the presence of titanium dioxide and TEMPO under the optimized conditions described earlier (**Scheme 60**)



**Scheme 60: Titanium dioxide coupling of 1-cyclohexyl-2-hydroxyethanone and *o*-phenylenediamine under microwave irradiation**

Titanium dioxide was removed and the mixture purified by radial chromatography to afford the title compound **218** in an isolated yield of 60%. The <sup>1</sup>H NMR spectrum (**Figure 14**) revealed the presence of the product with the expected peaks obtained at the anticipated chemical shifts. The integral ratios of product however, did not correspond with what was expected as the multiplet in the aliphatic region is expected to integrate for ten protons but was found to integrate for eighteen protons. The discrepancy in integral ratio was attributed to the residual petroleum ether which was used in the purification of **218**.<sup>§§§</sup> GC-MS analysis (**Figure 15**) revealed the product to be relatively pure with one major peak with a retention time of 23.4 min corresponding to the target compound mass of 212 g.mol<sup>-1</sup>. The yield of 60% is comparable to the palladium acetate/triethylamine procedure which also produced **218** a yield of 60% but in 3 hours.

<sup>§§§</sup> Although a yield of 60% has been quoted, this might be slightly lower owing to the presence of residual petroleum ether.

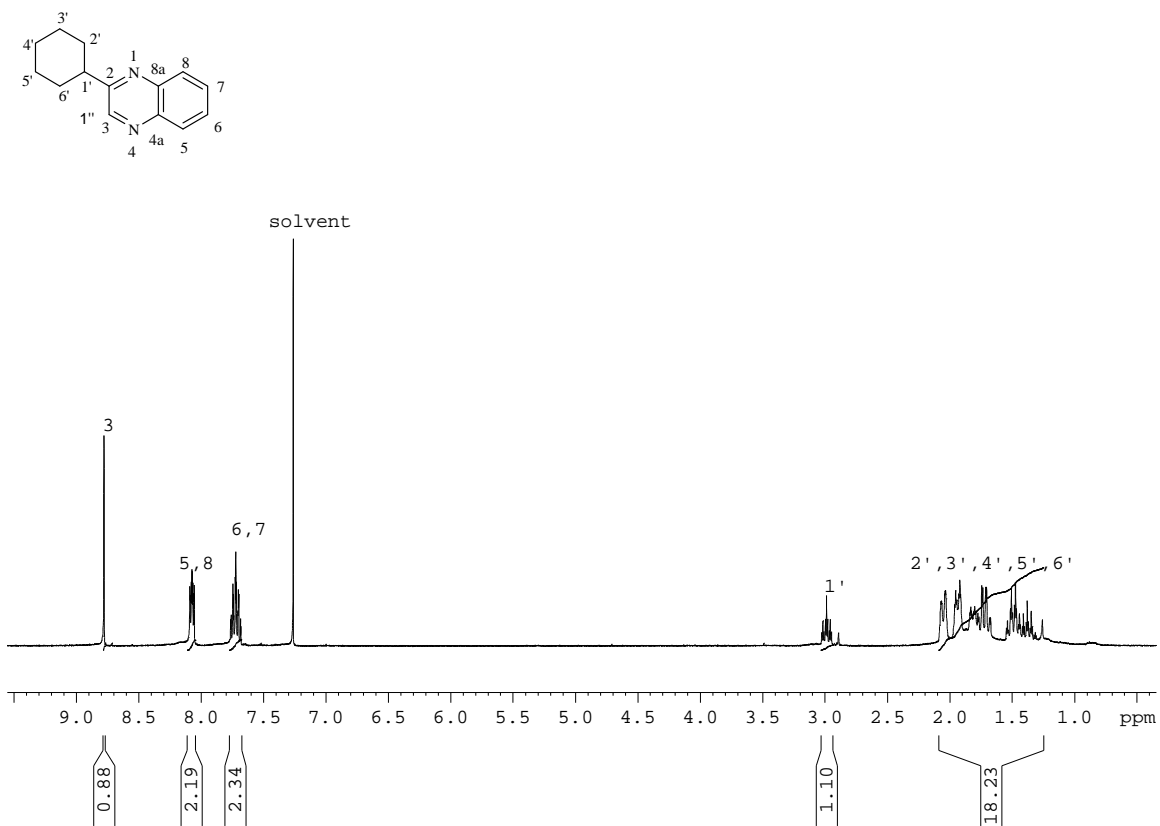
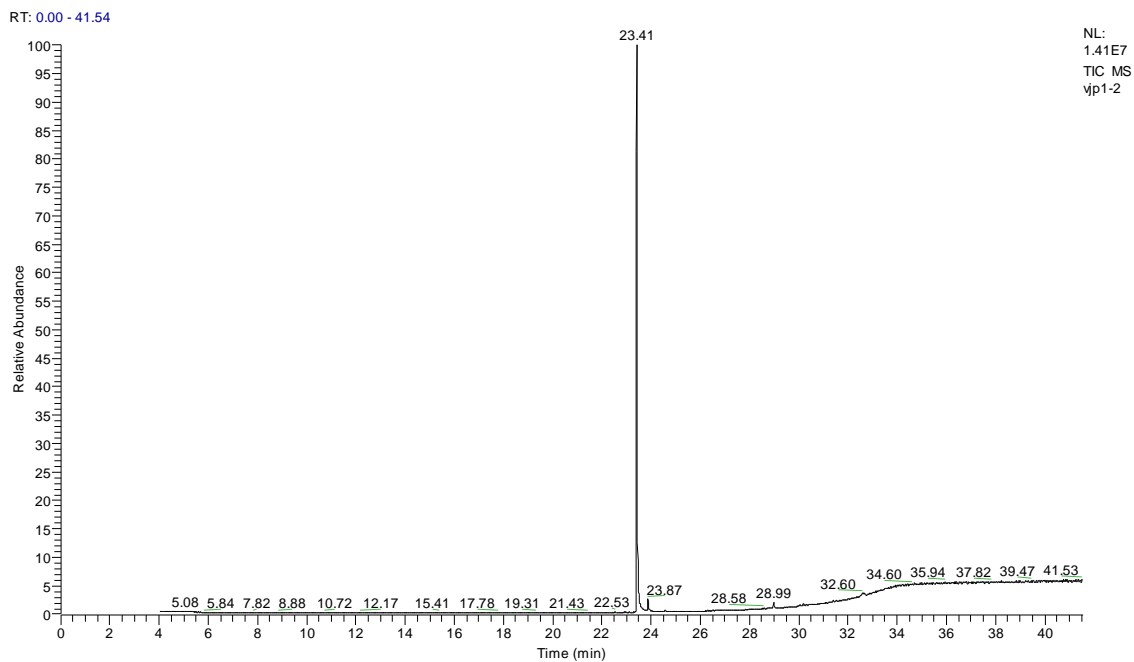


Figure 14:  $^1\text{H}$  NMR Spectrum for 2-Cyclohexylquinoxaline



vp1-2 #2445 RT: 23.41 AV: 1 NL: 2.42E6  
T: + c Full ms [20.00-400.00]

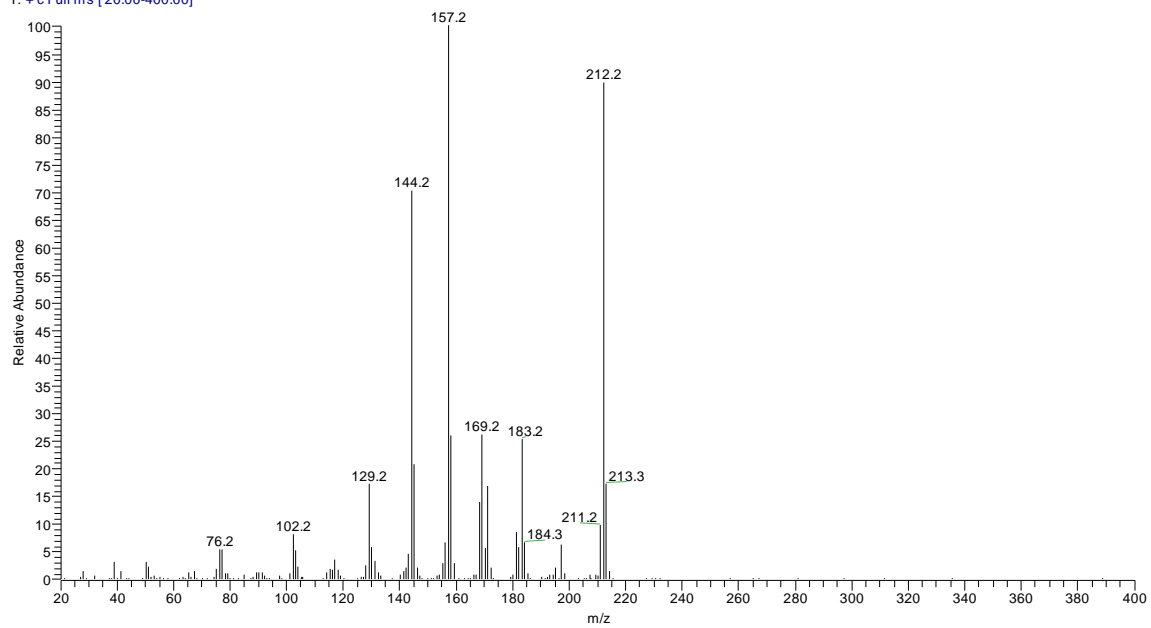
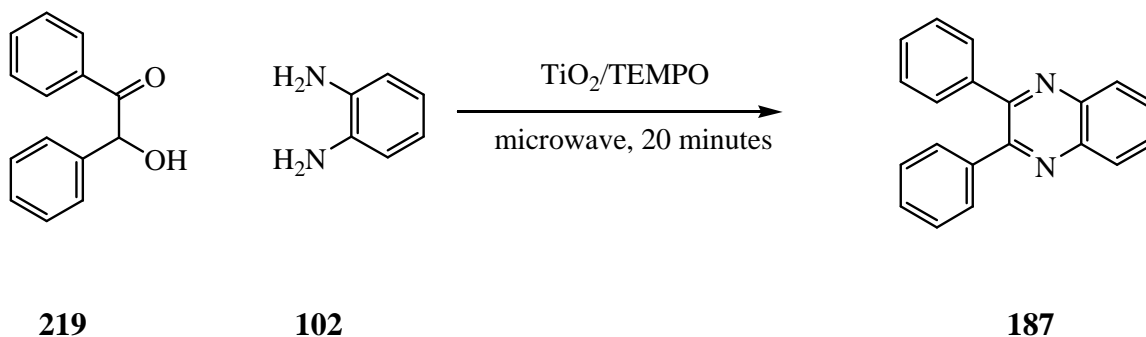


Figure 15



### 2.6.3 Synthesis of 2,3-diphenylquinoxaline

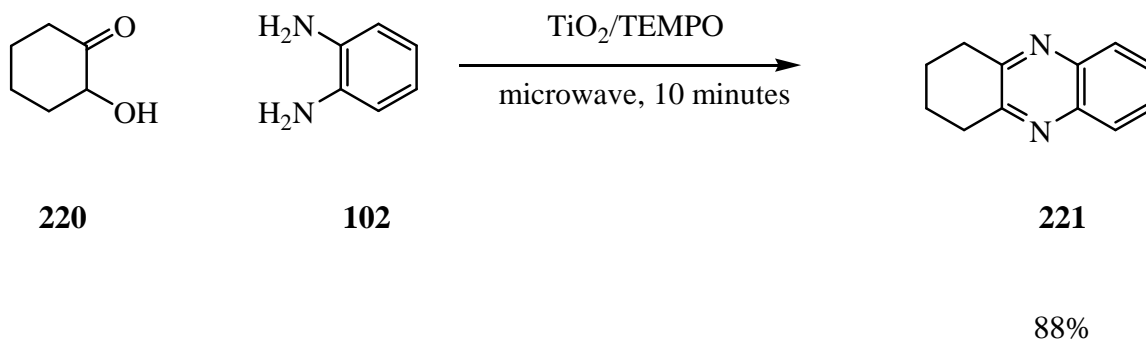
A bulky secondary alcohol was subjected to a titanium dioxide catalyzed oxidation. Benzoin **219**, *o*-phenylenediamine **102**, titanium dioxide and TEMPO were stirred under microwave irradiation for 10 minutes (**Scheme 61**). After this time period, the mixture was diluted with dichloromethane and passed through a short silica plug. The solvent was removed *in vacuo* to produce the crude product which was purified by radial chromatography to produce the title compound in an isolated yield of 35%. Since this yield was deemed to be too low, the reaction was repeated but with 20 minutes of microwave irradiation which produced **187** in an isolated yield of 81%. This result is satisfactory and compared favourably with other synthetic routes<sup>67,97</sup> towards compound **187**. Manganese dioxide catalyzed synthesis of compound **187** resulted in an isolated yield of 75% after 45 minutes while Pd(OAc)/Et<sub>3</sub>N catalyzed synthesis produced compound **187** in a yield of 40% in 3 hours. On increasing the reaction time to 24 hours the compound was obtained in an isolated yield of 74%. Thus, titanium dioxide compared favorably with other oxidants with higher yields in shorter reaction times.



**Scheme 61: Titanium dioxide coupling of benzoin and *o*-phenylenediamine under microwave irradiation**

## 2.6.4 Synthesis of 6,7,8,9-Tetrahydrophenazine

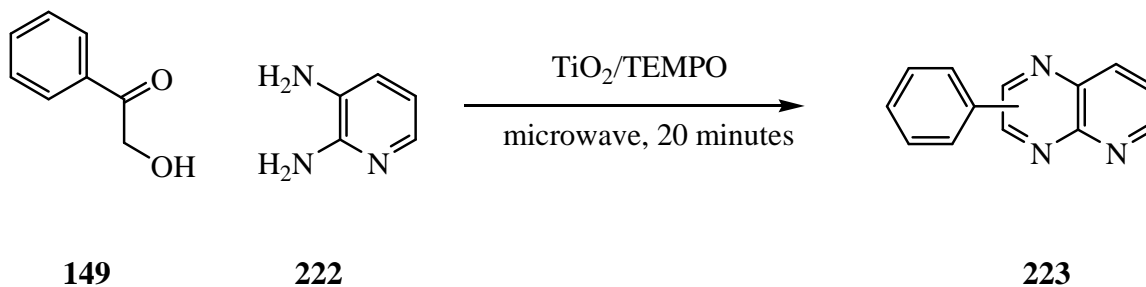
The effect of a non-hindered secondary alcohol was examined using 2-hydroxycyclohexanone dimer **220**, *o*-phenylenediamine **102**, titanium dioxide and TEMPO under microwave irradiation for 10 minutes (**Scheme 62**). The desired compound 6,7,8,9-tetrahydrophenazine **221** was isolated in a yield of 88%. The coupling of the secondary alcohol is comparable with that of primary alcohol **149** which afforded the quinoxaline derivative in a yield of 87% under the same reaction conditions. This result is superior to the  $\text{RuCl}_2(\text{PPh}_3)_3$  catalyzed oxidation which produced compound **221** in an isolated yield of 82% after 24 hours.



**Scheme 62: Titanium dioxide coupling of 2-cyclohexanone and *o*-phenylenediamine under microwave irradiation**

### 2.6.5 Synthesis of 2-/3-Phenylpyrido[2,3-*b*]pyrazines

The diamine component was then varied by using 2,3-diaminopyridine **222** instead of *o*-phenylenediamine. 2-hydroxyacetophenone, 2,3-diaminopyridine, titanium dioxide and TEMPO were stirred under microwave irradiation for 10 minutes (**Scheme 63**) to produce the desired compound 2-/3-phenylpyrido[2,3-*b*]pyrazine **223** as a mixture of regioisomers in an isolated yield of 34% in 10 minutes. The reaction was repeated using 20 minutes of microwave irradiation to produce the desired compound **223** in a yield of 83%.



**Scheme 63: Titanium dioxide coupling of 2-hydroxyacetophenone and 2,3-diaminopyridine under microwave irradiation**

On comparison with literature it was determined by <sup>1</sup>H NMR spectroscopy that 3-phenylpyrido[2,3-*b*]pyrazine was the predominant regioisomer formed and a <sup>1</sup>H NMR spectrum depicting these assignments is shown in **Figure 16**. The GC trace showed a major peak at 26.7 min and a minor peak at 27.0 min. Both peaks had a molecular mass of 207 Da indicative of the desired compound **223** (**Figure 17**).

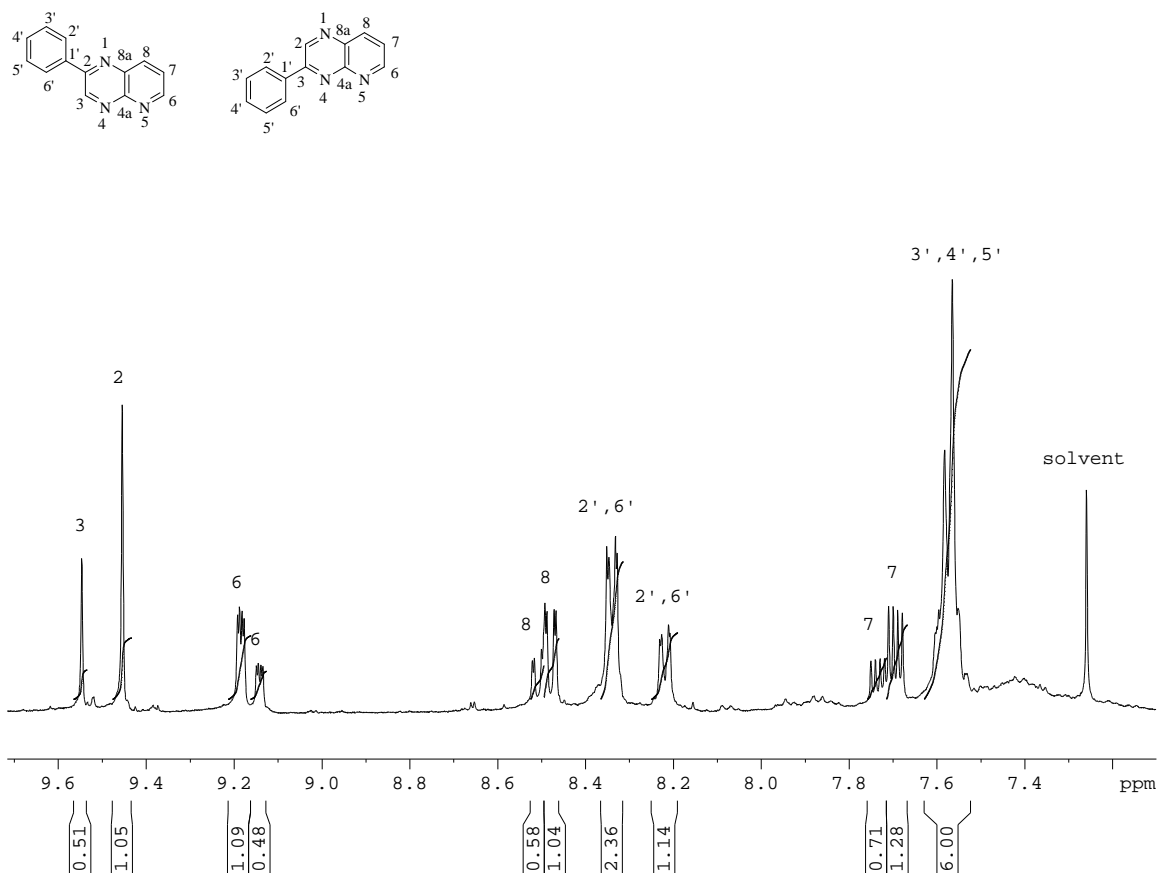
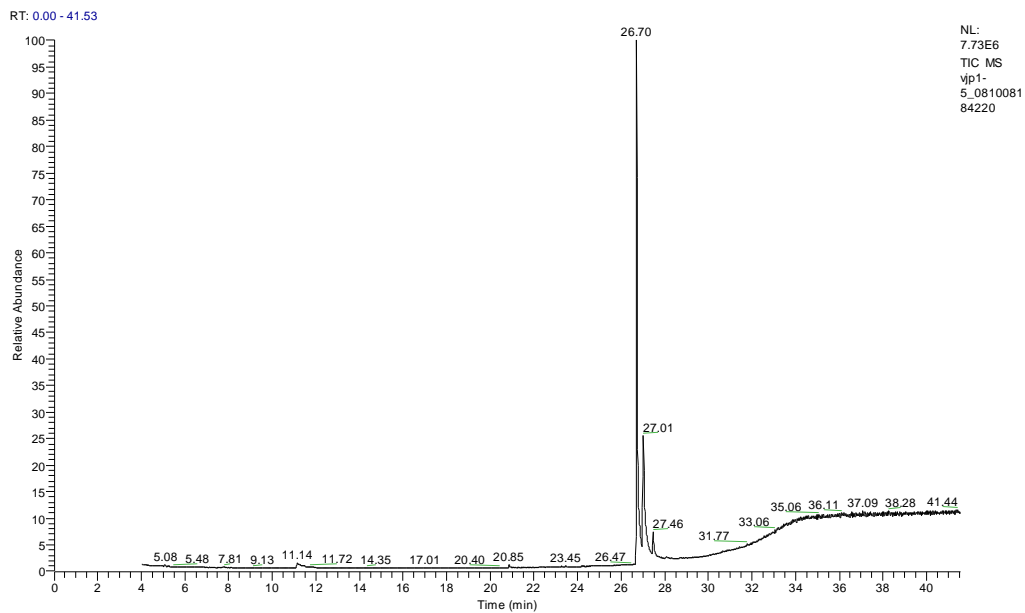


**Figure 16:**  $^1\text{H}$  NMR Spectrum for 2-/3-Phenylpyrido[2,3-*b*]pyrazine



vp1-5\_081008184220 #2893 RT: 26.70 AV: 1 NL: 2.18E6  
T: + c Full ms [20.00-400.00]

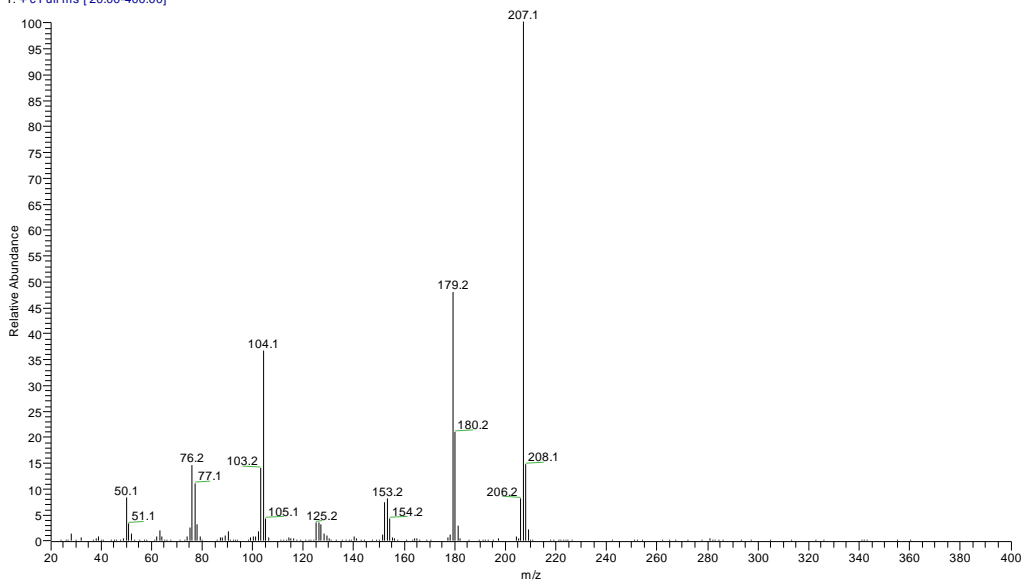
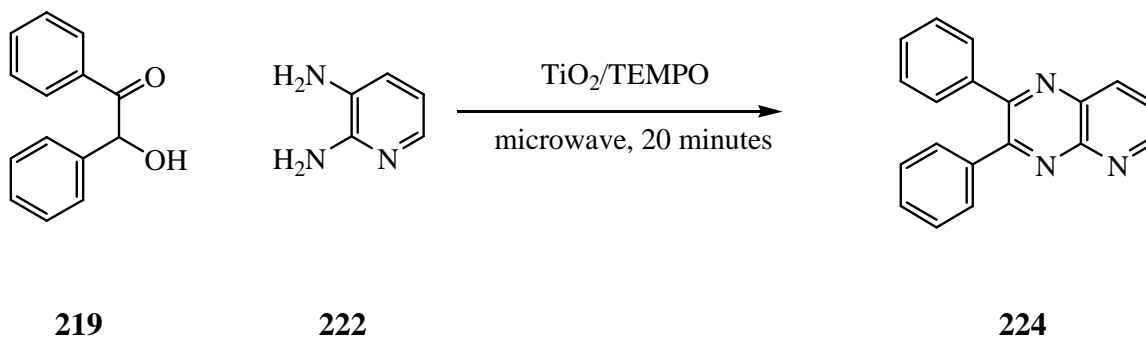


Figure 17

### 2.6.6 Synthesis of 2,3-Diphenyl[2,3-*b*]pyrazine

Benzoin **219** and 2,3-diaminopyridine **222** were stirred under microwave irradiation for 10 minutes to produce the product **224** in an isolated yield of 28%. The reaction was repeated for 20 minutes to produce the desired product **224** in an isolated yield of 54% \*\*\*\* (Scheme 64).



**Scheme 64: Titanium dioxide coupling benzoin and 2,3-diaminopyridine under microwave irradiation**

The <sup>1</sup>H NMR spectrum was assigned (**Figure 18**) and compared with Darabi and co-workers.<sup>116</sup> All the expected peaks were obtained but differed in the reported integral ratios. According to literature, the multiplet at 7.35 ppm should integrate for five protons while the doublet of doublet at 7.74 ppm should integrate for two protons. In our case, the multiplet integrated for six protons while the doublet of doublet integrated for one proton.

\*\*\*\* It is expected that an increasing the reaction time would result in an increase in yield beyond the 54% obtained after 20 minutes.

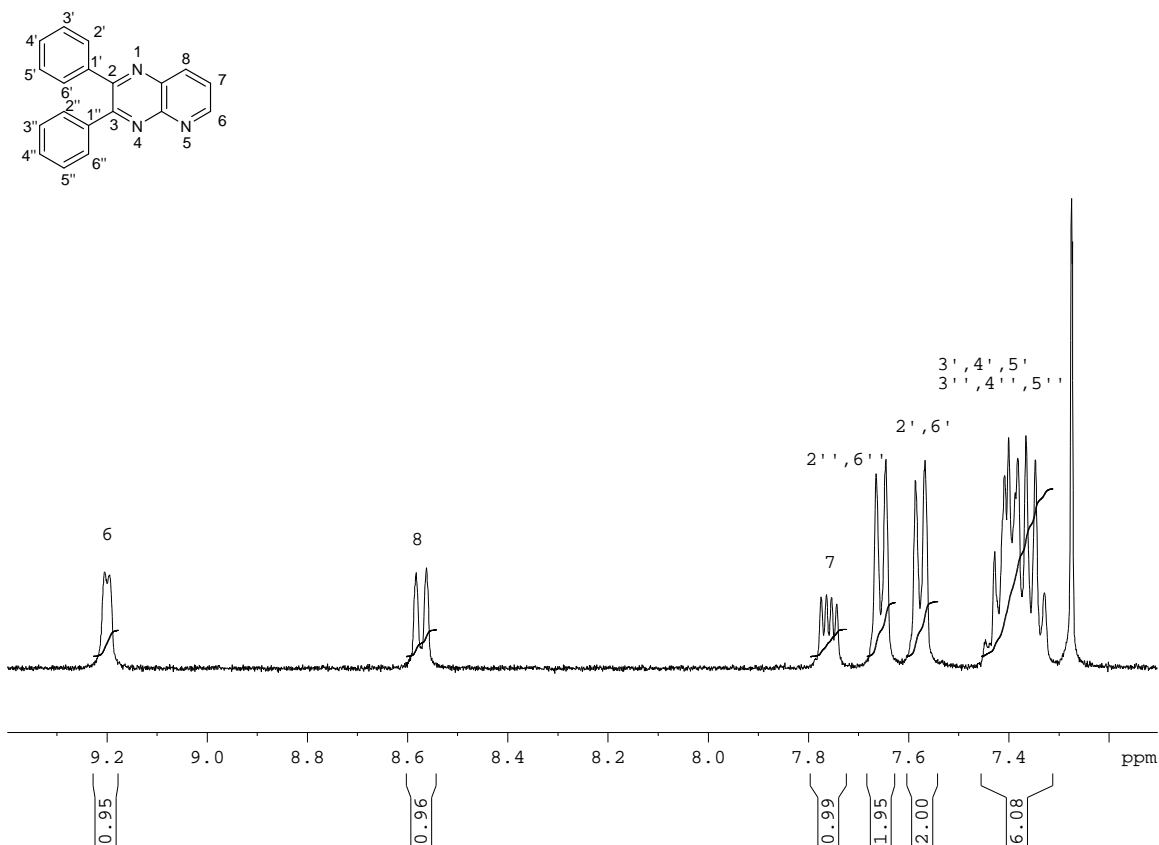


**Figure 18: <sup>1</sup>H NMR Spectrum of 2,3-Diphenyl[2,3-*b*]pyrazine**

Since there was debate as to the identity of the compound, it was submitted for high resolution mass spectrometry (HRMS) (**Figure 19**). HRMS revealed that the likely compound had a mass of 306.1006 [M+Na]<sup>+</sup> which corresponded to expected mass for 2,3-diphenyl[2,3-*b*]pyrazine **224**. Even more exciting was the presence of peak at a mass of 589.2120[2M+Na]<sup>+</sup> which was exactly double the molecular mass of the desired compound. This peak may be due to a dimer<sup>†††</sup> which would explain the observed molecular mass.

<sup>†††</sup> The dimer may be forming in the mass spectrometer as a sodium adduct.

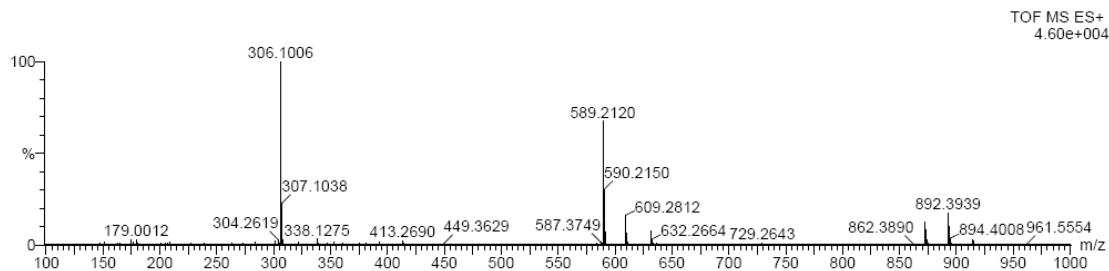
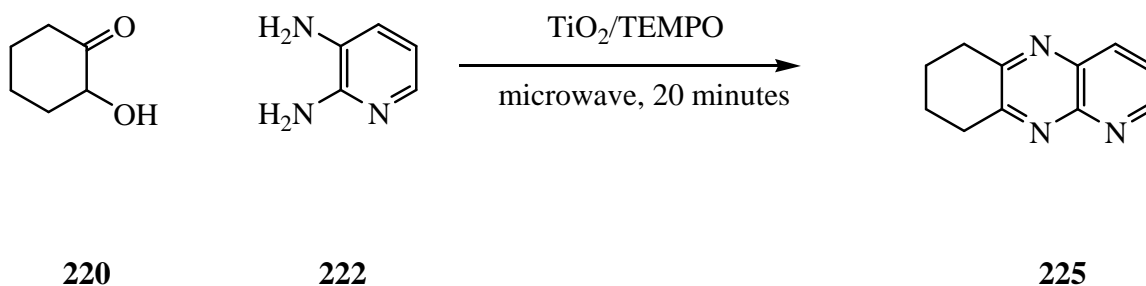


**Figure 19**

### 2.6.7 Synthesis of 6, 7, 8, 9-Tetrahydropyrido[2,3-*b*]quinoxaline

2-hydroxycyclohexanone dimer and 2,3-diaminopyridine were stirred under microwave irradiation (**Scheme 65**) for 10 minutes to provide the desired compound **225** in an isolated yield of 25%. The product was obtained in an isolated yield of 56% after 20 minutes. This result was somewhat surprising as the yield was comparable to that of the hindered alcohol (56% and 54%) which is in contrast to the reactions using *o*-phenylenediamine in which the yield for the unhindered alcohol was significantly higher in comparable times.



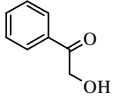
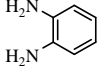
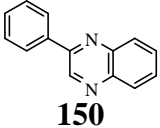
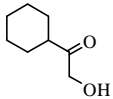
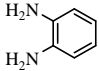
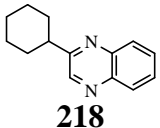
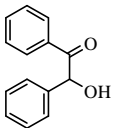
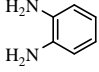
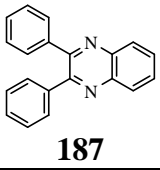
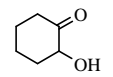
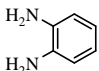
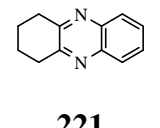
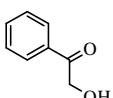
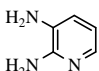
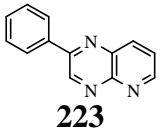
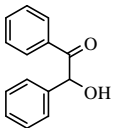
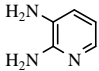
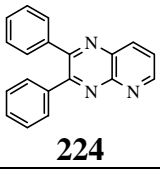
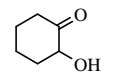
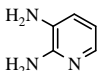
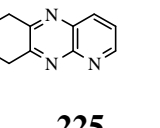
**Scheme 65: Titanium dioxide coupling of 2-hydroxycyclohexanone and 2,3-diaminopyridine under microwave irradiation**



## 2.7 SUMMARY OF RESULTS OBTAINED UNDER MICROWAVE IRRADIATION

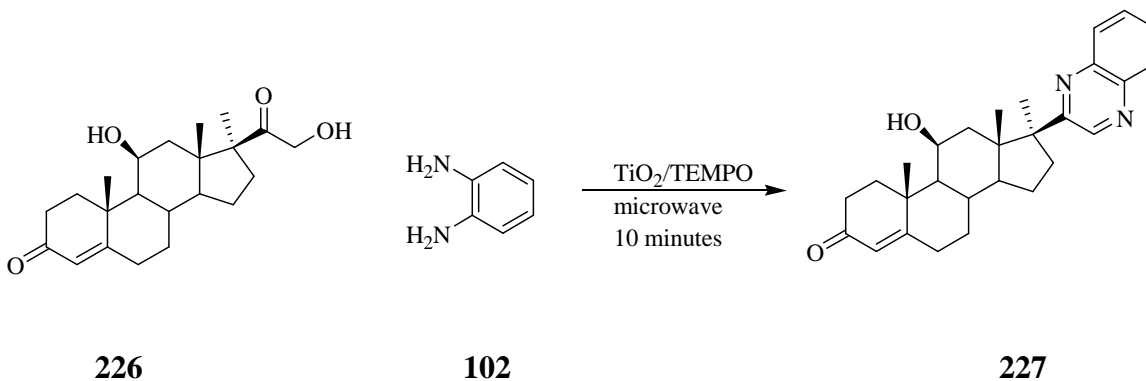
Titanium dioxide mediated tandem oxidation processes were explored under a number of energy sources such as sunlight, incandescent light and microwave energy. Microwave energy under solvent-free conditions under a moderately pressurized atmosphere provided the best results. Under these conditions, a range of quinoxaline derivatives were isolated in yields ranging from 54-88% in 10-20 minutes (**Table 8**). The yields obtained are in many cases superior to the other TOP type catalysts for the synthesis of quinoxalines. Compound **187**, as an example, was produced in a yield of 88% in 10 minutes which is far superior to the  $\text{Ru}(\text{Cl})_2(\text{PPh}_3)_3$  catalyzed procedure in which **187** was produced in a yield of 82% in 20 hours. The method has been shown to be successful on primary and secondary alcohols. Compound **187** was produced in a yield of 81% in 20 minutes, which is superior to the  $\text{Pd}(\text{OAc})_2/\text{NEt}_3$  mediated process which produced **187** in a yield of 40% in 3 hours. The procedure was also effective when varying the diamine component with the quinoxalines isolated in satisfactory yields of 54-83% in 20 minutes.

**Table 8: Summary of results obtained for the synthesis of quinoxalines under microwave irradiation.**

| entry | $\alpha$ -hydroxy ketone  | diamine   | time (min) | quinoxaline   | yield (%) |
|-------|---|---|------------|---|-----------|
| i.    |    |    | 10         | <br><b>150</b>   | 87        |
| ii.   |    |    | 10         | <br><b>218</b>   | 60        |
| iii.  |    |    | 20         | <br><b>187</b>   | 81        |
| iv.   |   |   | 10         | <br><b>221</b>  | 88        |
| v.    |  |  | 20         | <br><b>223</b> | 83        |
| vi.   |  |  | 20         | <br><b>224</b> | 54        |
| vii.  |  |  | 20         | <br><b>225</b> | 56        |

## 2.8 PRELIMINARY INVESTIGATION INTO A MULTIFUNCTIONAL SUBSTRATE

In order to further explore the scope of titanium dioxide, the general procedure was evaluated on a multifunctional substrate. Hydrocortisone **226**, *o*-phenylene diamine, titanium dioxide and TEMPO were stirred under microwave irradiation for 10 minutes (Scheme 66).

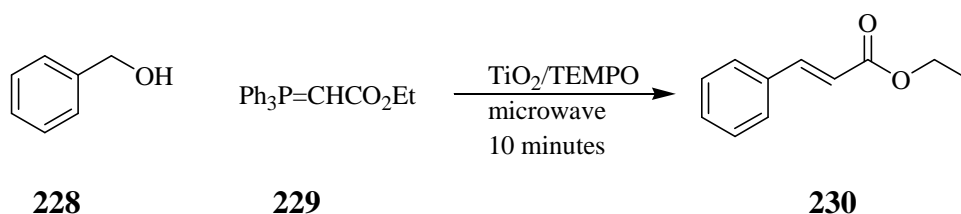


**Scheme 66: Titanium dioxide coupling of hydrocortisone and *o*-phenylenediamine under microwave irradiation**

Unfortunately, NMR spectroscopy revealed the absence of any product and the formation of other unidentifiable peaks. GC-MS revealed the presence of a multitude of peaks, none of which were attributable to the desired compound.

## 2.9 PRELIMINARY INVESTIGATION INTO THE WITTIG REACTION

In order to investigate the versatility of titanium dioxide, the methodology was extended to the Wittig reaction. Benzyl alcohol **228**, (ethoxycarbonylmethylenetriphenylphosphoran **229**, titanium dioxide and TEMPO were stirred under microwave irradiation and subsequently analyzed by NMR spectroscopy (Scheme 67).



**Scheme 67: Titanium dioxide/TEMPO mediated Wittig reaction**

The  $^1\text{H}$  NMR spectrum revealed the absence of any product with only benzyl alcohol present (**Figure 20**). The Wittig reagent was not present and a number of unidentifiable peaks were observed. The conclusion drawn was that titanium dioxide had degraded the Wittig reagent before attack of the carbonyl compounds could occur. The absence of benzaldehyde is also surprising and this may imply that the aldehyde is formed in small equilibrium quantities and must be elaborated further. If the small quantity of aldehyde is not elaborated further, the equilibrium shifts towards the starting reactant. A similar observation was made by Taylor and co-workers when carrying out the Wittig reaction on unactivated alcohols.<sup>30</sup> This reaction was not evaluated any further and will form part of future investigations.

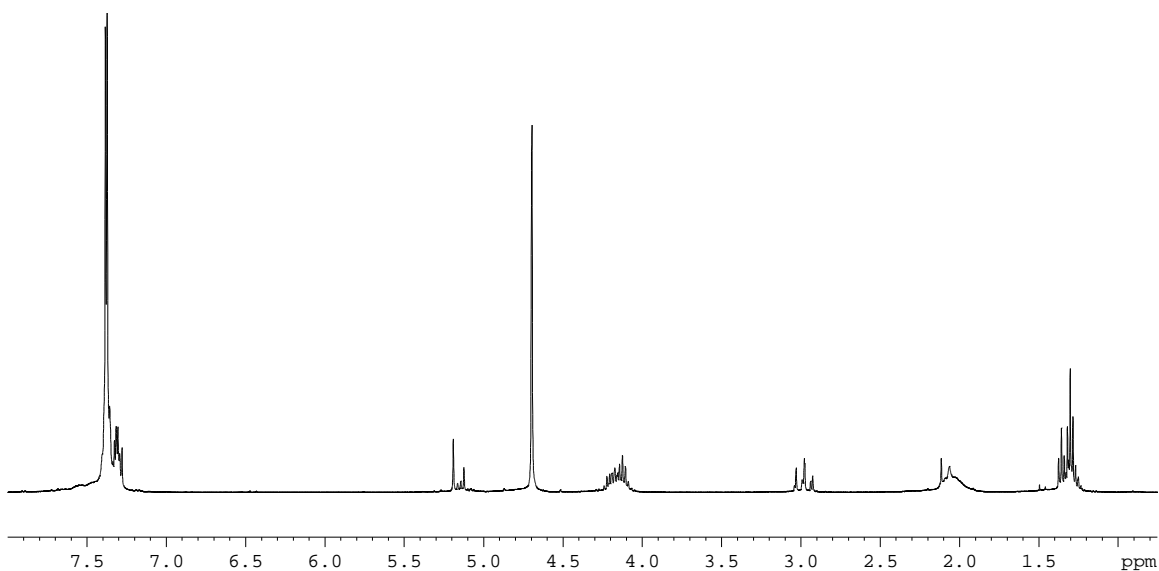


**Figure 20: Showing the degradation of the Wittig reagent**

Although success had been achieved using a microwave, the conditions were relatively harsh and thus, attempts were sought to conduct the tandem oxidation reaction under milder conditions. It was in this search that our attention focused on doping titanium dioxide in order to shift its absorbance and as a result, conduct the reaction under less strenuous conditions.

# Chapter 3

## Doping studies

### 3.1 Preface

The low cost, stability under irradiation and environmental friendliness make titanium dioxide an attractive oxidant within organic chemistry. There are however, significant drawbacks of a titanium dioxide catalyzed oxidation such as its large band gap of 3.2 eV, and the recombination of electrons with positive holes (**Figure 21**). Due to this large band gap, titanium dioxide requires ultraviolet irradiation ( $\lambda \leq 387$  nm) for activation while the recombination of electrons with holes results in a decrease of the active oxidizing species.

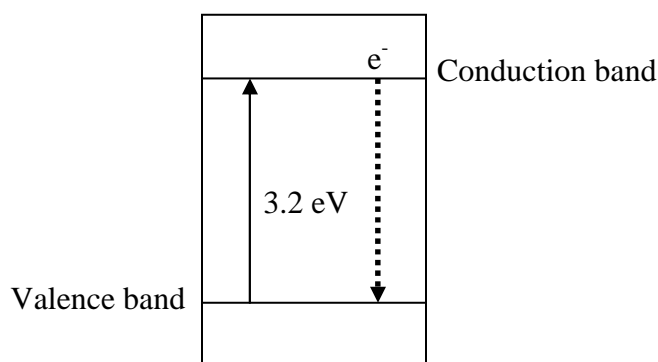


**Figure 21: Showing the large band gap of titanium dioxide and the recombination of electrons with the positive holes**

As a result, many research groups have focused on improving the photocatalytic ability of titanium dioxide,<sup>117</sup> with the most common methods being surface sensitization and doping.

## 3.2 IMPROVING THE PHOTOCATALYTIC RESPONSE OF TITANIUM DIOXIDE

### 3.2.1 Surface sensitization of titanium dioxide

The use of organic dyes is one commonly employed procedure to improve the photocatalytic response of titanium dioxide.<sup>118,119</sup> This method involves the attachment of a visible light absorbing dye to the surface of titanium dioxide in an attempt to shift its absorbance into the visible region. Chatterjee and co-workers adsorbed 8-hydroxyquinoline (**Figure 22**) onto titanium dioxide which resulted in a shift in titanium dioxide's absorbance into the visible region.

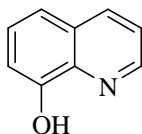
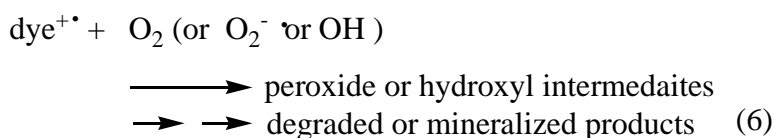
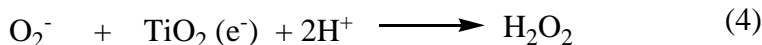
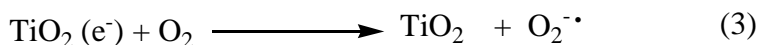
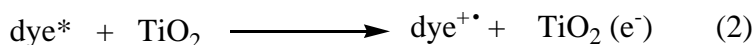


**Figure 22: 8-hydroxyquinoline**

The authors tested the photocatalytic activity of the dye sensitized titanium dioxide by monitoring the purification of waste water. The dye sensitized titanium dioxide was mixed with waste water and stirred under visible irradiation, and after 5 hours 70-80% of the pollutants had been degraded.

### 3.2.2 Mechanism of surface sensitized titanium dioxide

The mechanism of surface sensitized titanium dioxide differs from the general oxidation reaction in which the dye and not titanium dioxide is activated by visible light (**Scheme 68**):<sup>119</sup>



### Scheme 68: Hydroxyl radical formation on surface sensitized titanium dioxide

The mechanism begins with the excitation of the dye by an appropriate energy source (1). The excited dye molecule injects an electron into the conduction band of titanium dioxide (2), which reacts with preadsorbed oxygen to produce superoxide molecules (3). The superoxide molecules react with electrons, in acidic solution, to produce hydrogen peroxide (4). Hydrogen peroxide reacts with an electron to produce hydroxyl radicals (5). The superoxide molecules react with the hydroxyl radicals to generate the degraded products (6). The problems associated with the use of organic dyes are their long term stability which can result in detachment from titanium dioxide.<sup>120</sup>

### 3.3 DOPING OF TITANIUM DIOXIDE

The other commonly employed method to improve the photocatalytic ability of titanium dioxide is by a process described as doping. Doping refers to the purposeful addition of impurities to titanium dioxide and has been used to:



- decrease the band gap which results in a shift in absorbance into the visible region or
- increase the band gap which results in a higher absorbance under UV irradiation and confines the electrons to the conduction band for a longer period consequently resulting in an improved photocatalytic response.

### 3.3.1 History of doping

In 1971, Che and Naccache noticed a paramagnetic species by electron paramagnetic resonance (EPR), when titanium dioxide was treated with aqueous ammonia and calcined at 350-400°C.<sup>121</sup> They attributed the EPR signals to the presence of  $\text{NO}_2^{2-}$  radicals absorbed on the surface on titanium dioxide. They based this assumption by comparing the magnetic parameters of  $\text{NO}_2^{2-}$  radicals absorbed on other metal oxides. This represented the first synthesis of doped titanium dioxide although Che and Naccache never explored the photocatalytic properties of this substance.

In 1985, Sato noticed that titanium dioxide prepared by the calcination of commercially available  $\text{Ti}(\text{OH})_4$  displayed absorbance in the visible region.<sup>122</sup> By analysis of the  $\text{Ti}(\text{OH})_4$  sample, he found the presence of  $\text{NH}_4\text{OH}$  a consequence of the hydrolysis of  $\text{TiCl}_4$  and  $\text{NH}_4\text{OH}$  during the preparative stages of  $\text{Ti}(\text{OH})_4$ . Titanium dioxide prepared from  $\text{Ti}(\text{OH})_4$  without the use of  $\text{NH}_4\text{OH}$  showed no absorbance in the visible region. From these results, Sato concluded that the absorbance in the visible region was due to the nitrogen impurity resulting from the preparation of  $\text{Ti}(\text{OH})_4$ . Since the discovery, many research groups have attempted to dope titanium dioxide by the insertion of a variety of impurities.<sup>123</sup>

### 3.3.2 Physical doping of titanium dioxide- metal ion implantation

The metal ion implantation technique is a commonly employed physical method for the doping of titanium dioxide.<sup>124,125</sup> Metal ions are accelerated with such velocity that they are able to insert into titanium dioxide resulting in a shift in absorbance. Zheng and co-workers described a procedure for the doping of titanium dioxide using Sn ions *via* the ion implantation method.<sup>126</sup> The band gap of Sn doped titanium dioxide was estimated to be 3.25 eV corresponding to a wavelength of 382 nm while the band gap of undoped titanium dioxide was estimated to be 3.34 eV corresponding to a wavelength of 371 nm. Since the band gap of titanium dioxide had decreased, the authors reasoned that Sn doped titanium dioxide should display superior activity as it can absorb energy over a wider range of wavelengths.<sup>\*\*\*</sup> They confirmed this hypothesis by monitoring the degradation of Rhodamine B with the Sn doped powder degrading 80% of a Rhodamine B solution while the undoped powder degraded only 68% of the Rhodamine B solution. While improving the activity of titanium dioxide, a significant drawback of this procedure is the high cost associated with the instrumentation.

### 3.3.3 Chemical doping of titanium dioxide- the sol gel process

The sol gel process is a commonly employed chemical method for the doping of titanium dioxide. Using this methodology, Wu and co-worker reported a process for the synthesis of a series of vanadium doped titanium dioxide powders.<sup>127</sup> The vanadium doped powders were analyzed by diffuse reflectance spectroscopy and revealed a shift in absorbance into the visible region when compared with undoped titanium dioxide. In this procedure, titanium butoxide was mixed with acetic acid and added to a butanolic solution of vanadyl acetylacetonate. The solution was stirred for 24 hours and dried at 150°C. The obtained precipitates were calcined at 400°C for 30 minutes to produce vanadium doped titanium dioxide powders of varying vanadium content. The vanadium doped powders were analyzed by the degradation of methyl blue under visible irradiation

---

<sup>\*\*\*</sup> Sn doped titanium dioxide is activated by photons of wavelength  $\leq 382\text{nm}$  while undoped titanium dioxide is activated by photons of wavelength  $\leq 371\text{nm}$ .

and showed superior degradative ability when compared to undoped titanium dioxide. The authors ascribed the superior performance of vanadium doped titanium dioxide to its shift in absorbance into the visible region.

### **3.3.4 ANALYSIS OF DOPED TITANIUM DIOXIDE**

Two common techniques used to analyze the doped powder are powder X-ray diffraction (XRD) and diffuse reflectance spectroscopy. XRD provides information about the crystallinity and phase composition of titanium dioxide while the diffuse reflectance reveals the effect of the dopant on the band gap. Thus, diffuse reflectance in particular can be used to predict the activity of the doped titanium dioxide by providing an indication of the shift in light absorbance. Since XRD and diffuse reflectance spectroscopy are techniques not commonly employed by organic chemists a basic explanation of these procedures will be provided.

#### **3.3.4.1 Powder X-ray diffraction**

Powder X-ray diffraction has found widespread application ranging from the identification of unknown materials and phase determination to crystal size estimations.<sup>128</sup> In an X-ray tube, a tungsten filament is heated leading to the generation of electrons which are accelerated with high voltage to strike a metal target such as copper, chromium, cobalt or iron. The striking of the metal target gives rise to a series of wavelengths such as  $K\alpha_1$ ,  $K\alpha_2$  and  $K\beta$ . For powder X-ray diffraction, the  $K\alpha_1$  wavelength is chosen as it is the most intense of the three dominant wavelengths. Thus for a typical powder X-ray diffraction study,  $CuK\alpha_1$  is chosen as the single wavelength. X-rays of this single chosen wavelength are passed through a slit to remove any unwanted wavelengths before interaction with the sample. The interaction between the X-rays and sample give rise to a series of diffraction cones in all directions. The detector cuts through the cones at diffraction maxima which are displayed as a function of the detector angle  $2\theta$ .<sup>128</sup> The intensity of the diffraction pattern is related to the amount of a

particular phase in the sample. The phases can be identified by comparing the diffractions with a set of standard data, which accompanies the processing software, or with literature.

#### **3.3.4.2 Diffuse reflectance spectroscopy**

Diffuse reflectance spectroscopy is primarily used to measure the energy gap of a solid, usually a semiconductor.<sup>129,130</sup> The absorption edge is defined as the transition from strong short wavelength and weak long wavelength absorbance. The position of this edge is determined by the energy gap between the conduction and valence band. Monitoring the absorbance (or percentage reflectance) of semiconductors over the UV/VIS range can be used to estimate its band gap.

In a diffuse reflectance spectroscopy study, light of a particular wavelength is projected onto a horizontal sample and the diffusely reflected light is collected by two mirrors located above the sample. In this case, the wavelength of light projected and the percentage reflectance (% R) is recorded. A graph of % R vs. wavelength is plotted and the onset of the transition (strong short wavelength to weak long wavelength) determined – allowing for band gap estimation.

## 3.4 DISCUSSION OF DOPING RESULTS

### 3.4.1 Preface

In order to investigate the effect of the doping on the band gap of titanium dioxide, a series of doped titanium dioxide powder were prepared. Titanium dioxide was doped with silver, phosphorus, boron, nitrogen, sulfur, and iodine and the effect of the dopant monitored by powder X-ray diffraction (XRD) and diffuse reflectance. Nano-titanium dioxide was also evaluated by XRD and diffuse reflectance spectroscopy to determine the effect of particle size on the photocatalytic activity of titanium dioxide.

### 3.4.2 Nano - titanium dioxide

Nano crystalline titanium dioxide has been reported to have superior photocatalytic capabilities compared to crystalline titanium dioxide. This superior photocatalytic performance of the nanoparticles has been attributed to the smaller particles having a larger specific surface area resulting in an increase in surface sites and surface charge carrier transfer rate.<sup>131</sup> There is however, an optimum particle size resulting in the highest photocatalytic activity. Ying and co workers reported an optimum size of 10 nm for the degradation of chloroform,<sup>132</sup> while Anpo<sup>133</sup> and Yue<sup>134</sup> have reported an optimum size of 7 nm. Decreasing the particle size beyond this point does not result in an increase in photocatalytic activity due to amplified electron/hole recombination.<sup>131</sup> Thus, nano-titanium powder purchased from Aldrich was analyzed by XRD and diffuse reflectance spectroscopy. XRD revealed, as expected, characteristic reflections of anatase titanium dioxide (25.3°, 37.8°, and 48°) but with one obvious difference. The smaller particle size of the nano-powder resulted in peak broadening (**Figure 23**). The peak broadening is evident by comparing the peaks at 37.8° which in the case of crystalline titanium dioxide was shown be a 'triplet' while in the case of the nano crystalline powder appears as a broad hump (**Figure 24**).

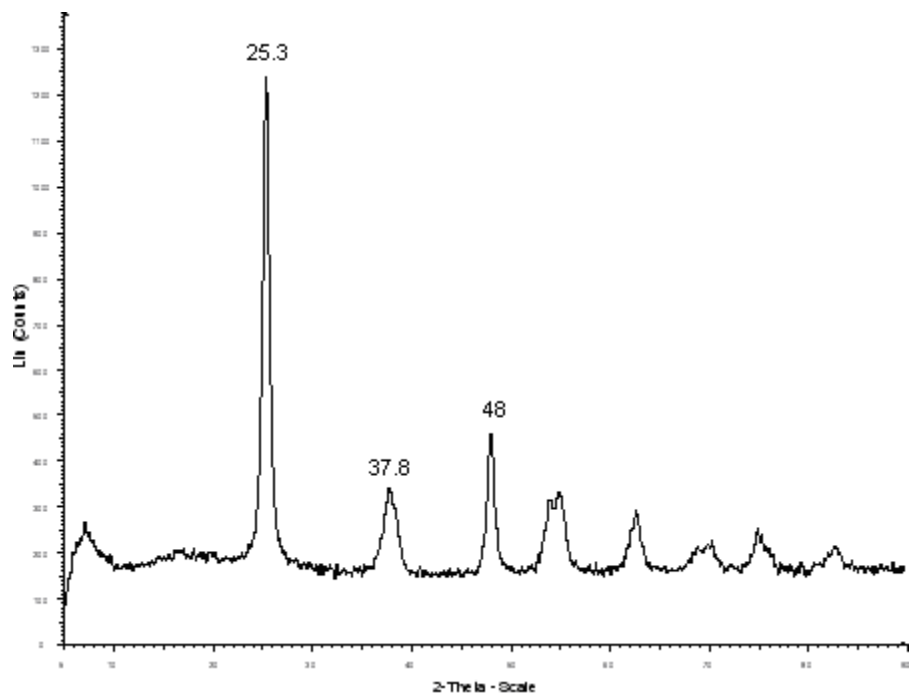


**Figure 23: Powder x-ray diffraction pattern of nano-titanium dioxide**

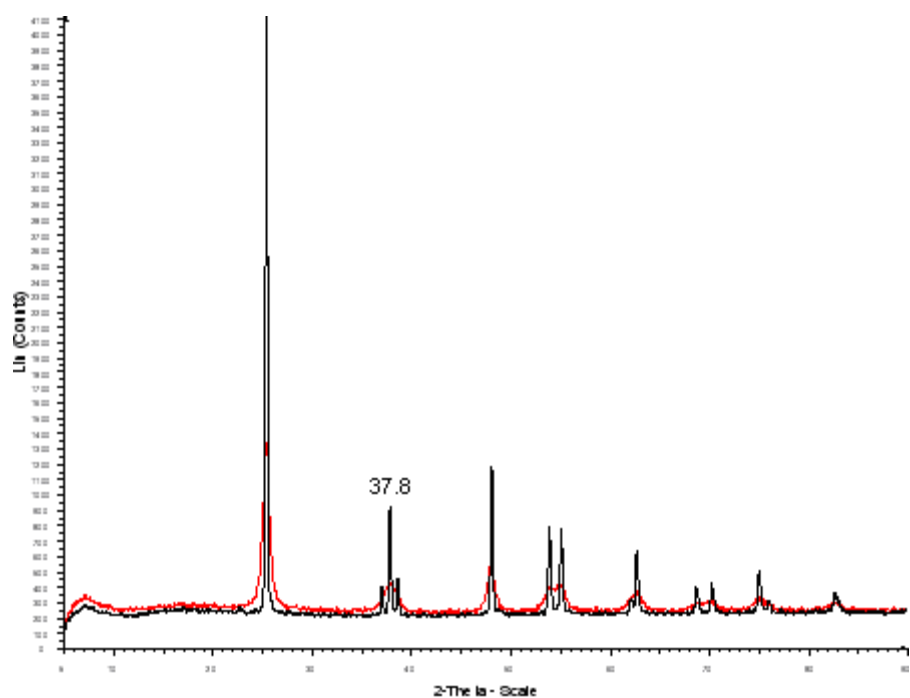


**Figure 24: Comparison of powder x-ray diffraction pattern of nano and crystalline titanium dioxide**

Of interest was the effect of particle size on the band gap of titanium dioxide. The onset of the transition for titanium dioxide was estimated by extrapolation to occur at 365 nm (See **Figure 25**). Similarly the onset of the transition was determined for nano crystalline titanium dioxide. Using this information, the band gap of nano crystalline titanium was estimated to be 3.5 eV for nano crystalline titanium dioxide and 3.4 eV for crystalline titanium dioxide.<sup>§§§§</sup> In addition, throughout the spectral window, nano crystalline titanium dioxide displays a lower absorbance of light (higher % R implies low absorbance) compared to titanium dioxide. Thus for the tandem oxidation reaction crystalline titanium dioxide is expected to give superior results than its nano-powder counterpart.

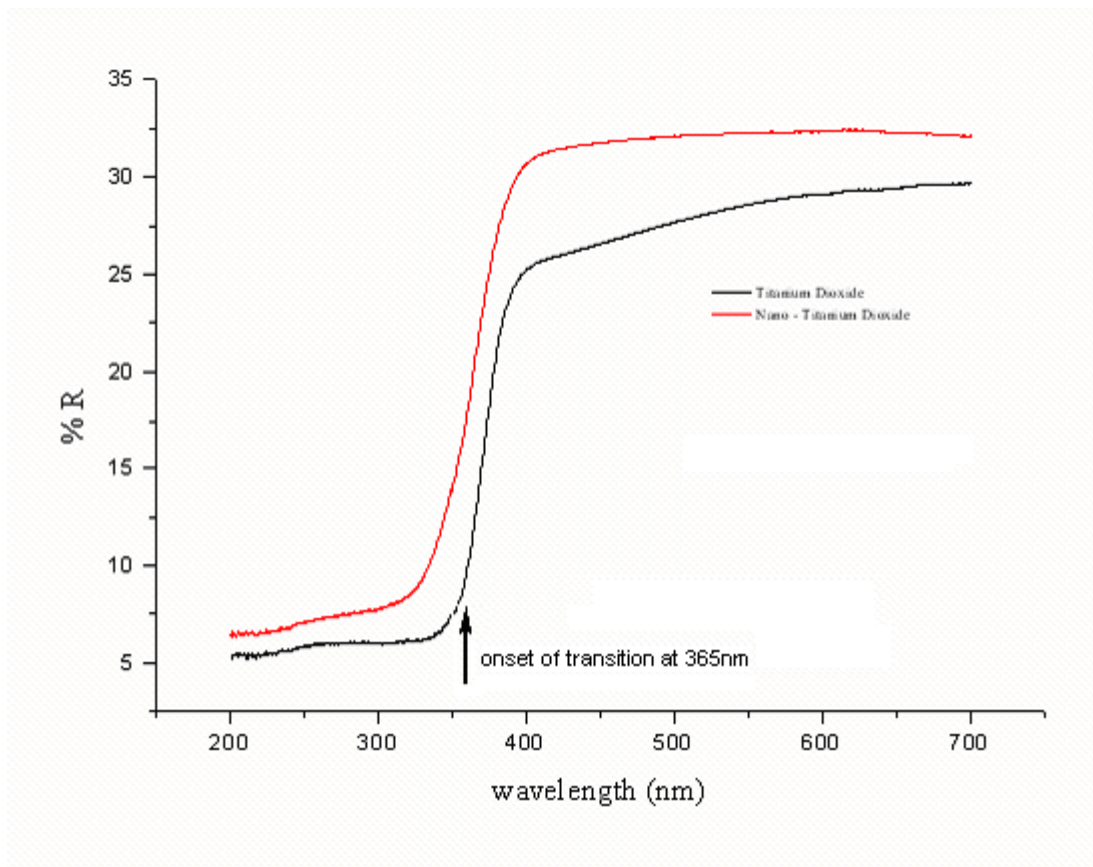


**Figure 25: Diffuse reflectance spectrum of nano and crystalline titanium dioxide**

<sup>§§§§</sup> Band gap determined using the equation  $E=1239.8/\lambda$  where E=band gap

### 3.4.3 Silver-doped titanium dioxide

Silver doped titanium dioxide powders were prepared using silver nitrate as a source of silver using the procedure outlined by Pal and co-workers.<sup>135</sup> Titanium dioxide was added to a solution of silver nitrate and water which was stirred thoroughly. The mixture was aged at room temperature for 24 hours and dried in an oven at 100°C followed by calcination at 400°C for 3 hours to produce a grey powder. Unfortunately, Pal and co-workers did not report an XRD pattern or diffuse reflectance spectrum so a direct comparison of spectra is not possible. In the present case, XRD revealed the powder to be purely anatase in crystalline phase as all the characteristic anatase peaks were present (Figure 26).

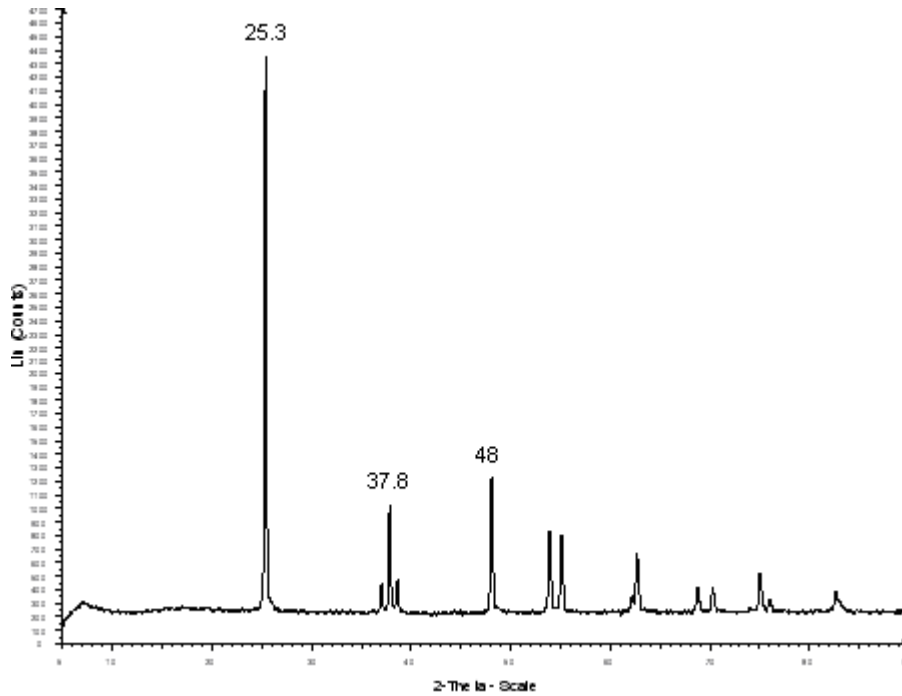
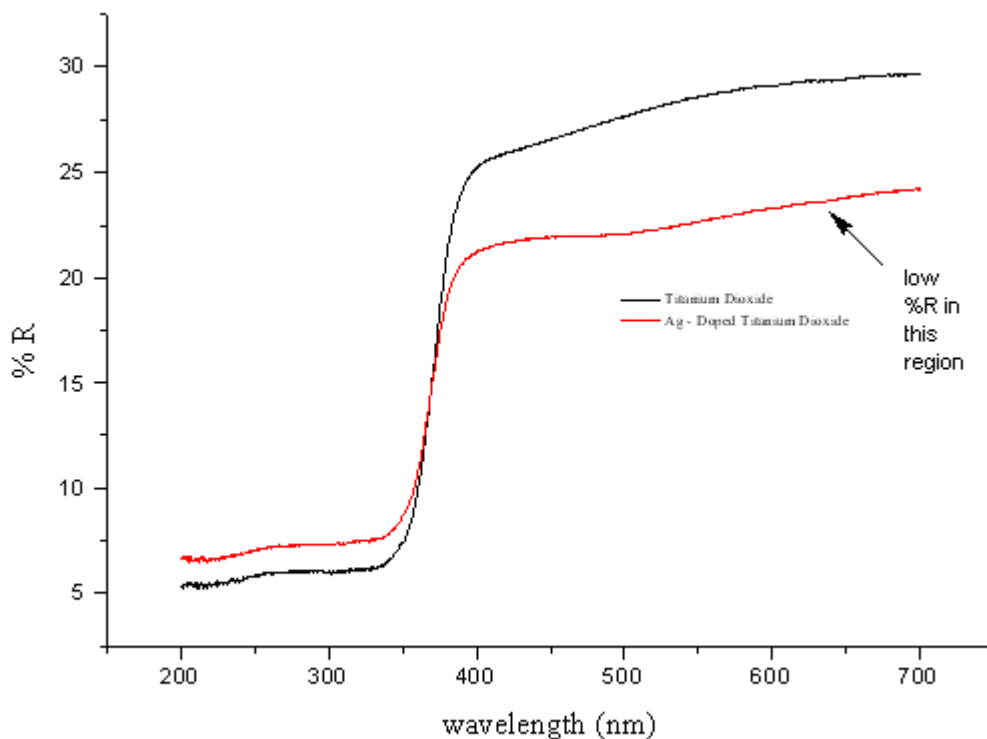


Figure 26: Powder x-ray diffraction pattern of silver doped titanium dioxide



The band gap of silver doped titanium dioxide was estimated to be 3.4 eV but the silver doped powder displayed a higher degree of absorbance in the visible region ( $\lambda > 400$  nm) when compared to undoped titanium dioxide (**Figure 27**).



**Figure 27; Diffuse reflectance spectra of silver doped titanium dioxide and crystalline titanium dioxide**

A similar spectrum has been obtained by Liu and co-workers who attempted to provide mechanistic detail for the photocatalytic activity of silver doped titanium dioxide.<sup>136</sup> Liu and co-workers firstly focused their efforts on determining the effect of silver loading on the photocatalytic oxidation of phenol. In the absence of silver only 18% of a phenol solution had been degraded after 2 hours while various loadings of silver doped titanium dioxide showed a higher degradation of phenol till an optimal silver loading of 1.026wt.% was reached. An increase in silver content beyond this optimal value results in:

- the formation of bulk silver which could serve as a recombination site for the photogenerated species.
- a decrease in the contact time between titanium dioxide and the organic species.
- obstruction of irradiation reaching titanium dioxide and consequently a decrease in active oxidizing species.

The silver doped powder was analyzed for its elemental weight distribution and found to have a carbon distribution of 10.61wt.%, oxygen distribution of 31.11wt.%, silver loading of 1.98wt.% and titanium distribution of 56.3wt.% (**Diagram 2**). The carbon present in this analysis was due to the carbon tape used in the preparation of the sample. It was evident that the doped powder's silver content of 1.98wt.% compared favourably with the requirements outlined by Liu and co-workers.

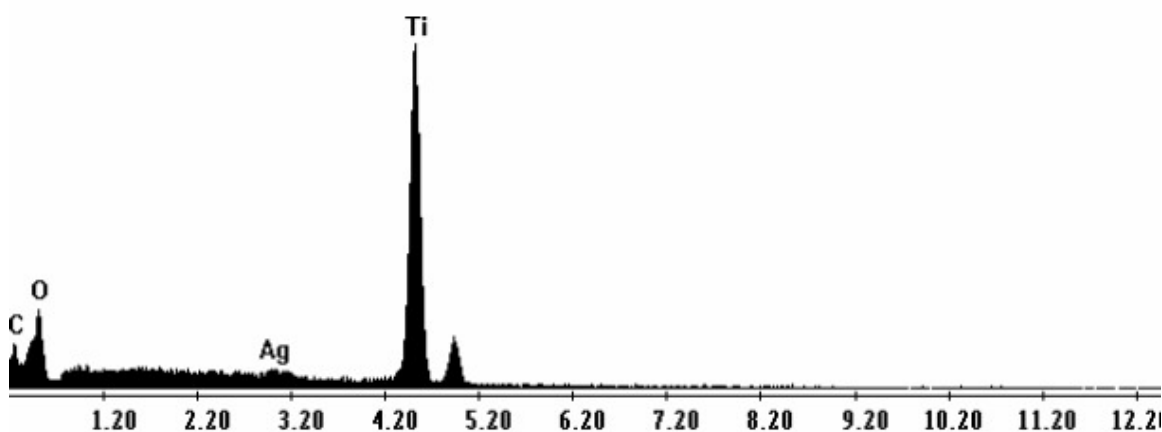
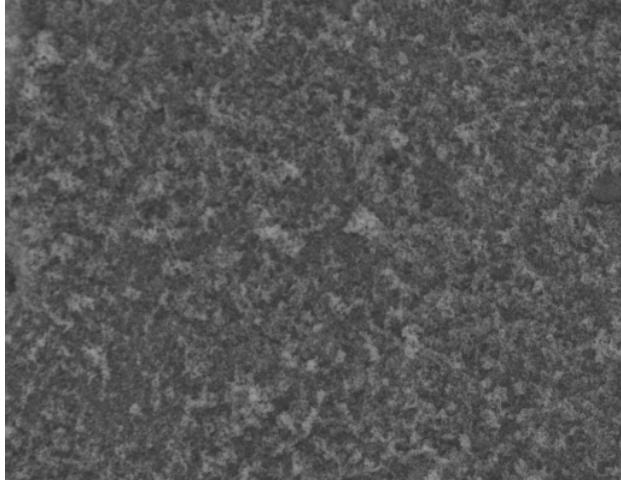


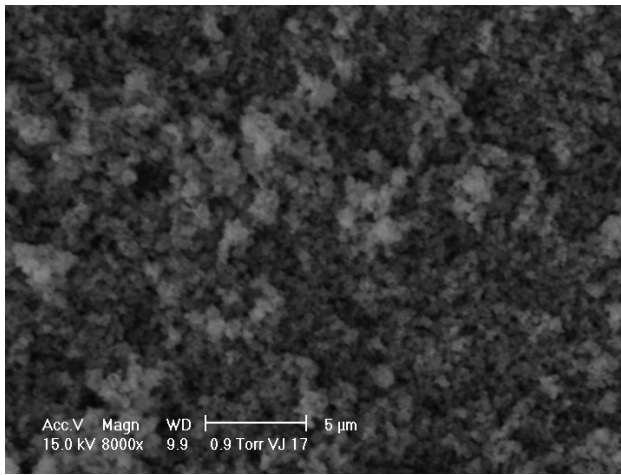
**Diagram 2**

Since the band gap of silver doped titanium dioxide is relatively unchanged, there must be other factors contributing to the photocatalytic activity of titanium dioxide. Liu and co-workers proposed a mechanism for the superior results obtained under silver doped titanium dioxide. It was proposed by Liu that the deposited silver serves as an accumulation site for photogenerated electrons. These electrons could react with adsorbed oxygen to produce  $O_2^-$  or they could react with  $Ti^{4+}$  to produce surface  $Ti^{3+}$  which is the most reactive center for the photocatalytic process.

The powder was analyzed by scanning electron microscopy (SEM) and compared to undoped titanium dioxide (**Figure 28**). The powders were similar in appearance, which is unsurprising since both powders consist of anatase titanium dioxide.



(a)



(b)

**Fig 28: SEM images of (a) undoped titanium dioxide and (b) Ag doped titanium dioxide.**

### 3.4.4 Phosphorus doped titanium dioxide

Phosphorus doped titanium dioxide was prepared by adding titanium isopropoxide to phosphoric acid and heating the mixture to reflux for four hours using the procedure outlined by Yu.<sup>137</sup> After this time the mixture was cooled and the solids filtered and calcined at 400°C for 4 hours to afford a grey powder. XRD revealed that the powder was purely amorphous<sup>\*\*\*\*\*</sup> as a diffuse hump was obtained and no assignable peaks could be identified (**Figure 29**). While this was unexpected it was not necessarily detrimental to the titanium dioxide catalyzed oxidation as amorphous powders are known to exhibit high photocatalytic ability.<sup>138</sup> The diffuse reflectance results showed a definite increase in band gap when compared to undoped titanium dioxide (**Figure 30**) which may result in a confinement of electrons in the conduction band and improved photocatalytic activity. The phosphorus doped powder does display a lower absorbance when compared with undoped titanium dioxide throughout the spectral window. The band gap of phosphorus doped titanium dioxide was estimated to be 3.7 eV corresponding to 335 nm. SEM images showed, as expected, the powder to consist of randomly orientated crystals – indicative of an amorphous powder (**Figure 31**).

---

\*\*\*\*\* Amorphous powders do not contain a definite crystalline phase

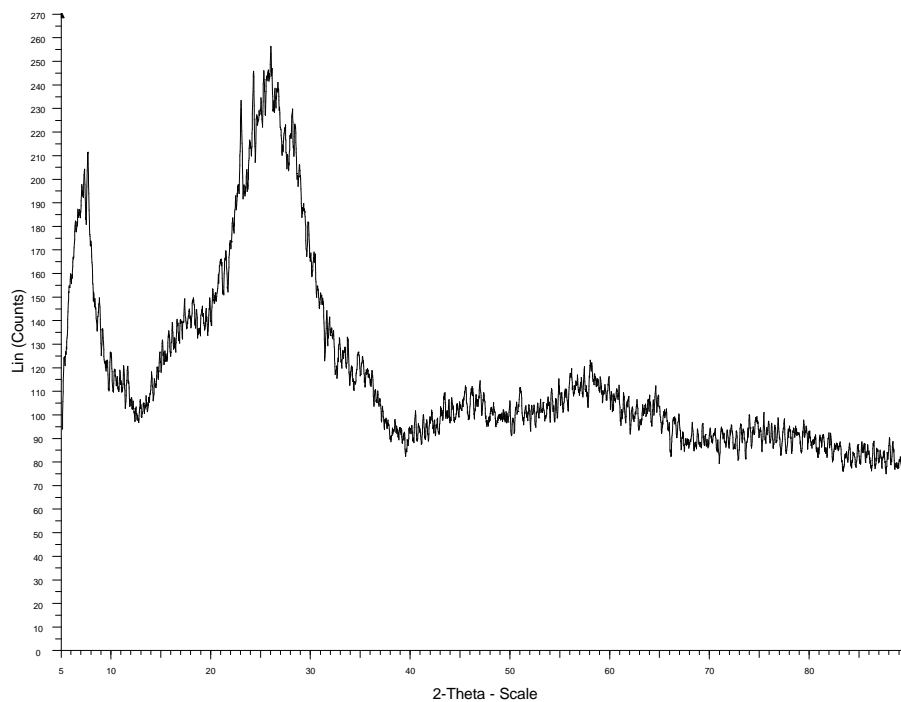


**Figure 29: Powder x-ray diffraction pattern of phosphorus doped titanium dioxide**

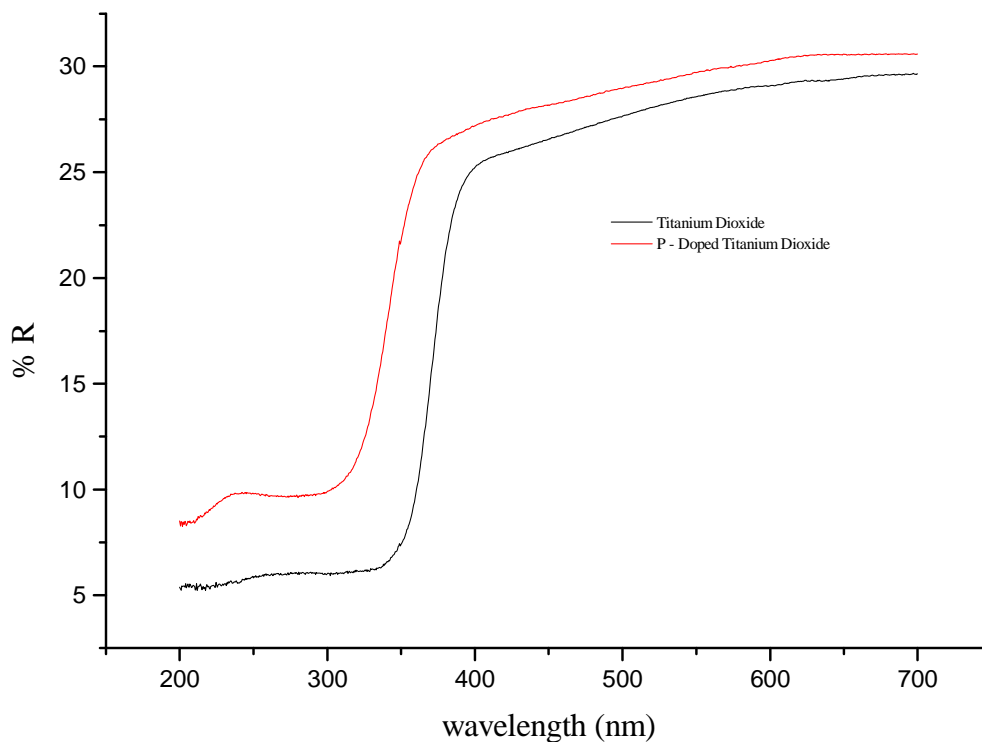
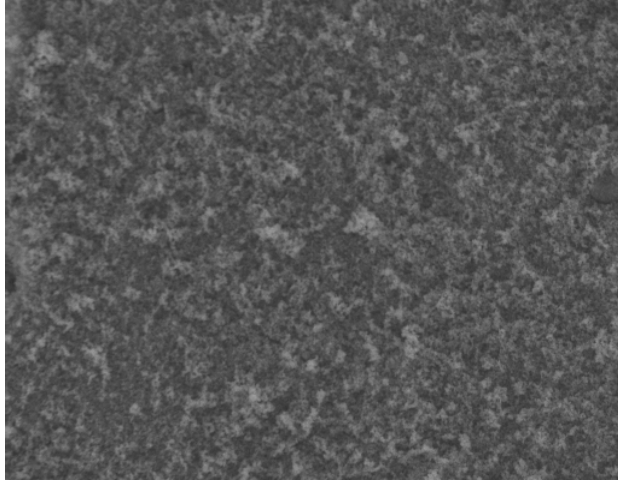
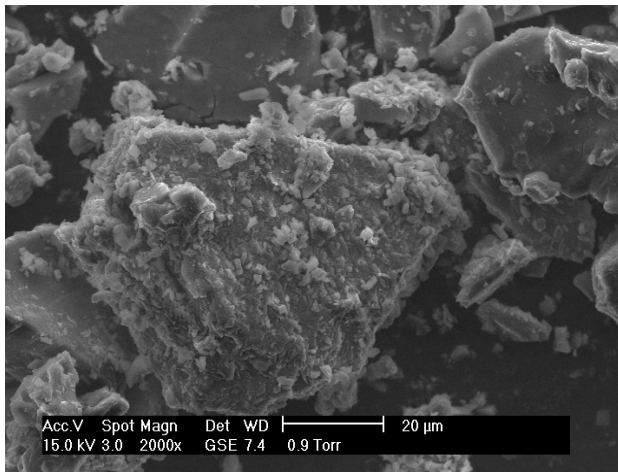


**Figure 30: Diffuse reflectance spectra of phosphorus doped titanium dioxide and crystalline titanium dioxide**



(a)



(b)

**Fig 31: SEM images of (a) undoped titanium dioxide and (b) phosphorus doped titanium dioxide**

### 3.4.5 Boron doped titanium dioxide

The effect of boron on the photocatalytic activity of titanium dioxide was examined using a method outlined by Jiang and co-workers in which the boron doped titanium dioxide displayed an increase in band gap.<sup>139</sup> Titanium isopropoxide was added to water, to generate titanium dioxide, followed by the addition of boric acid. The mixture was stirred for 12 hours at room temperature and dried in an oven at 100°C for 8 hours followed by calcination at 500°C for 1 hour. According to the XRD pattern (**Figure 32**) there was a characteristic peak at 28° which, according to the structure database, might correspond to the rutile phase of titanium dioxide. This theory was however, disband as rutile crystallization *commences* at 700-800 °C<sup>139</sup> which was unlikely to occur in our situation. There was however, a small peak at 25.3° which corresponded to anatase titanium dioxide. This led to conclusion that a mixed powder was present consisting of trace anatase phase titanium dioxide and another phase. Moon *et al.*<sup>140</sup> had reported that boron doped titanium dioxide initially forms an amorphous powder consisting of diboron trioxide which upon calcination crystallizes into firstly anatase, and at higher temperatures rutile phase titanium dioxide. They reported XRD patterns of boron doped titanium dioxide calcined over the temperature range 400-900°C. At 400°C, diboron trioxide dominates the x-ray pattern. As the temperature was increased the diboron trioxide phase decreased and the anatase phase dominated till 700°C when traces of rutile titanium dioxide appeared. Temperatures beyond 700°C, showed a decrease in anatase phase titanium dioxide and an increase in rutile titanium dioxide. The X-ray pattern that was obtained in our case matched that of the powder calcined at 500 °C. Thus, the peaks at 14.6° and 28.1° were assigned to diboron trioxide and the powder was determined to be amorphous with traces of anatase titanium dioxide. More useful information was obtained from the diffuse reflectance spectrum (**Figure 33**) which showed this powder to have undergone a decrease in band gap which was in contrast to Jiang and co-workers prediction of an increase in band gap. Even more interesting was that the powder showed two distinct band transitions – one in the UV region due to the titanium dioxide fundamental band transition and the second in the visible region due to boron doping. The band gap of boron doped titanium dioxide was estimated to be 2.3 eV corresponding



to a wavelength of 539 nm. Thus, for activation of boron doped titanium dioxide, a minimum energy of 2.3 eV is required.

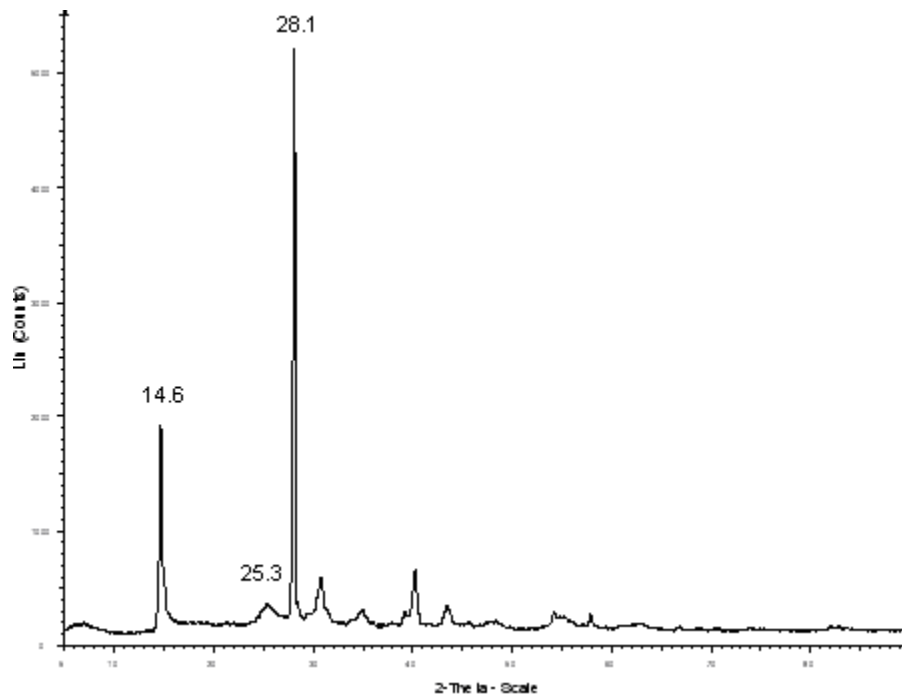


**Figure 32: Powder x-ray diffraction pattern of boron doped titanium dioxide**

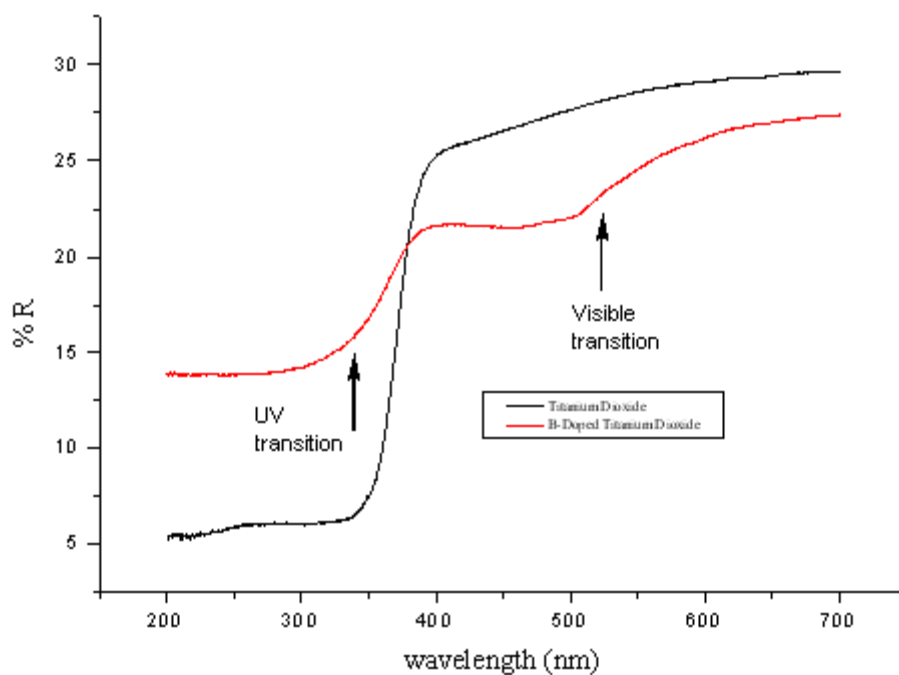
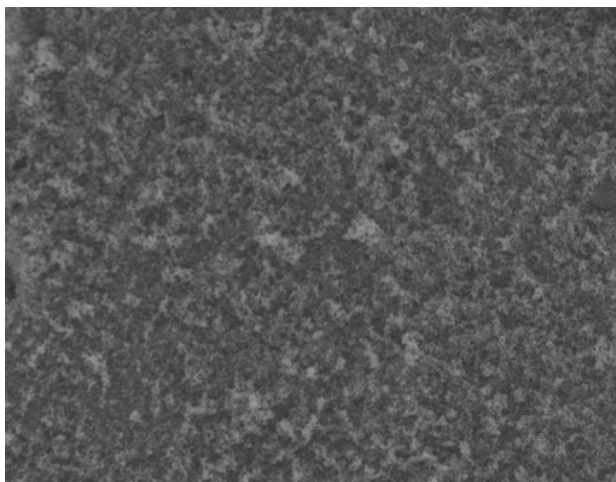
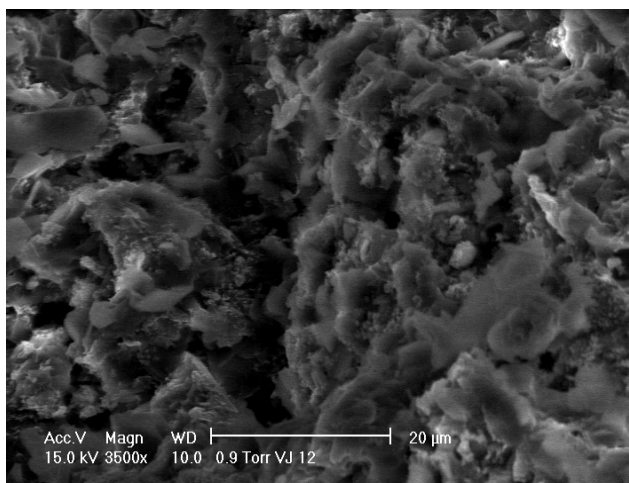


**Figure 33: Diffuse reflectance spectra of boron doped titanium dioxide and crystalline titanium dioxide**

In order to verify our observation that the doped powder was indeed amorphous the powder was analyzed by scanning electron microscopy. The SEM image of pure anatase titanium dioxide was compared with boron doped titanium dioxide (**Figure 34**). The anatase titanium dioxide shows a higher degree of ‘order’ when compared to boron doped titanium dioxide which consisted of randomly orientated and sized crystals.



(a)



(b)

**Figure 34: SEM images of (a) titanium dioxide and (b) boron-doped titanium dioxide**

### 3.4.6 Nitrogen doped titanium dioxide

Nitrogen doped titanium dioxide was prepared by the addition of titanium isopropoxide to water, after which nitric acid and aqueous ammonium hydroxide was added to produce a brown floccule, which was filtered and calcined at 400°C to produce a brown powder.<sup>138</sup> The powder was analyzed by XRD (**Figure 35**), which revealed it to be

marginally crystalline as there were no sharp, definite peaks. There were however, 'peaks' that did not correspond to titanium dioxide. Analysis of the database revealed that the observed peaks at 18.1, 22.6, 29.0 and 33.1° matched that of ammonium nitrate. Since the method of preparation<sup>138</sup> involved the addition of aqueous ammonia and nitric acid to titanium isopropoxide, these peaks must result from the reaction between aqueous ammonia and nitric acid. From the comparison of the counts (y-axis) it is evident that the proportion of ammonium nitrate is minute.<sup>††††</sup> Thus, it is concluded that the powder is partially crystalline – with a large portion in the amorphous state. Diffuse reflectance spectroscopy showed that the shift in band gap was not significant but, more importantly, the powder showed a greater absorbance in the visible region when compared to titanium dioxide (**Figure 36**). In addition, the doped powder did not show a sharp absorption edge evident in undoped titanium dioxide. This observation has been attributed to a number of surface states across the band gap which results in a diffuse spectrum. A similar observation was made by Manorama and co-workers in the case of carbon doped titanium dioxide. The band gap of nitrogen doped titanium dioxide was estimated to be 3.4 eV. Despite the unchanged band gap, nitrogen doped titanium dioxide is predicted to exhibit superior photocatalytic ability under visible light compared with undoped titanium dioxide.

---

<sup>††††</sup> Intensity of diffraction pattern is related to the amount of a particular phase.

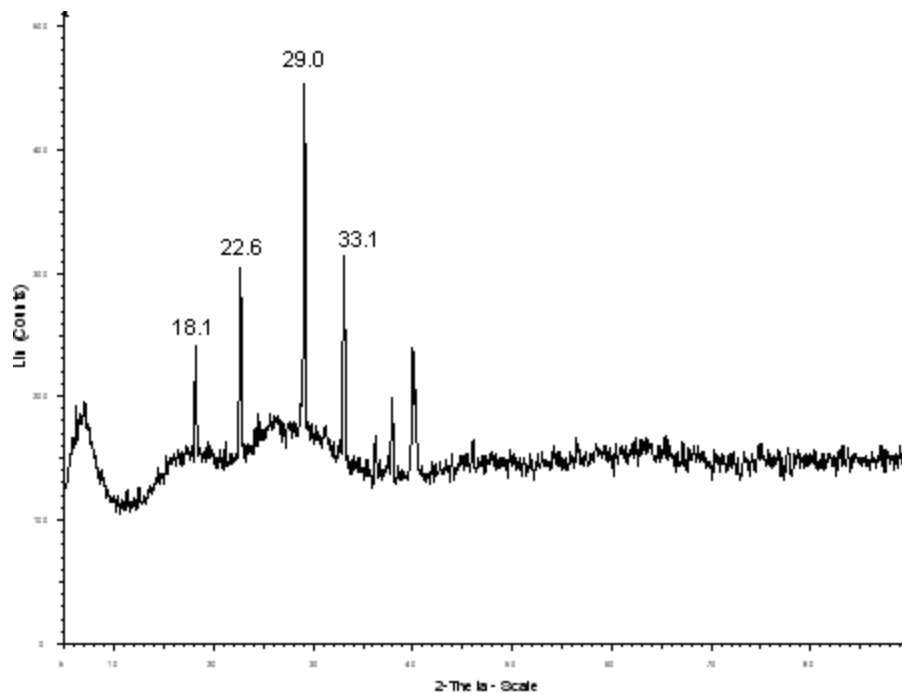


**Figure 35: Powder X-ray diffraction pattern for nitrogen doped titanium dioxide**

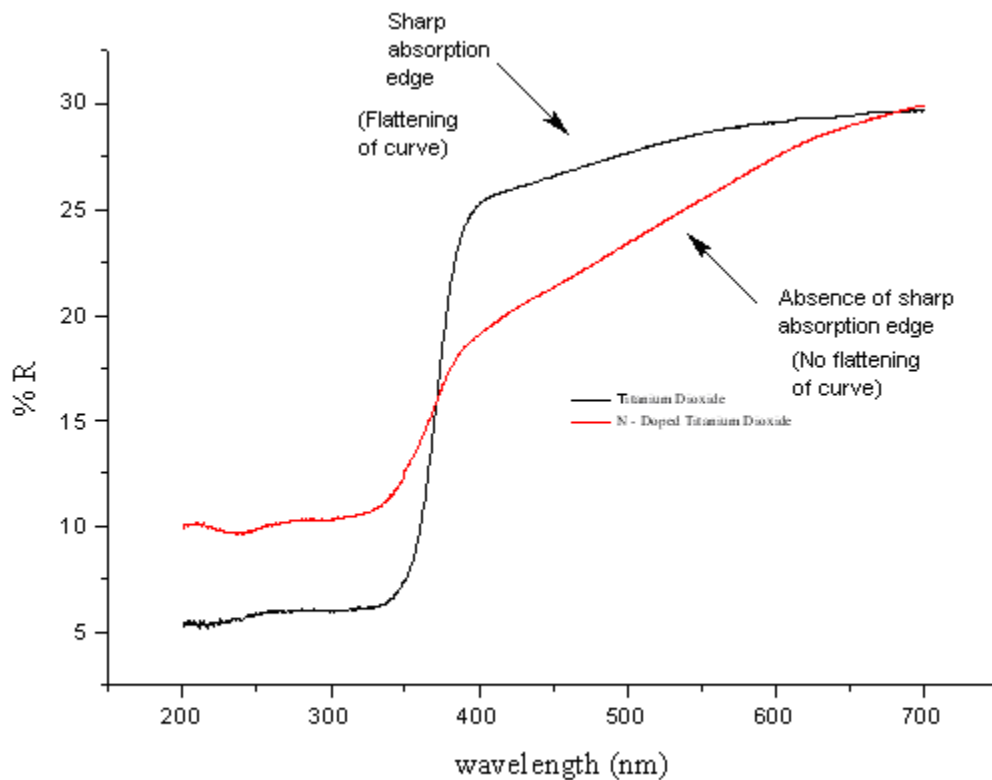
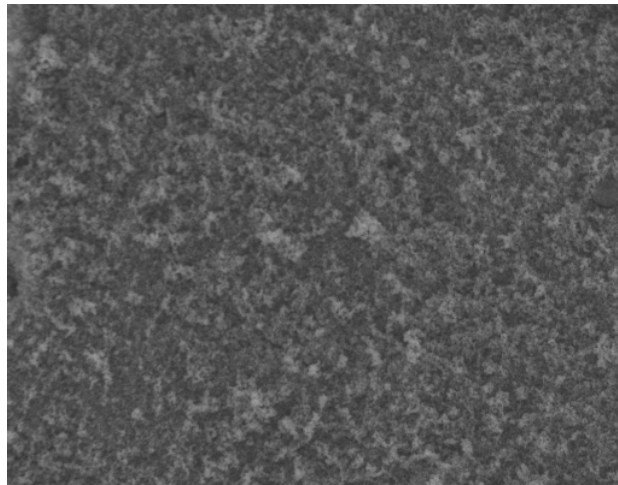
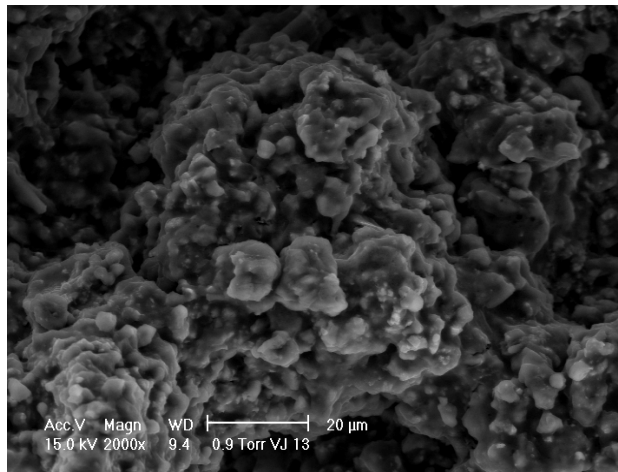


**Figure 36: Diffuse reflectance spectra for nitrogen doped titanium dioxide and crystalline titanium dioxide**

Again, the nitrogen doped titanium dioxide SEM image was compared with pure anatase titanium dioxide (**Figure 37**). The nitrogen doped powder showed a higher degree of disarray when compared to pure titanium dioxide which further validated our prediction of the amorphous nature of the powder.



(a)



(b)

**Figure 37: SEM images of (a) undoped titanium dioxide and (b) nitrogen doped titanium dioxide**

### 3.4.7 Sulfur doped titanium dioxide

To prepare sulfur doped titanium dioxide, titanium isopropoxide was added to a solution of thiourea dissolved in ethanol to produce a white powder which was filtered and calcined at 400 °C.<sup>141</sup> XRD revealed the presence of a highly crystalline powder evidenced by the definite, sharp peaks. A peak at 25.5° was present which may indicate the presence of anatase titanium dioxide. XRD also revealed the presence of characteristic thiourea peaks at 19.9, 20.9, 23.3, 25.5 and 28.5° (**Figure 38**). Thus the peak at 25.5° could be due to thiourea and *not* anatase titanium dioxide. From these observations it was concluded that the powder might contain thiourea doped anatase titanium dioxide, thiourea doped amorphous titanium dioxide or no titanium dioxide and just thiourea. Diffuse reflectance spectroscopy showed that this powder displayed an absorbance curve over the scanned region which could imply the presence of titanium dioxide. If titanium dioxide was present there was no shift in absorbance with the band gap of 3.4 eV which is comparable to the undoped titanium dioxide (**Figure 39**). SEM results showed the presence of randomly orientated crystal structures which was in accord with our prediction that this was an amorphous powder (**Figure 40**).

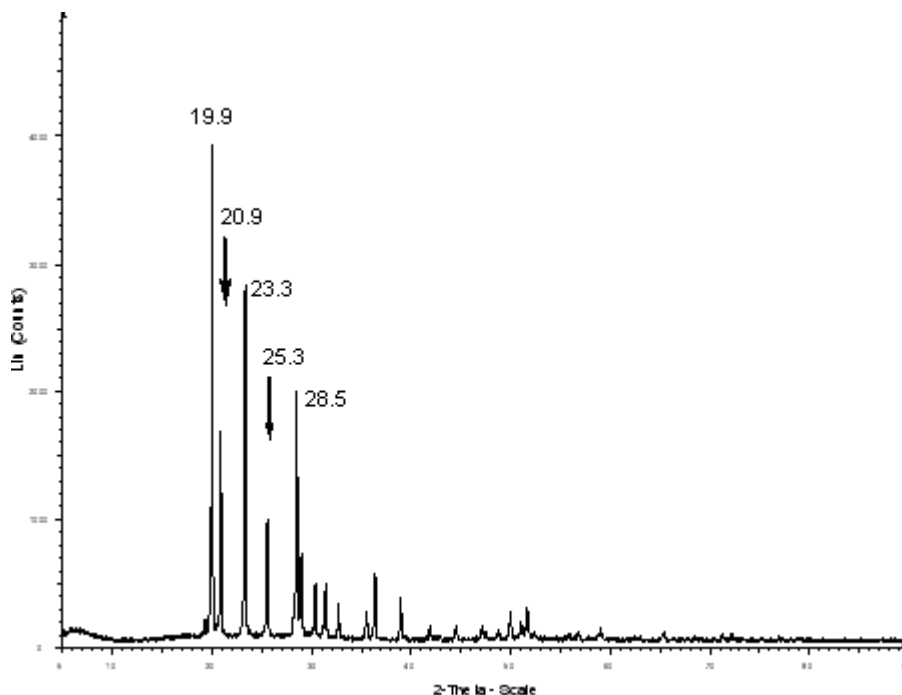


**Figure 38: Powder x-ray diffraction pattern for sulfur doped titanium dioxide**

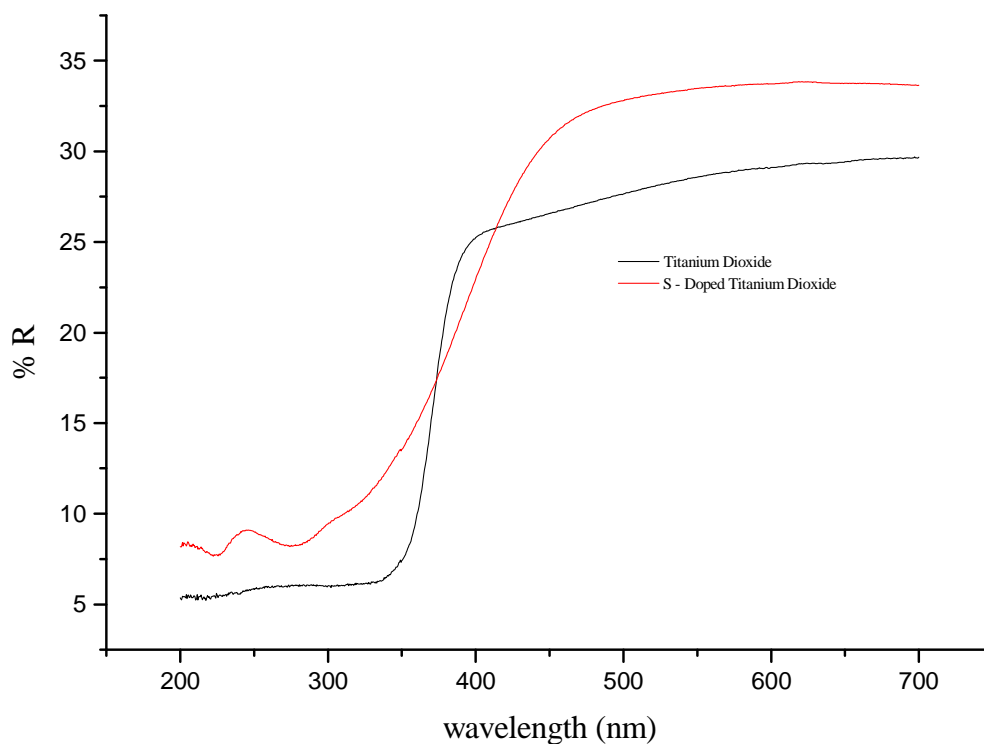
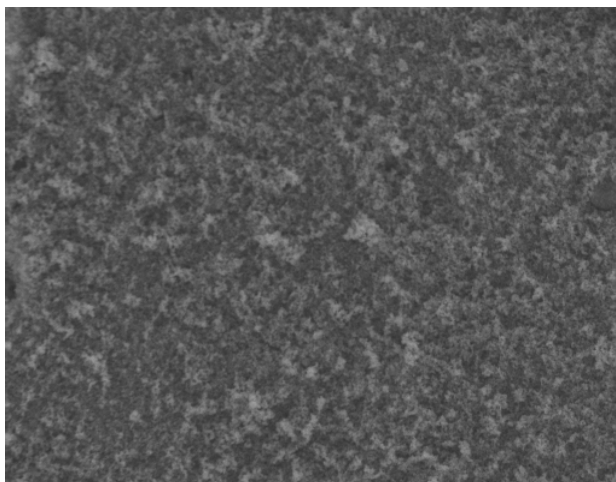
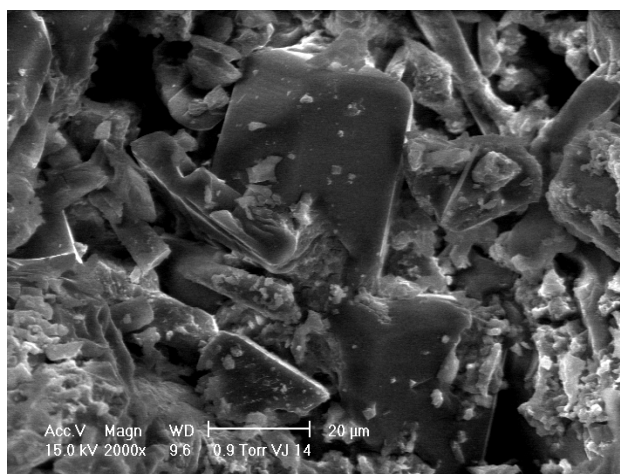


**Figure 39: Diffuse reflectance spectra for sulfur doped titanium dioxide and crystalline titanium dioxide**





(a)



(b)

**Figure 40: SEM image of (a) titanium dioxide and (b) sulfur doped titanium dioxide**

The sulfur doped titanium dioxide was ‘mapped’ in order to gain an understanding of the elemental distribution in the powder and provide conclusive proof for the presence of titanium dioxide. The process involves taking an SEM image and scanning that image for elemental distribution. The dots indicate the distribution of the various elements across that image. Ideally, it would be useful to have all four images together to compare the distribution of the elements. However, this would require an adjustment of image size

which consequently, affects the image quality and results in an inaccurate assessment of element distribution. For this study, the image and each elements distribution is provided separately for a clear and definite element distribution (**Figures 41-43**). From the mapped image, it is evident that titanium and oxygen are present (and by implication titanium dioxide). Based on this result (and the XRD and diffuse reflectance spectroscopy) it was concluded that titanium dioxide is present in the amorphous state with thiourea present.

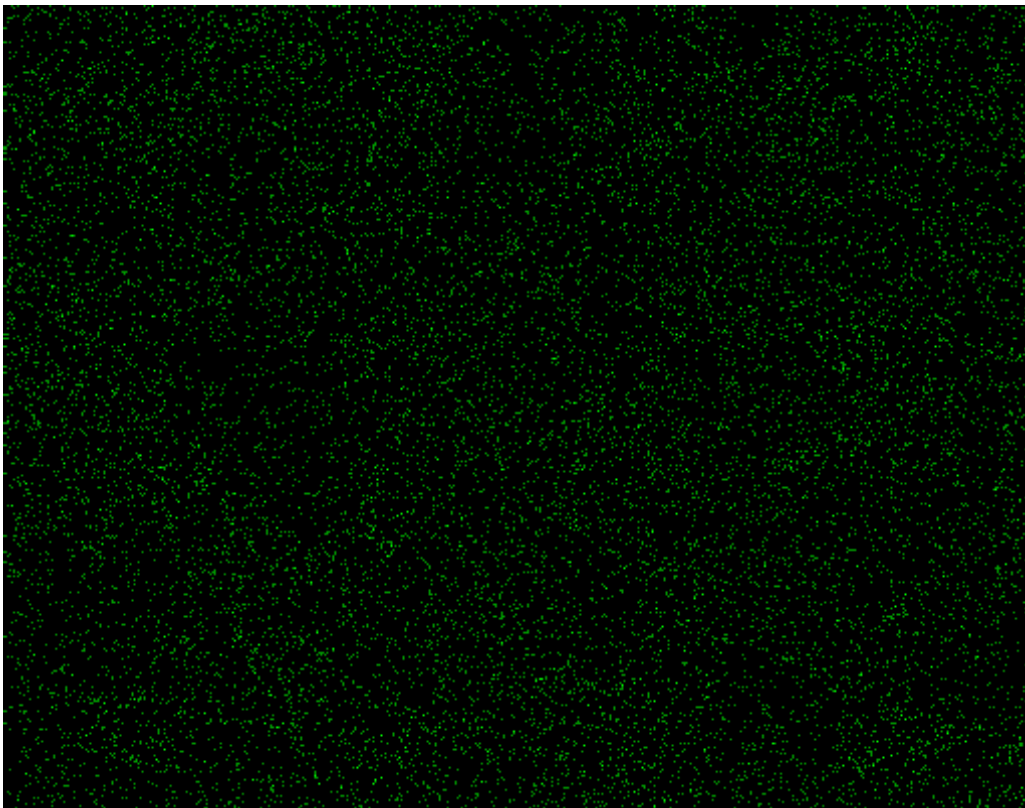
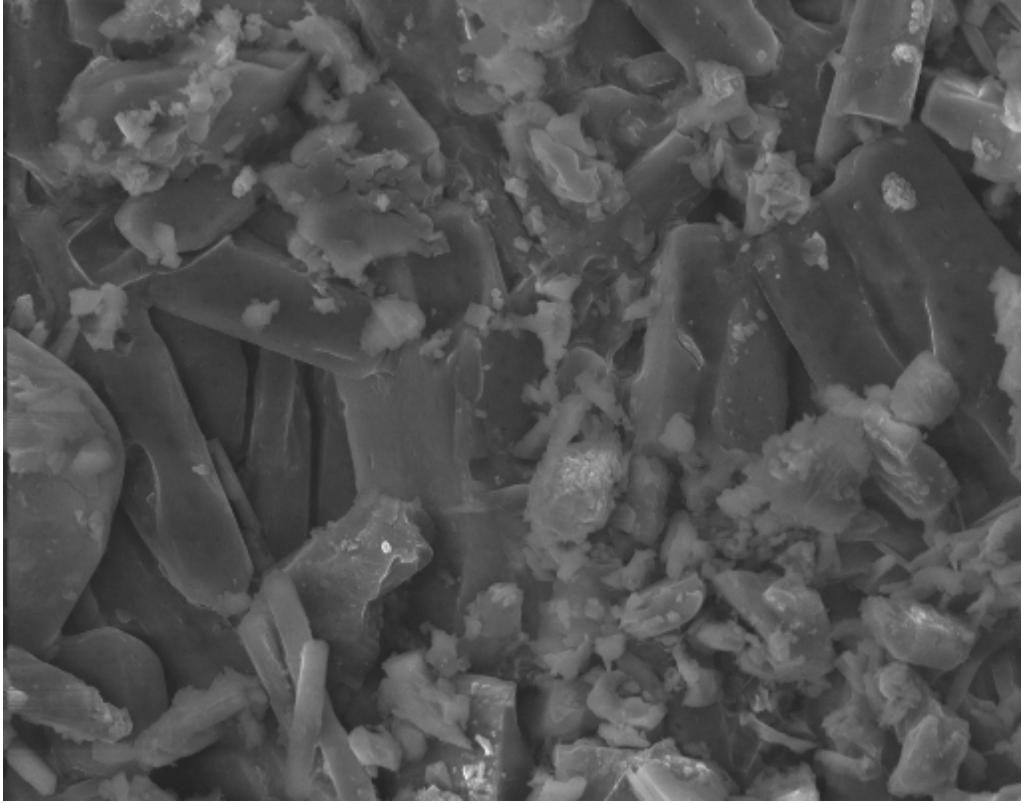


**Figure 41: Oxygen distribution throughout the scanned region**

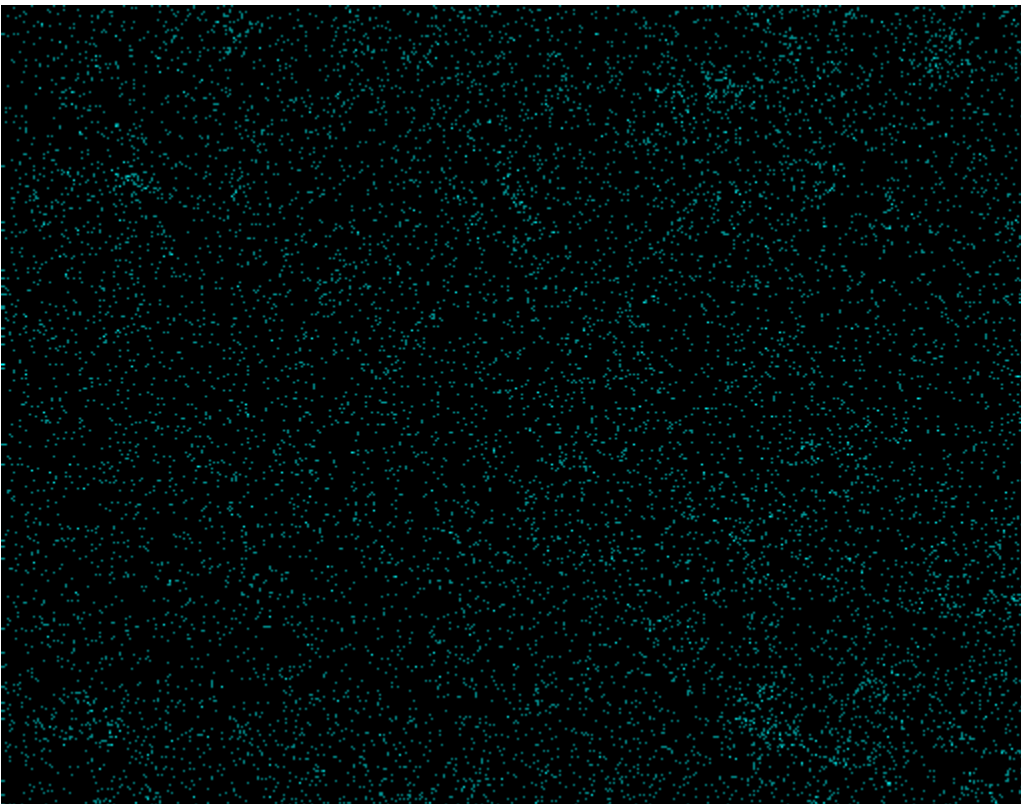
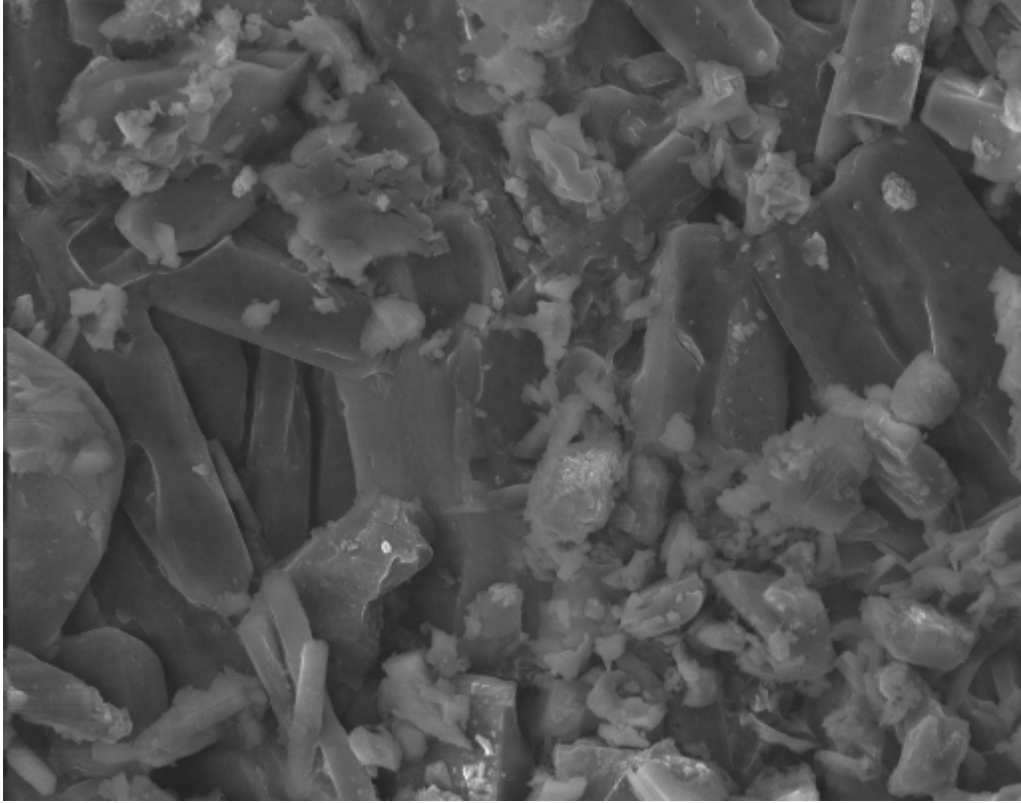


**Figure 42: Titanium distribution throughout the scanned region**

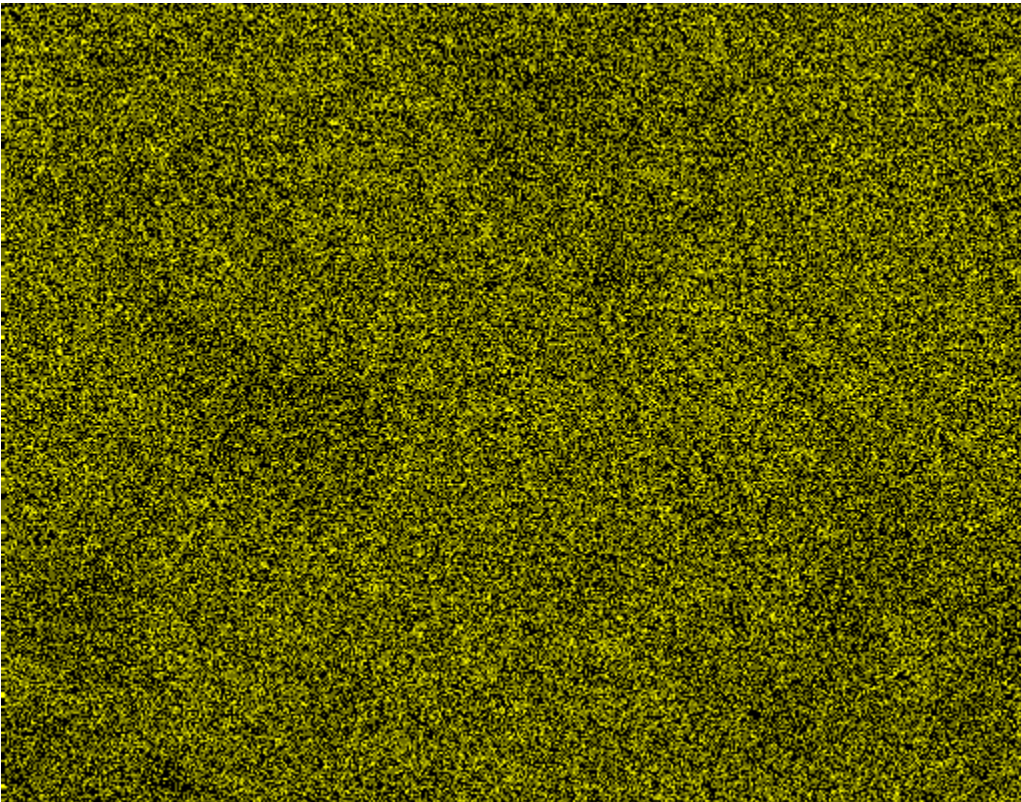
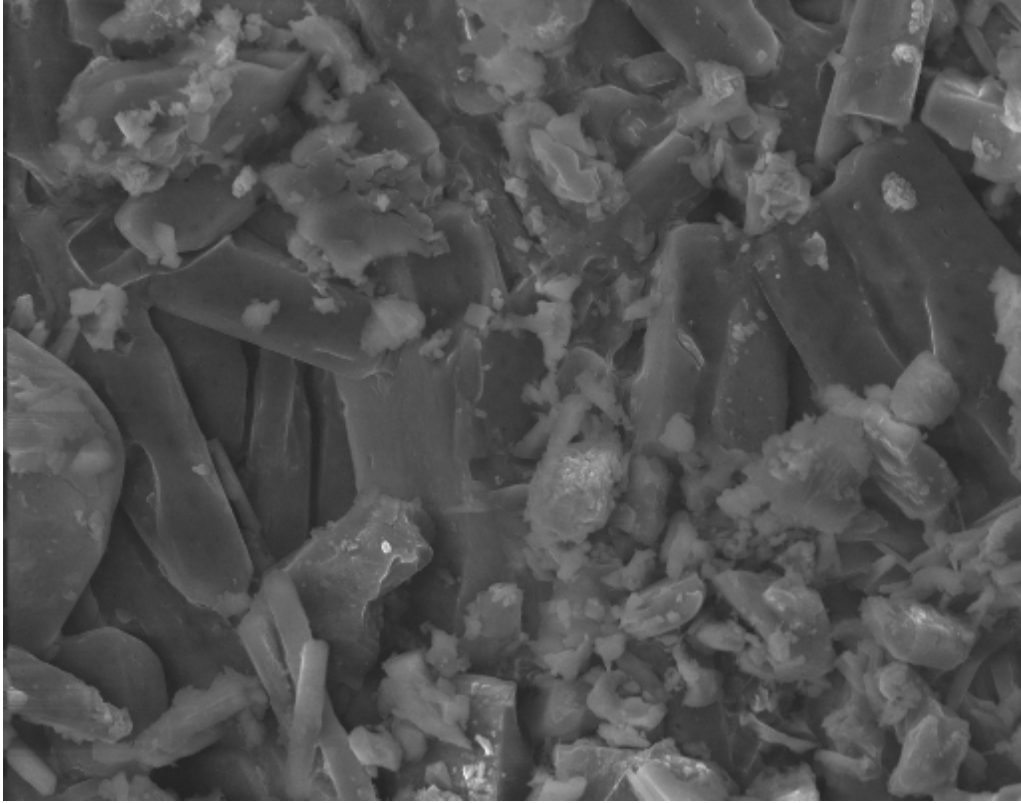


**Figure 43: Sulfur distribution throughout the scanned region**

### 3.4.8 Iodine doped titanium dioxide

Iodine doped titanium dioxide was prepared using a modified procedure to that outlined by Cai and co workers<sup>142</sup> in which titanium isopropoxide was added to a solution containing iodic acid dissolved in deionized water. The mixture was stirred for 5 hours and placed in an oven at 100°C for 3 hours followed by calcination at 400°C for 3 hours to afford a pink powder. Since anatase iodine doped titanium dioxide are known to be yellow in colour,<sup>142</sup> this was a most surprising result. XRD showed that this powder was purely amorphous (which may explain the pink powder) as indicated by the presence of no assignable peaks and a diffuse hump indicative of amorphous powders (**Figure 44**). Diffuse reflectance revealed that a definite decrease in band gap had occurred as well as two transitions being present – the fundamental UV transition and a visible transition as a result of the iodine doping (**Figure 45**). The band gap of iodine doped titanium dioxide was estimated to be 2.3 eV corresponding to a wavelength of 539 nm.

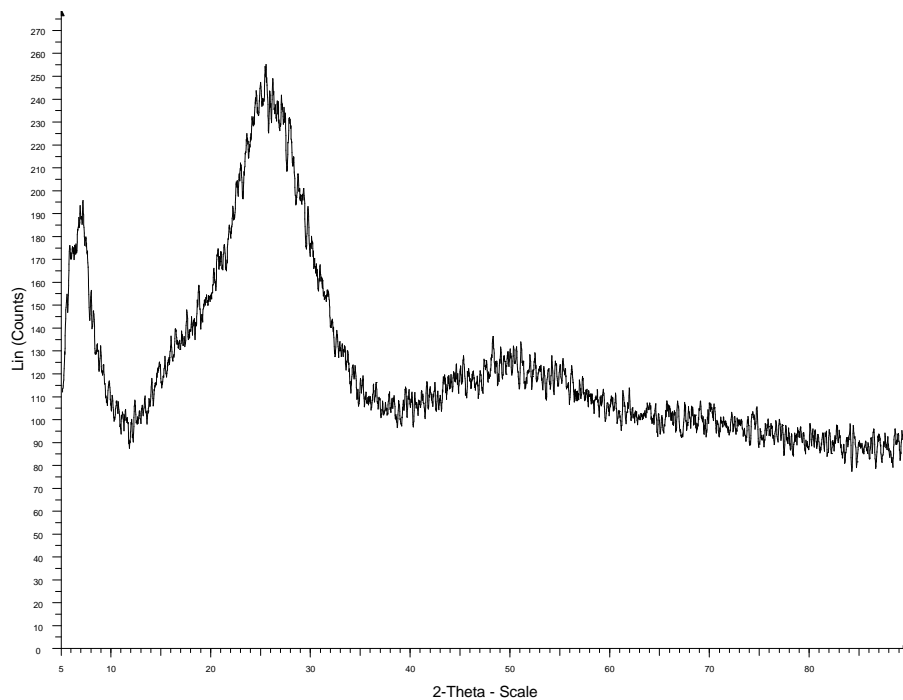


**Figure 44: Powder x-ray diffraction pattern for iodine doped titanium dioxide**

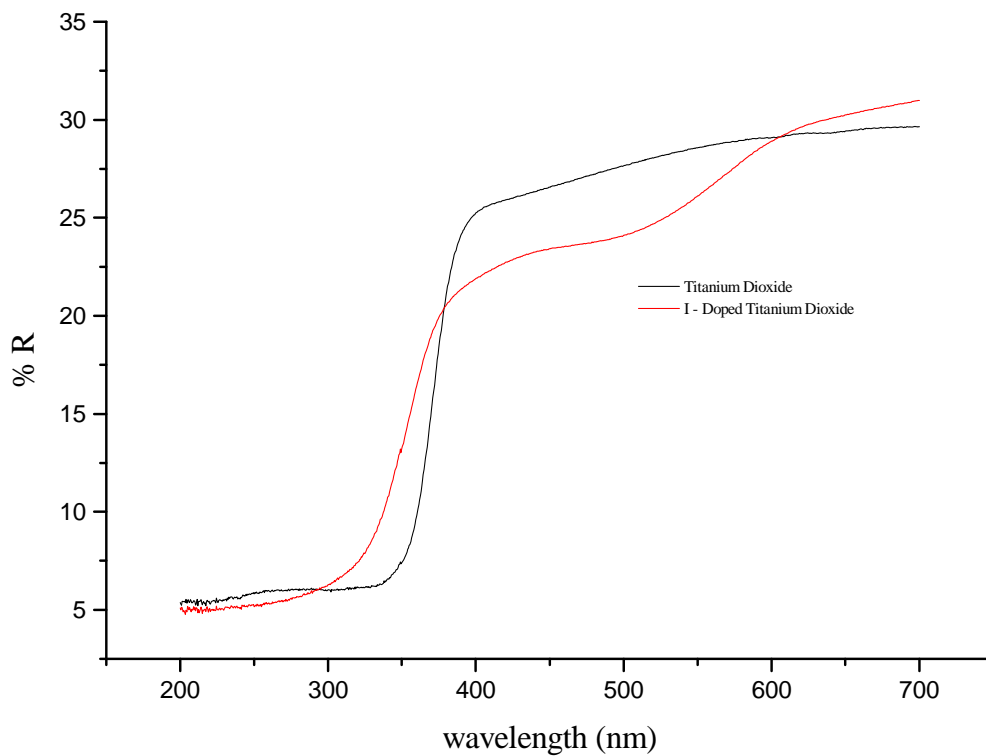


**Figure 45: Diffuse reflectance spectra for iodine doped titanium dioxide and crystalline titanium dioxide**

### 3.5 SUMMARY OF DOPING RESULTS

The results of the doping study have been summarized in Table 9. A series of doped titanium dioxide powders were prepared and the effect of the dopant monitored by XRD and diffuse reflectance spectroscopy. In all cases, the doped titanium dioxide powder was compared with undoped anatase titanium dioxide to gauge any improvement in photocatalytic ability. Nano and Ag-doped titanium dioxide displayed negligible changes in band gap but Ag-doped titanium dioxide displayed a higher absorbance in the visible region (400-700 nm) compared to undoped anatase titanium dioxide. P-doped titanium dioxide was prepared in an amorphous state with an increase in band gap but displayed a lower absorbance than titanium dioxide throughout the spectral window. B-doped titanium dioxide was synthesized in a partially crystalline phase, demonstrating a decrease in band gap with a UV and visible light transition present. N and S-doped powders showed negligible changes in band gap but the N-doped powder showed a higher absorbance in the visible region compared to titanium dioxide. I-doped titanium dioxide was synthesized in an amorphous state, as evidenced by XRD, with a decrease in band gap with the presence of two transitions corresponding to a fundamental UV transitions and visible transition as a result of the iodine doping.



**Table 9: Summary of results obtained from doping study**

| <b>Powder</b>             | <b>Band gap (eV)</b> | <b>Crystal phase</b>  | <b>Comment<sup>a</sup></b>   |
|---------------------------|----------------------|-----------------------|--|
| TiO <sub>2</sub>          | 3.4                  | anatase               | -  |
| nano-TiO <sub>2</sub>     | 3.5                  | anatase               | -larger band gap<br>-lower absorbance throughout spectral window           |
| Ag-doped TiO <sub>2</sub> | 3.4                  | anatase               | -no significant change in band gap<br>-higher absorbance in visible region |
| P-doped TiO <sub>2</sub>  | 3.7                  | amorphous             | -increase in band gap<br>-lower absorbance throughout spectral window      |
| B-doped TiO <sub>2</sub>  | 2.3                  | partially crystalline | -decrease in band gap<br>-higher absorbance in visible region              |
| N-doped TiO <sub>2</sub>  | 3.4                  | partially crystalline | -no significant change in band gap<br>-higher absorbance in visible region |
| S-doped TiO <sub>2</sub>  | 3.4                  | partially crystalline | -no significant change in band gap<br>-lower absorbance                    |
| I-doped TiO <sub>2</sub>  | 2.3                  | amorphous             | -decrease in band gap<br>-higher absorbance                                |

<sup>a</sup> Compared to undoped anatase titanium dioxide

### 3.6 MECHANISM OF DOPING

#### 3.6.1 Literature models for the response of doped titanium dioxide

The doping of titanium dioxide results in a definite improvement in the photocatalytic ability of titanium dioxide. Accordingly, it is appropriate to offer some insight into the mechanism of the response of the doped material. At the outset it is worth mentioning that there is some debate in the literature concerning the doping mechanism and, in the present case attempts have been made to correlate the experimentally obtained results with literature rationalization. Attention will be focused specifically on boron and iodine doped titanium dioxide due to their interesting diffuse reflectance spectra. Since nitrogen doped titanium dioxide is the most widely investigated doped material, it is unsurprising that the two most common models are based on nitrogen doped titanium dioxide.

The first model, reported by Asahi and co-workers<sup>143</sup> suggested that the doping of titanium dioxide with nitrogen results in a mixing of the 2p nitrogen states and the 2p oxygen states to produce a new band resulting in a net decrease in band gap (**Figure 46**) Asahi and co-workers based this mechanism on X-ray photoelectron spectroscopy (XPS) and first principle calculations.

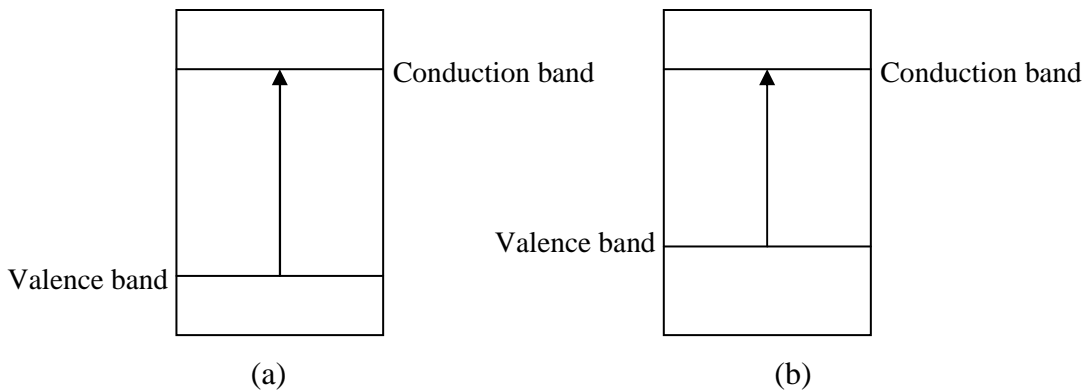


**Figure 46: Schematic representation of (a) undoped titanium dioxide and (b) doped titanium dioxide resulting from mixing of energy states**

The alternative theory suggested by Hashimoto and co-workers claimed that the introduction of nitrogen gives rise to a separate energy level above the valence band.<sup>144</sup> They monitored the degradation of isopropyl alcohol under UV and visible irradiation. Consistently higher results were obtained under UV irradiation which is only possible if two separate energy levels are present. Under UV irradiation, an electron is promoted from the valence band and the impurity level while under visible light irradiation an electron is promoted from the impurity level only (**Figure 47**).

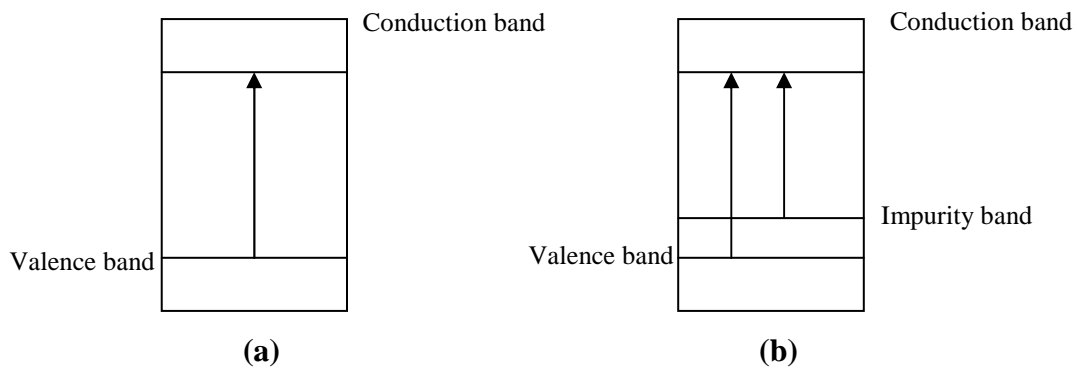


**Figure 47: Schematic representation of (a) titanium dioxide and (b) doped titanium dioxide showing the presence of two separate energy levels**

#### 4.6.2 Boron and Iodine doped titanium dioxide

In 2005, Manorama and co-workers reported the presence of two distinct band transitions based on diffuse reflectance spectroscopy for the doping of titanium dioxide with nitrogen (**Figure 48**).<sup>141</sup> Manorama assigned the two transitions as the fundamental UV transition (385 nm) and a visible transition (495 nm) which arise from nitrogen doping and claimed that this confirmed the presence of two different surface states that were characteristic of doped and undoped titanium dioxide.

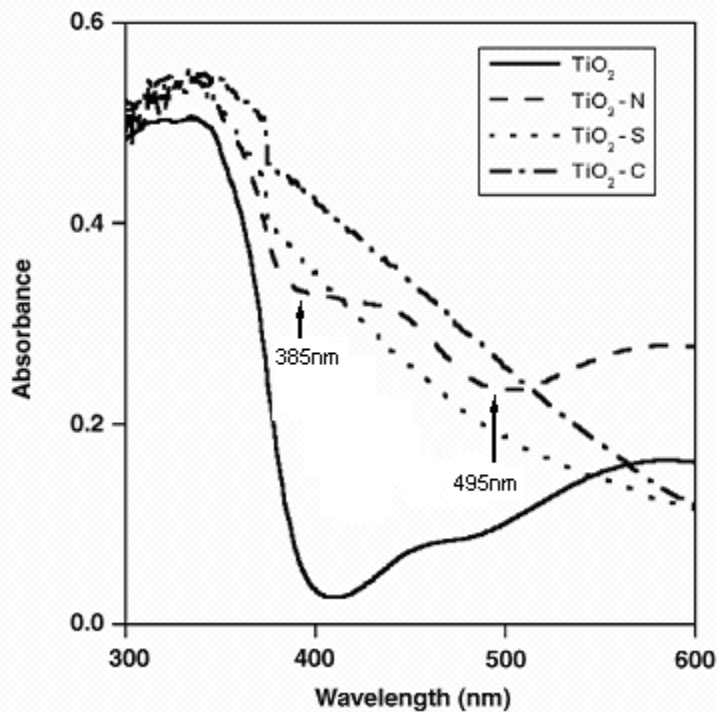


**Figure 48: Diffuse reflectance spectrum obtained by Manorama and co workers<sup>141</sup>**

The mechanism proposed is similar to Hashimoto and co-workers except that Hashimoto claimed an isolated narrow band formed above the valence band, while Manorama claimed that doping introduces a series of intermediate levels (**Figure 49**).

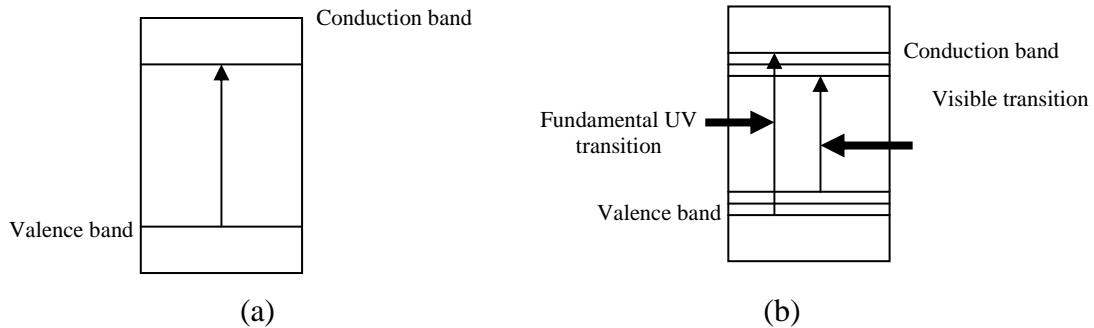


**Figure 49: Schematic representation of (a) titanium dioxide and (b) doped titanium dioxide resulting from the formation of intermediate levels**

In the case of iodine and boron doped titanium dioxide, evidence exists for the model proposed by Manorama and co-workers. The diffuse reflectance spectrum of boron and iodine doped titanium dioxide display two distinct transitions (**Figure 50**), similar to those reported by Manorama, corresponding to the fundamental band transition and the visible transition arising from boron and iodine doping. This confirms the presence of two different surface states characteristic of doped and undoped titanium dioxide.

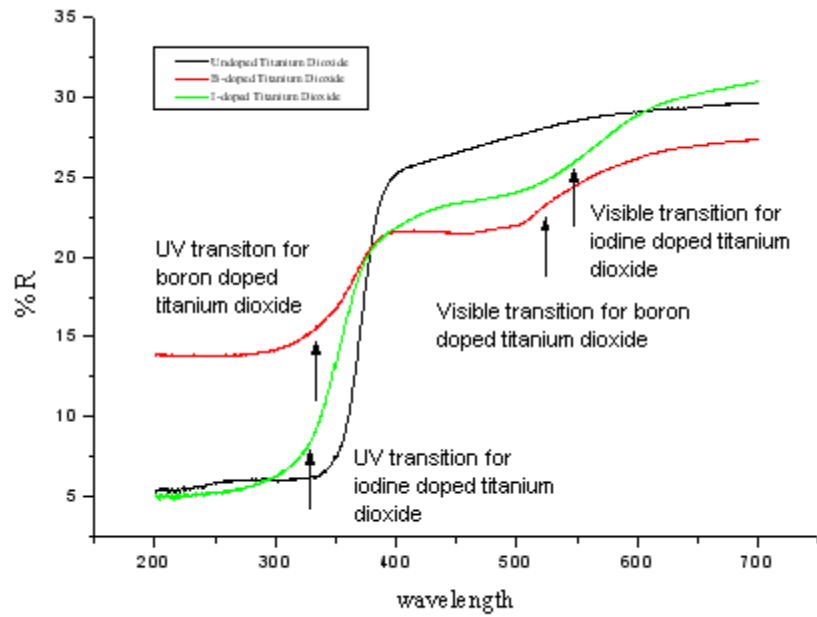
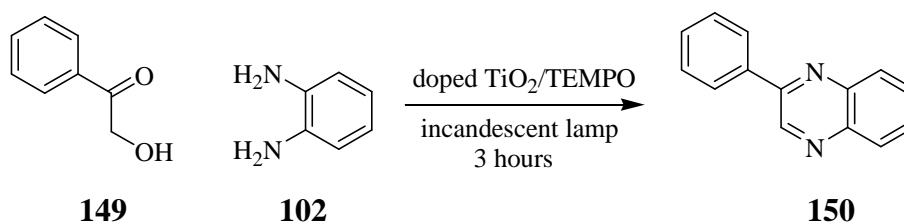


**Figure 50: Diffuse reflectance spectra for boron and iodine doped titanium dioxide showing the ultraviolet and visible transition**

### 3.7 APPLICATION OF DOPED TITANIUM DIOXIDE TOWARDS THE SYNTHESIS OF QUINOXALINES

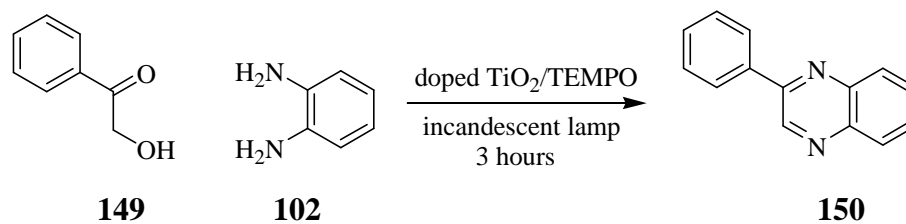
As previously highlighted, the efficiency of doped titanium dioxide is tested by the degradation of dyes. In our case, the efficiency of boron and iodine doped titanium dioxide was tested by the synthesis of quinoxalines. 2-hydroxyacetophenone, *o*-phenylenediamine, doped titanium dioxide and TEMPO were stirred in methanol under an incandescent lamp for 3 hours (**Scheme 69**).



**Scheme 69: Doped titanium dioxide mediated synthesis of quinoxalines**

The mixtures were passed through a short silica plug and the solvent removed *in vacuo* to produce a crude product which was purified using radial chromatography to give the title compound 2-phenylquinoxaline as an orange solid. A summary of the results are given below:

### 3.7.1 Summary of results obtained for the synthesis of 2-phenyl quinoxaline under incandescent lamp irradiation



anatase titanium dioxide: 25%

B-doped titanium dioxide: 60%

I-doped titanium dioxide: 73%

#### Scheme 70: Comparison of doped and crystalline titanium dioxide for the synthesis of quinoxalines

During the preliminary investigations using undoped titanium dioxide, 2-phenylquinoxaline was obtained in an isolated yield of 25% in 3 hours. Under identical conditions, boron doped titanium dioxide produced the desired quinoxaline in a superior yield of 60%. The use of iodine doped titanium dioxide for this coupling reaction produced the quinoxaline in an isolated yield of 73% in 3 hours. This result validated the hypothesis that the photocatalytic ability of titanium dioxide can be improved by doping. The significant improvement may be attributed to the decrease in band gap as well as the low crystallinity of boron and iodine doped titanium dioxide.



## Conclusions

Titanium dioxide was evaluated as a potential tandem oxidation process type catalyst in the synthesis of a series of quinoxaline derivatives. Titanium dioxide, being a photocatalyst, was evaluated under a number of different energy sources with the best results obtained under microwave irradiation. Under microwave irradiation, quinoxaline derivatives were synthesized in yields ranging from 54-88% in 10-20 minutes. The yields obtained under a titanium dioxide mediated tandem oxidation process were compared with other established tandem oxidation type catalysts and in most cases were shown to be significantly superior.

This project also illustrated the emergence of a new electron acceptor/co-catalyst with the use of TEMPO resulting in shorter reaction times, cleaner product distributions and higher yields.

The titanium dioxide mediated oxidation was less successful on complex, multifunctional substrates such as hydrocortisone as well as in the Wittig reaction. Nevertheless, the results obtained suggest a degradation of the starting reactants which reinforces the notion of the strong oxidizing strength of titanium dioxide.

In an attempt to improve the reactivity of a titanium dioxide mediated oxidation a doping study was undertaken. Titanium dioxide was doped with silver, phosphorus, boron, nitrogen, sulfur and iodine and the effect of the dopant monitored by powder X-ray diffraction (XRD) and diffuse reflectance spectroscopy. Of the powders synthesized, boron and iodine showed the greatest shift in absorbance into the visible region. Both the boron and iodine doped powders were in agreement with a literature model for the photocatalytic response of doped titanium dioxide powders. The quinoxaline derivative was synthesized in a yield of 60% and 73% for boron and iodine doped titanium dioxide, compared with a yield of 25% for the undoped powder.

To the best of our knowledge, very few reports exist showing the application of titanium dioxide in organic synthesis, nevertheless results from the present study are highly encouraging although much research still needs to be undertaken.

### **Future work**

Titanium dioxide has been shown in this study to be a highly efficient oxidant for the synthesis of quinoxalines *via* the tandem oxidation process. Preliminary investigations into a more complex substrate and the Wittig reaction were unfortunately unsuccessful, indicative of the high oxidative potential of titanium dioxide. Future studies should be directed towards tempering the reactivity of titanium dioxide which would allow for expansion into the Wittig reaction. During the course of these studies, the complexity of the mechanism by which titanium dioxide operates was highlighted and consequently future studies should be directed at addressing this issue. A mechanistic study should be carried out using EPR to monitor hydroxyl radical formation. The EPR will provide detail of the quantity of hydroxyl radicals formed, consequently resulting in information about the active oxidizing species. Gaining insight into the mechanism will allow for further understanding of titanium dioxide chemistry leading to new and exciting tandem oxidation reactions.

# Chapter 4: Experimental

## 4.1 GENERAL METHODS

### *Instrumentation:*

NMR spectra were recorded using a Bruker Avance III 400 spectrometer equipped with a 5 mm BBO-Z probe at 30°C.

<sup>1</sup>H NMR spectra were recorded at 400 MHz, <sup>13</sup>C NMR spectra were recorded at 100 MHz.

Spectra were referenced against either the CDCl<sub>3</sub> singlet at 7.26 ppm or the central line of CDCl<sub>3</sub> triplet at 77.0 ppm.

IR spectra were recorded on either Perkin Elmer Spectrum One or a Bruker ALPHA spectrometer.

Powder X-ray diffraction was obtained from the University of Witwatersrand using Cu K $\alpha$  irradiation.

Low resolution (Electron Impact) mass spectra were recorded using a ThermoFinnigan trace GC, coupled with PolarisQ mass spectra.

Melting points were determined using a Kofler hot-stage melting apparatus.

Scanning Electron Microscope (SEM) images were recorded on Philips XL30 ESEM.

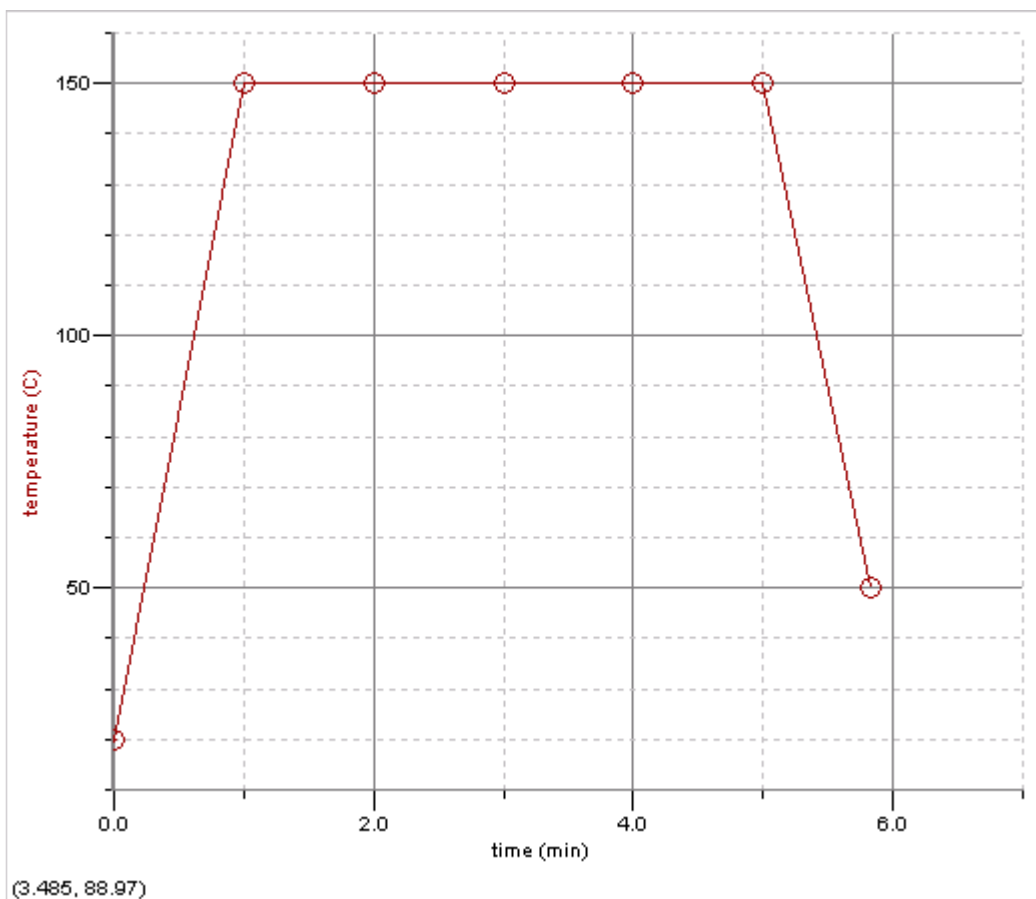
Diffuse Reflectance Spectra were obtained using a Cary 500 UV-Vis-NIR spectrophotometer.

High resolution mass spectra were obtained using a Waters Acquity (LCT premier) ultra performance liquid chromatography-mass spectrometry instrument.

### *Microwave:*

All reactions were conducted using a CEM Focused Microwave™ Synthesis system which uses an infrared sensor located below the microwave cavity floor to measure temperature

## **Temperature/Time profile for 2-phenylquinoxaline [100]**



- Reaction temperature and profile was monitored every minute during a 5 minute run.
- After the 5 minutes, the reaction vessel was rapidly cooled to 50 °C by the instrument.
- Once a temperature of 50 °C was reached, the instrument stopped cooling and released the residual pressure.

NOTE: The reaction time of 5 minutes includes the time taken for the microwave instrument to increase the temperature from room temperature to 150°C.

### *Chemicals:*

Reagents were used as received from the supplier except for  $\alpha$ -hydroxy ketone **124** which was synthesized from the corresponding methyl ketone using the method described by Moriarty *et al.*<sup>114</sup>

### *Chromatography:*

Radial chromatography was performed on the Harrison Research Chromatatron (Model 7924T) with the solvent system delivered by gravity flow using a 1mm layer of Merck silica gel (7749). Thin layer chromatography was carried out using silica gel 60 F<sub>254</sub> aluminum backed plates. The plates were viewed under UV light and developed in anisaldehyde thereafter.

### *Explanation of NMR abbreviations:*

s – singlet; d – doublet, dd – doublet of doublet, tt – triplet; tt – triplet of triplet; m – multiplet (Any, non-first order, signal with a multiplicity greater than a quartet.)

### *Spectra:*

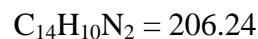
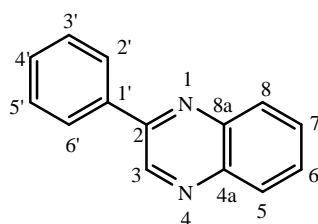
All spectra referred to in the discussion have been included within the text with supplementary spectra included in an electronic format. NMR spectra have been included as word documents. The original FIDs have also been submitted to facilitate the viewing process. IR, GC/MS and HRMS as well as diffuse reflectance data tables for the doped samples have been included as word documents. Each folder has been designated its IUPAC name and numbered as it appears in the text.

## 4.2 PROCEDURES AND SPECTROMETRIC DATA

### Optimization of reaction conditions using the synthesis of 2-phenylquinoxaline as a test reaction

#### Under natural sunlight in the absence of TEMPO

#### 2-Phenylquinoxaline [150]



To a solution of 2-hydroxyacetophenone (0.068g, 0.50mmol) in methanol was added *o*-phenylenediamine (0.054g, 0.50mmol) and  $\text{TiO}_2$  (0.040g, 0.50mmol) and the mixture stirred under natural sunlight. After 3 hours, the reaction mixture was filtered through a short silica plug and the solid residues washed well with dichloromethane. The solvent was removed *in vacuo* to produce a crude product which was purified using radial chromatography to afford the title compound as an orange solid (m.p. 75-76°C) (lit.<sup>145</sup> 79-80 °C); (0.028 g, 27%);  $R_f$  0.46 (3 : 1 PE : EtOAc).

$^1\text{H}$  NMR (400MHz,  $\text{CDCl}_3$ ):  $\delta$  (ppm) = 7.55-7.60 (3H, m, *H*- 3', 4', 5'), 7.79-7.82 (2H, m, *H*- 2', 6'), 8.15 (2H, m, *H*- 6, 7), 8.21 (m, 2H, *H*- 5, 8), 9.35 (s, 1H, *H*- 3).

$^{13}\text{C}$  NMR (100MHz,  $\text{CDCl}_3$ ):  $\delta$  (ppm) = 127.5 (*C*- 2', 6'), 127.6 (*C*- 4'), 129.2 (*C*- 6, 7), 129.6 (*C*- 3'), 129.7 (*C*- 5'), 130.2 (*C*- 5), 130.4 (*C*- 8), 136.8 (*C*- 1'), 141.4 (*C*- 8a), 142.4 (*C*- 4a), 143.2 (*C*- 2), 151.9 (*C*- 3).

$\nu_{\text{max}}$  (neat) = 1599, 1541, 1488, 1445, 1305  $\text{cm}^{-1}$ .

MS (EIMS):  $m/z$  (%) = 206 [ $\text{M}^+$ ] (100); 179 (38), 178 (22), 32 (20), 28 (48).

### **Under the incandescent lamp in the absence of TEMPO**

To a solution of 2-hydroxyacetophenone (0.068g, 0.50mmol) in methanol was added *o*-phenylenediamine (0.054g, 0.50mmol) and TiO<sub>2</sub> (0.040g, 0.50mmol) and the mixture stirred under the incandescent lamp irradiation. After 48 hours, the reaction mixture was filtered through a short silica plug and the solid residues washed well with dichloromethane. The solvent was removed *in vacuo* to produce a crude product. Analysis by NMR spectroscopy revealed only the presence of starting material, with no evidence of the desired product.

### **Under an incandescent lamp in the presence of TEMPO**

To a solution of 2-hydroxyacetophenone (0.068g, 0.50mmol) in methanol was added *o*-phenylenediamine (0.054g, 0.50mmol), TiO<sub>2</sub> (0.040g, 0.50mmol) and TEMPO (0.008g, 0.050mmol) and the mixture stirred under incandescent lamp irradiation. After 3 hours, the reaction mixture was filtered through a short silica plug and the solid residues washed well with dichloromethane. The solvent was removed *in vacuo* to produce a crude product which was purified using radial chromatography to afford the title compound as an orange solid in a yield of 25%. Spectroscopic data consistent with previously reported data.

### **Under an incandescent lamp in the presence of TEMPO**

To a solution of 2-hydroxyacetophenone (0.068g, 0.50mmol) in methanol was added *o*-phenylenediamine (0.054g, 0.50mmol), TiO<sub>2</sub> (0.040g, 0.50mmol) and TEMPO (0.008g, 0.050mmol) and the mixture stirred under incandescent lamp irradiation overnight. The reaction mixture was filtered through a short silica plug and the solid residues washed well with dichloromethane. The solvent was removed *in vacuo* to produce a crude product which was determined by NMR spectroscopic analysis to contain the desired quinoxaline in quantitative yield.

### **Under natural sunlight in the absence of TEMPO**

To a solution of 2-hydroxyacetophenone (0.068g, 0.50mmol) in methanol was added *o*-phenylenediamine (0.054g, 0.50mmol) and TiO<sub>2</sub> (0.040g, 0.50mmol) and TEMPO (0.008g, 0.50mmol) and the mixture stirred under natural sunlight. After 3 hours, the reaction mixture was filtered through a short silica plug and the solid residues washed well with dichloromethane. The solvent was removed *in vacuo* to produce a crude product which was purified using radial chromatography to afford the title compound as an orange solid in an isolated yield of 90%. Spectroscopic data was in agreement with previously reported data.

### **Under open vessel microwave irradiation**

(1) To a solution of 2-hydroxyacetophenone (0.068g, 0.50mmol) in methanol was added *o*-phenylenediamine (0.054g, 0.50mmol) and TiO<sub>2</sub> (0.040g, 0.50mmol) and the mixture stirred under microwave irradiation. After 10 minutes, the reaction mixture was filtered through a short silica plug and the solid residues washed well with dichloromethane. The solvent was removed *in vacuo* to produce a crude product which by NMR spectroscopic analysis was found to consist of starting material only.

(2) To a solution of 2-hydroxyacetophenone (0.068g, 0.50mmol) in methanol was added *o*-phenylenediamine (0.054g, 0.50mmol) and TiO<sub>2</sub> (0.040g, 0.50mmol) and the mixture stirred under microwave irradiation. After 90 minutes, the reaction mixture was filtered through a short silica plug and the solid residues washed well with dichloromethane. The solvent was removed *in vacuo* to produce a crude product which by NMR spectroscopic analysis to contain the desired quinoxaline in quantitative yield. Spectroscopic data was in agreement with previously reported data.

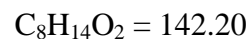
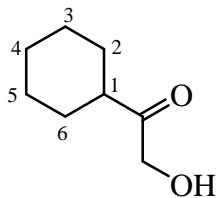


### Under closed vessel microwave irradiation

2-hydroxyacetophenone (0.068g, 0.50mmol), *o*-phenylenediamine (0.054g, 0.50mmol), TiO<sub>2</sub> (0.040g, 0.50mmol) and 2, 2, 6, 6-Tetramethylpiperidine-1-oxyl (TEMPO) (0.0080g, 0.050mmol) were added to a sealed 10mL CEM Discover<sup>®</sup> reaction vial equipped with a magnetic stirrer bar. The reaction vial was irradiated (with cooling) for 10 min (2 x 5 min) at 150°C, after which the vessel was rapidly cooled to 50°C by the unit. The reaction mixture was diluted with dichloromethane (DCM) and passed through a short silica plug. The solvent was removed *in vacuo* to produce a crude product which was purified using radial chromatography (3:1 PE:EtOAc) to produce the title compound **100** as an orange solid (0.089g, 87%).

### Synthesis of quinoxaline derivatives

#### 1-Cyclohexyl-2-hydroxyethanone [217]



Cyclohexyl methyl ketone (0.63g, 5.0 mmol) was added to a stirred solution of trifluoroacetic acid (0.77 ml, 10 mmol), water (5.0 ml), and acetonitrile (25 ml). [Bis(trifluoroacetoxy)] iodobenzene (4.3g, 10 mmol) was added and the mixture heated to reflux for four hours. The reaction mixture was concentrated *in vacuo* to remove the acetonitrile. The residue was portioned between dichloromethane (125 ml) and water (50 ml). The aqueous phase was extracted with dichloromethane (3 x 25 ml). The combined organic extracts were then washed with a saturated solution of sodium hydrogen carbonate (3 x 25 ml), dried over magnesium sulfate and concentrated *in vacuo*

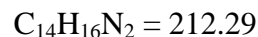
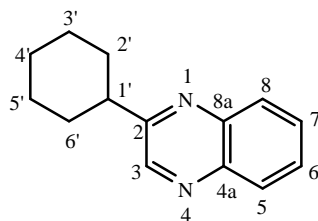
to produce a crude product which was purified using radial chromatography to produce the title compound **217** as a yellow oil; (0.64 g; 90%);  $R_f$  0.34 (1: 1 PE : EtOAc).

$^1\text{H}$  NMR (400 MHz,  $\text{CDCl}_3$ ):  $\delta$  (ppm) = 1.14 – 1.30 (4H, m, *H*- 3, 5), 1.31 – 1.44 (2H, m, *H*- 4), 1.71 – 1.84 (4H, m, *H*- 2, 6), 2.36 (1H, m, *H*- 1), 4.30 (2H, s,  $\text{CH}_2$ ).

$^{13}\text{C}$  NMR (400 MHz,  $\text{CDCl}_3$ ):  $\delta$  (ppm) = 25.4 (*C*- 3, 5), 25.6 (*C*- 4), 28.3 (*C*- 2, 6), 47.1 (*C*- 1), 66.4 ( $\text{CH}_2\text{OH}$ ), 212.7 ( $\text{C}=\text{O}$ ).

MS (EIMS): ( $m/z$ ) (%) = 142 [ $\text{M}^+$ ] (1%), 111 (28), 83 (87), 55 (100), 39 (26).

## 2-Cyclohexylquinoxaline [218]



Prepared by the procedure given for **150** under microwave irradiation using 1-cyclohexyl-2-hydroxyethanone (0.106g, 0.50mmol) and *o*-phenylenediamine (0.054g, 0.50mmol). Purified using radial chromatography (2: 1 PE : EtOAc) to produce the title compound **218** as a brownish solid (m.p. 41 °C) (lit.<sup>97</sup> 48 °C); (0.064 g, 60%);  $R_f$  0.80 (2: 1 PE : EtOAc).

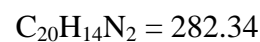
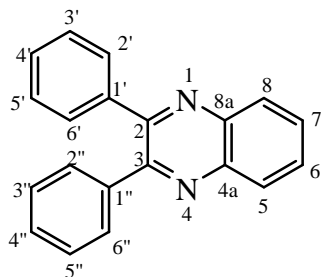
$^1\text{H}$  NMR (400MHz,  $\text{CDCl}_3$ ):  $\delta$  (ppm) = 1.40-2.06 (10H, m, *H*- 2', 3', 4', 5', 6'), 3.00 (1H, tt,  $J$  12.0 Hz  $J$  3.5, *H*- 1'), 7.70 (2H, m, *H*- 6, 7); 8.07 (2H, m, *H*- 5, 8); 8.79 (1H, s, *H*-3);

$^{13}\text{C}$  NMR (100MHz,  $\text{CDCl}_3$ ):  $\delta$ (ppm) = 25.2 (*C*- 4'), 25.8 (*C*- 3', 5'), 31.7 (*C*- 2', 6'), 44.4 (*C*- 1'), 128.8 (*C*- 6), 129.1 (*C*- 7), 129.1 (*C*- 5) 129.7 (*C*- 8), 140.7 (*C*- 4a), 141.4 (*C*- 8a), 144.3 (*C*- 3), 160.4 (*C*-2).

$\nu_{\text{max}}$  (neat) = 1559, 1491, 1449, 1368  $\text{cm}^{-1}$

MS (EIMS) :  $m/z$  (%) = 212 [ $\text{M}^+$ ] (84), 183 (25), 169 (27), 157 (100), 144 (71).

## 2,3-Diphenylquinoxaline [187]



Prepared using the procedure given for **150** under microwave irradiation using benzoin (0.106 g, 0.50mmol) and *o*-phenylenediamine (0.054 g, 0.50mmol) but reactants irradiated for 20 minutes. Purified using radial chromatography (9:1 PE : EtOAc) to give the title compound **187** as a yellow solid: (m.p. 123 °C) (lit.<sup>116</sup> 124 °C); (0.114 g, 81%);  $R_f$  0.59 (9 : 1 PE : EtOAc);

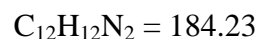
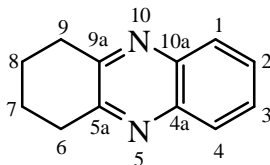
$^1\text{H}$  NMR (400 MHz,  $\text{CDCl}_3$ ):  $\delta$  (ppm) = 7.33-7.40 (6H, m, *H*- 3', 4', 5', 3'', 4'', 5''), 7.53-7.56 (4H, m, *H*- 2', 6', 2'', 6''), 7.78 (2H, m, *H*- 6, 7), 8.19 (2H, m, *H*- 5, 8)

$^{13}\text{C}$  NMR (100 MHz,  $\text{CDCl}_3$ ):  $\delta$  (ppm) = 127.3 (*C*- 2', 6', 2'', 6''), 128.8 (*C*- 4', 4''), 129.2 (*C*- 6, 7), 129.9 (*C*- 3', 5', 3'', 5''), 129.9 (*C*- 5, 8), 139.1 (*C*- 1', 1''), 141.3 (*C*- 4a, 8a), 153.5 (*C*- 2, 3).

$\nu_{\text{max}}$  (neat) = 1596, 1514, 1448, 1346  $\text{cm}^{-1}$ .

MS (EIMS):  $m/z$  = 283 [ $\text{M}+1$ ] (21), 282 [ $\text{M}^+$ ] (92), 281 (100), 178 (23), 178 (21).

### 1,2,3,4-Tetrahydrophenazine [221]



Prepared using the procedure given for **150** using 2-hydroxycyclohexanone dimer (0.057g, 0.500mmol) and *o*-phenylenediamine (0.054g, 0.50mmol). Purified using radial chromatography (1 : 1 PE : EtOAc) to give the title compound **221** as a white solid: (m.p. 90 °C) (lit.<sup>146</sup> 93 – 94 °C); (0.810 g, 88%);  $R_f$  0.54 (1 : 1 PE : EtOAc).

$^1\text{H}$  NMR (400MHz,  $\text{CDCl}_3$ ):  $\delta$ (ppm) = 2.04-2.08 (4H, m, *H*- 6, 9), 3.19-3.20 (4H, m, *H*- 7, 8), 7.66 (2H, m, *H*- 2, 3), 7.97 (2H, m, *H*- 1, 4)

$^{13}\text{C}$  NMR (100MHz,  $\text{CDCl}_3$ ):  $\delta$  (ppm) = 22.8 (*C*- 7, 8), 33.2 (2*C*- 6, 9), 128.3 (2*C*- 2, 3), 128.9 (2*C*- 1, 4), 141.2 (2*C*- 4a, 10a), 154.1 (*C*- 5a, 9a).

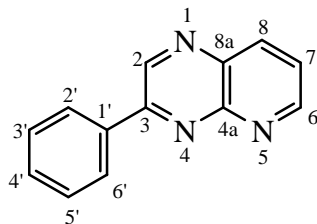
$\nu_{\text{max}}$  (neat) = 1459, 1423, 1384, 1330, 1291, 1238  $\text{cm}^{-1}$ .

MS (EIMS) :  $m/z$  = 185 [ $\text{M}+1$ ] (15), 184 [ $\text{M}^+$ ] (100), 183 (67), 169 (42).

### 2-/3-Phenylpyrido[2,3-*b*]pyrazine [223]

Prepared by the procedure given for **150** using 2-hydroxyacetphenone (0.068g, 0.50 mmol) and 2,3-diaminopyridine (0.054g, 0.50 mmol) but reactants irradiated for 20 minutes. Purified using radial chromatography (EtOAc) to give the title compound **223**, a brown solid, as a mixture of regioisomers with 3-phenylpyrido[2,3-*b*] pyrazine predominating: (0.087 g, 83%);  $R_f$  0.70 (EtOAc).

### 3-phenylpyrido[2,3-*b*] pyrazine



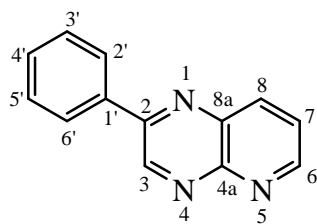
$^1\text{H}$  NMR (400 MHz,  $\text{CDCl}_3$ ):  $\delta$ (ppm) = 7.57-7.62 (3H, m, *H*- 3', 4', 5' ), 7.71 (1H, dd, *J* 8.3Hz, *J* 4.2Hz, *H*- 7), 8.35-8.37 (2H, m, *H*- 2', 6'), 8.49 (1H, dd, *J* 8.3Hz, *J* 1.8Hz, *H*- 8), 9.20 (1H, dd, *J* 4.1Hz, *J* 1.8Hz, *H*- 6), 9.47 (1H, s, *H*- 2).

$^{13}\text{C}$  NMR (400 MHz,  $\text{CDCl}_3$ ):  $\delta$ (ppm) = 124.8 (*C*- 7), 128.1 (*C*- 2', 6'), 129.3 (*C*- 4'), 131.1 (*C*- 3', 5'), 135.8 (*C*- 8), 136.8 (*C*- 1'), 138.2 (*C*- 2), 144.4 (*C*- 8a), 150.9 (*C*- 4a), 153.5 (*C*- 6), 154.5 (*C*- 3).

$\nu_{\text{max}}$  (neat) = 1645, 1561, 1457, 1419, 1363, 1327  $\text{cm}^{-1}$ .

MS (EIMS) :  $m/z$  = 208 [ $\text{M}+1$ ] (17), 207 [ $\text{M}^+$ ] (100), 180 (28), 179 (38).

### 2-phenylpyrido[2,3-*b*] pyrazine



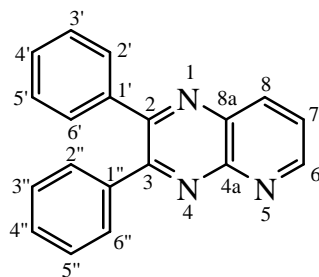
$^1\text{H}$  NMR (400 MHz,  $\text{CDCl}_3$ ):  $\delta$ (ppm) = 7.57-7.61 ( 3H, m, *H*- 3', 4', 5'), 7.74 (1H, dd, *J* 8.4Hz, *J* 4.2Hz, *H*- 7), 8.23-8.25 (2H, m, *H*- 2', 6'), 8.51 (1H, dd, *J* 8.4Hz *J* 1.8Hz, *H*- 8), 9.20 (1H, dd *J* 4.1Hz *J* 1.8Hz, *H*- 6), 9.56 (1H, s, *H*- 3)

$^{13}\text{C}$  NMR (400 MHz,  $\text{CDCl}_3$ ):  $\delta$ (ppm) = 125.7 (C- 7), 127.8 (C- 2', 6'), 129.3 (C- 4'), 130.8 (C- 3', 5'), 135.9 (C- 8), 137.6 (C- 1'), 138.6 (C- 3), 146.3 (C- 8a), 150.5 (C- 4a), 153.5 (C- 6), 154.7 (C- 2).

$\nu_{\text{max}}$  (neat) = 1645, 1561, 1457, 1419, 1363, 1327  $\text{cm}^{-1}$ .

MS (EIMS) :  $m/z$  = 208 [M+1] (17), 207 [M $^+$ ] (100), 180 (18), 179 (38).

### 2,3-Diphenylpyrido[2,3-*b*]pyrazine [224]



Prepared by the procedure given for **150** using benzoin (0.106g, 0.50 mmol) and 2,3-diaminopyridine (0.054g, 0.50 mmol) but reactants irradiated for 20 minutes. Purified using radial chromatography (9 : 1 DCM : EtOAc) to produce the title compound **224** as a yellow solid (m.p. 132 °C) (lit.<sup>62</sup> 135 °C); (0.076g, 54%);  $R_f$  0.30 (9 : 1 DCM : EtOAc).

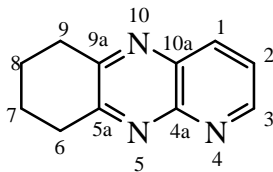
$^1\text{H}$  NMR (400 MHz,  $\text{CDCl}_3$ ):  $\delta$ (ppm) = 7.35-7.45 (6H, m, *H*- 3', 4', 5', 3'', 4'', 5''), 7.59 (2H, d, *J* 7.8Hz, *H*- 2', 6'), 7.65 (2H, d, *J* 7.8Hz, *H*- 2'', 6''), 7.74-7.78 (1H, dd, *J* 8.4Hz *J* 4.1Hz, *H*- 7), 8.56-8.59 (1H, d, *J* 8.2Hz, *H*- 8), 9.19 (1H, d, *J* 4.2Hz, *H*- 6).

$^{13}\text{C}$  NMR (400 MHz,  $\text{CDCl}_3$ ):  $\delta$ (ppm) = 125.1 (C- 7), 128.2 (C- 3', 5'), 128.5 (C- 3'', 5''), 129.4 (C- 4'), 129.6 (C- 4''), 129.8 (C- 2', 6'), 130.3 (C- 2''), 136.2 (C- 6''), 138.0 (C- 1', 1''), 138.5 (C- 8), 149.4 (C- 6), 153.6 (C- 4a, 8a), 155.0 (C- 2), 156.7 (C-3).

$\nu_{\text{max}}$  (neat) = 1587, 1545, 1429, 1382  $\text{cm}^{-1}$ .

HRMS : found  $m/z$  = 306.1006 (M +Na),  $\text{C}_{19}\text{H}_{13}\text{N}_3$  + Na requires 306.1007  
= 589.2120 (2M +Na),  $\text{C}_{38}\text{H}_{26}\text{N}_6$  + Na requires 589.2117

## 6, 7, 8, 9-Tetrahydropyrido[2,3-b]quinoxaline [225]



Prepared by the procedure given for **150** using 2-hydroxycyclohexanone dimer (0.057g, 0.50 mmol) and 2,3-diaminopyridine (0.054g, 0.50 mmol) but reactants irradiated for 20 minutes. Purified for radial chromatography (9 : 1 DCM : EtOAc) to produce the title compound as a purple solid (m.p. ), (0.052g, 52%),  $R_f$  0.40 (9 : 1 DCM : EtOAc).

$^1\text{H}$  NMR (400 MHz,  $\text{CDCl}_3$ ):  $\delta$ (ppm) = 1.07–2.08 (4H, m, *H*- 7, 8), 3.17 (2H, m, *H*- 9), 3.25 (2H, m, *H*- 6), 7.55-7.63 (1H, dd,  $J$  8.3 Hz  $J$  4.2 Hz, *H*- 2), 8.25-8.33 (1H, dd,  $J$  8.3 Hz 1.6 Hz, *H*- 1), 9.00-9.05 (1H, dd,  $J$  3.9 Hz  $J$  1.5 Hz, *H*- 3).

$^{13}\text{C}$  NMR (400 MHz,  $\text{CDCl}_3$ ):  $\delta$ (ppm) = 22.4 (*C*- 8), 22.6 (*C*- 7), 33.1 (*C*- 9), 33.5 (*C*- 6), 124.3 (*C*- 2), 136.1 (*C*- 1), 137.3 (*C*- 3), 150.1 (*C*- 10a), 152.9 (*C*- 4a), 155.7 (*C*- 9a), 157.9 (*C*- 5a).

$\nu_{\text{max}}$  (neat) = 1460, 1426, 1381, 1327, 1262.

MS (EIMS) :  $m/z$  = 186 [ $\text{M}+1$ ] (13), 185 [ $\text{M}^+$ ] (100), 184 (53), 170 (31), 157 (8).

## Attempted synthesis of 11,17-Dihydroxy-10,13-dimethyl-17-quinoxalin-2-yl-1,2,6,7,8,9,10,11,12,13,14,15,16,17-tetradecahydrocyclopenta-[a]phenanthren-3-one [227]

Hydrocortisone (0.072g, 0.020mmol), *o*-phenylene diamine (0.022g, 0.20mmol),  $\text{TiO}_2$  (0.016g, 0.20mmol) and TEMPO (3.2mg, 0.2mmol) were added to a sealed 10mL CEM Discover<sup>®</sup> reaction vial equipped with a magnetic stirrer bar. The reaction vial was irradiated (with cooling) for 10 min (2 x 5 min) at 150°C, after which the vessel was rapidly cooled to 50°C by the unit. The reaction mixture was diluted with dichloromethane (DCM) and passed through a short silica plug. The solvent was removed

*in vacuo* to produce a crude product which through NMR analysis was shown to consist of unidentifiable peaks with none of which were attributable to the product.

### **Attempted synthesis of ethyl cinnamate [230]**

Benzyl alcohol (0.054ml, 0.50mmol), (ethoxycarbonylmethylen)-triphenylphosphoran (0.17g, 0.50mmol), TiO<sub>2</sub> (0.040g, 0.50mmol) and TEMPO (0.008g, 0.050mmol) ) were added to a sealed 10mL CEM Discover<sup>®</sup> reaction vial equipped with a magnetic stirrer bar. The reaction vial was irradiated (with cooling) for 10 min (2 x 5 min) at 150°C, after which the vessel was rapidly cooled to 50°C by the unit. The reaction mixture was diluted with dichloromethane (DCM) and passed through a short silica plug. The solvent was removed *in vacuo* to produce a crude product which through NMR analysis was shown to consist of benzyl alcohol and other unidentifiable peaks.

### **Synthesis of doped titanium dioxide powders**

#### **Synthesis of silver doped titanium dioxide<sup>135</sup>**

AgNO<sub>3</sub> (0.01mol) was dissolved in 100ml water and titanium dioxide (0.99mol) was added with continuous stirring. The solution was allowed to stand at room temperature for 24 hours after the mixture was poured into a Petri dish and placed in an oven for 3 hours. Thereafter, the dried powder was placed in an oven at 400°C for 3 hours to produce a grey powder.

#### **Phosphorus doped titanium dioxide<sup>137</sup>**

Titanium (IV) isopropoxide Ti(OCH)(CH<sub>3</sub>)<sub>2</sub>)<sub>4</sub> was added to phosphoric acid and the solution refluxed at 90 °C for four hours. The mixture was poured into a Petri dish and placed in an oven for 3 hours. Thereafter, the dried powder was placed in an oven at 400°C for 3 hours to produce a grey powder.



### **Boron doped titanium dioxide<sup>139</sup>**

Titanium isopropoxide (0.02 mol) was added dropwise to a water/H<sub>3</sub>BO<sub>3</sub> mixture under continuous stirring. The solution was allowed to stir for twelve hours at room temperature and thereafter, placed in a oven at 100 °C for 8 hours. The mixture was calcined at 500 °C for one hour to produce a brown powder.

### **Nitrogen doped titanium dioxide<sup>138</sup>**

Titanium (IV) isopropoxide Ti(OCH)(CH<sub>3</sub>)<sub>2</sub>)<sub>4</sub> (2.05 ml) was added dropwise to 15.0 ml water under continuous stirring. A gel solution immediately formed after contact between water and titanium (IV) isopropoxide. Concentrated nitric acid (4.0ml) was added was then added to translucent solution which was stirred vigorously for half an hour. Aqueous ammonium hydroxide with an ammonium content of 25% was added dropwise till pH = 9 to produce a yellow precipitate which got darker with increasing amount of added ammonia. The yellow precipitate was washed with deionized water and dried at room temperature after which it was calcined at 400 °C for 2 hours.

### **Sulfur doped titanium dioxide<sup>141</sup>**

Titanium (IV) isopropoxide Ti(OCH)(CH<sub>3</sub>)<sub>2</sub>)<sub>4</sub> (2.48 ml) was added to Thiourea (2.80 g) dissolved in 50 ml ethanol. The mixture was stirred for 2 hours. Ethanol was allowed to evaporate at room temperature to produce a pale yellow powder which was calcined at 400 °C for 3 hours.

### **Iodine doped titanium dioxide**

Titanium (IV) isopropoxide Ti(OCH)(CH<sub>3</sub>)<sub>2</sub>)<sub>4</sub> (7 ml) was in 40 ml isopropyl alcohol was added to 60 ml water with iodic acid (3.00 g) dissolved in it. The solution was allowed to

stir for 5 hours. After this time, the solution was poured into a Petri dish and placed in an oven at 100 °C for 3 hours. Thereafter, the dried powder was placed in an oven at 400°C for 3 hours to produce a pink powder.

#### **Synthesis of 2-phenylquinoxaline using B-doped titanium dioxide**

To a solution of 2-hydroxyacetophenone (0.068g, 0.50mmol) in methanol was added *o*-phenylenediamine (0.054g, 0.50mmol), B-doped TiO<sub>2</sub> (0.040g, 0.50mmol) and TEMPO (0.008g, 0.050mmol) and the mixture stirred under incandescent lamp irradiation. After 3 hours, the reaction mixture was filtered through a short silica plug and the solid residues washed well with dichloromethane. The solvent was removed *in vacuo* to produce a crude product which was purified using radial chromatography to afford the title compound as an orange solid in a yield of 60%. Spectroscopic data consistent with previously reported data.

#### **Synthesis of 2-phenylquinoxaline using I-doped titanium dioxide**

To a solution of 2-hydroxyacetophenone (0.068g, 0.50mmol) in methanol was added *o*-phenylenediamine (0.054g, 0.50mmol), I-doped TiO<sub>2</sub> (0.040g, 0.50mmol) and TEMPO (0.008g, 0.050mmol) and the mixture stirred under incandescent lamp irradiation. After 3 hours, the reaction mixture was filtered through a short silica plug and the solid residues washed well with dichloromethane. The solvent was removed *in vacuo* to produce a crude product which was purified using radial chromatography to afford the title compound as an orange solid in a yield of 73%. Spectroscopic data consistent with previously reported data.

## References

1. Sheldon, R. A.; Kochi, J. K. *Metal Catalyzed Oxidations of Organic Compounds*; Academic Press: New York, 1981.
2. Zhan, B.; Thompson, A. *Tetrahedron* **2004**, *60*, 2917-2935.
3. Weissermel, K.; Arpe, H.-J. In *Industrial organic chemistry*; Lindley, C. R. Ed.; VCH: New York, 1997.
4. Dess, D. B.; Martin, J. C. *J. Org. Chem.* **1983**, *48*, 4155-4156.
5. Dess, D. B.; Martin, J. C. *J. Am. Chem. Soc.* **1991**, *113*, 7277-7287.
6. Boeckman, R. K.; Shao, P.; Mullins, J. J. *Org. Synth.* **2000**, *77*, 141-152.
7. Yadav, J. S.; Reddy, B. V. S.; Basak, A. K.; Narsaiah, A. V. *Tetrahedron* **2004**, *60*, 2131-2135.
8. Surendra, K.; Krishnaveni, N. S.; Reddy, M. A.; Nageswar, Y. V. D.; Rao, K. R. *J. Org. Chem.* **2003**, *68*, 2058-2059.
9. Kuhakarn, C.; Kittigowittana, K.; Pohmakotr, M.; Reutrakul, V. *Tetrahedron* **2005**, *61*, 8995-9000.
10. Mancuso, J. A.; Brownfain, D. S.; Swern, D. *J. Org. Chem.* **1979**, *44*, 4148-4150.
11. Heilbron, I.; Jones, E. R. H.; Sondheimer, F. *J. Chem. Soc.* **1947**, 1586-1590.
12. Heilbron, I.; Jones, E. R. H.; Sondheimer, F. *J. Chem. Soc.* **1949**, 604-607.
13. Harding, K. E.; May, L. M.; Dick, K. F. *J. Org. Chem.* **1975**, *40*, 1664-1665.
14. Corey, E. J.; Suggs, J. W. *Tetrahedron Lett.* **1975**, *31*, 2647-2650.
15. Watanabe, K.; Takada, Y.; Matsuo, N.; Nishimura, H. *Biosci. Biotech. Biochem.* **1996**, *59*, 1979-1980.
16. Carter, R. *Vaccine* **2001**, *19*, 2309-2314.
17. Takikawa, H.; Yamazaki, Y.; Mori, K. *Eur. J. Org. Chem.* **1998**, 229-232.
18. Wellington, K. D.; Cambie, R. C.; Rutledge, P. S.; Bergquist, P. R. *J. Nat. Prod.* **2000**, *63*, 79-85.
19. Taber, D. F.; Tian, W. *J. Org. Chem.* **2008**, *73*, 7560-7564.
20. Corey, E. J.; Ensley, H. E. *J. Am. Chem. Soc.* **1975**, *97*, 6908-6909.
21. Corey, E. J.; Ensley, H. E.; Suggs, J. W. *J. Org. Chem.* **1976**, *41*, 380-381.
22. Huang, C. C. *J. Labelled Compd. Radiopharm.* **1987**, *24*, 676-681.
23. Taylor, R. J. K.; Alcaraz, L.; Kapfer-Eyer, I.; Macdonald, G.; Wei, X.; Lewis, N. *J. Synthesis* **1998**, 775-790.
24. Macdonald, G.; Alcaraz, L.; Wei, X.; Lewis, N. J.; Taylor, R. J. K. *Tetrahedron* **1998**, *54*, 9823-9836.
25. Alcaraz, L.; Macdonald, G.; Ragot, J.; Lewis, N. J.; Taylor, R. J. K. *J. Org. Chem.* **1998**, *63*, 3526-3527.
26. Alcaraz, L.; Macdonald, G.; Ragot, J.; Lewis, N. J.; Taylor, R. J. K. *Tetrahedron* **1999**, *55*, 3707-3716.
27. Meyers, A. I.; Babiak, K. A.; Campbell, A. L.; Comins, D. L.; Fleming, M. P.; Henning, R.; Heuschmann, M.; Hudspeth, J. P.; Kane, J. M.; Reider, P. J.; Roland, D. M.; Shimizu, K.; Tomioka, K.; Walkup, R. D. *J. Am. Chem. Soc.* **1983**, *105*, 5015-5024.
28. Ireland, R. E.; Norbeck, D. W. *J. Org. Chem.* **1985**, *50*, 2198-2200.
29. Wei, X.; Taylor, R. J. K. *Tetrahedron Lett.* **1998**, *39*, 3815-3818.

30. Blackburn, L.; Wei, X.; Taylor, R. J. K. *Chem. Commun.* **1999**, 1337-1338.
31. Lang, S.; Taylor, R. J. K. *Tetrahedron Lett.* **2006**, *47*, 5489-5492.
32. Crich, D.; Mo, X.-S. *Synlett* **1999**, *1*, 67-68.
33. Barrett, A. G. M.; Hamprecht, D.; Ohkubo, M. *J. Org. Chem.* **1997**, *62*, 9376-9378.
34. Barrett, A. G. M.; Hamprecht, D.; White, A. J. P.; Williams, D. J. *J. Am. Chem. Soc.* **1997**, *119*, 8608-8615.
35. Shuto, S.; Niizuma, S.; Matsuda, A. *J. Org. Chem.* **1998**, *63*, 4489-4493.
36. Hamada, Y.; Shibata, M.; Sugiura, T.; Kato, S.; Shioiri, T. *J. Org. Chem.* **1987**, *52*, 1252-1255.
37. Blackburn, L.; Taylor, R. J. K. *Org. Lett.* **2001**, *3*, 1637-1639.
38. Raw, S. A.; Wilfred, C. D.; Taylor, R. J. K. *Chem. Commun.* **2003**, 2286-2287.
39. Quesada, E.; Raw, S. A.; Reid, M.; Roman, E.; Taylor, R. J. K. *Tetrahedron* **2006**, *62*, 6673-6680.
40. Laphookhieo, S.; Jones, S.; Raw, S. A.; Sainz, Y. F.; Taylor, R. J. K. *Tetrahedron Lett.* **2006**, *47*, 3865-3870.
41. Wilfred, C. D.; Taylor, R. J. K. *Synlett* **2004**, *9*, 1628-1630.
42. Taylor, R. J. K.; Reid, M.; Foot, J.; Raw, S. A. *Acc. Chem. Res.* **2005**, *38*, 851-869.
43. Toshima, K.; Kimura, T.; Takano, R.; Ozawa, T.; Ariga, A.; Shima, Y.; Umezawa, K.; Matsumura, S. *Tetrahedron* **2003**, *59*, 7057-7066.
44. Sanna, P.; Carta, A.; Loriga, M.; Zanetti, S.; Sechi, L. *IL Farmaco* **1998**, *53*, 455-461.
45. Kim, Y. B.; Kim, Y. H.; Park, J. Y.; Kim, S. K. *Bioorg. Med. Chem. Lett.* **2004**, *14*, 541-544.
46. Hazeldine, S. T.; Polin, L.; Kushner, J.; White, K.; Corbett, T. H.; Horwitz, J. P. *Bioorg. Med. Chem.* **2005**, *13*, 3910-3920.
47. Porter, A. E. A. *Comprehensive Heterocyclic Chemistry*; Pergamon: Oxford, 1984.
48. Woo, G. H. C.; Snyder, J. K.; Wan, Z.-K. *Prog. Heterocycl. Chem.* **2002**, *14*, 279.
49. Brown, D. J. *The Chemistry of Heterocyclic Compounds*; John Wiley & Sons: New Jersey, 2004.
50. Das, B.; Venkateswarlu, K.; Suneel, K.; Majhi, A. *Tetrahedron Lett.* **2007**, *48*, 5371-5374.
51. Chakraborti, A. K.; Gulhane, R. *Chem. Commun.* **2003**, 1896-1897.
52. Antoniotti, S.; Dunach, E. *Tetrahedron Lett.* **2002**, *43*, 3971-3973.
53. Taylor, E. C.; Maryanoff, C. A.; Skotnicki, J. S. *J. Org. Chem.* **1980**, *45*, 2512-2515.
54. Santosusso, T. M.; Swern, D. *J. Org. Chem.* **1975**, *40*, 2764-2769.
55. Coin, C.; Le Boisselier, V.; Favier, I.; Postel, M.; Dunach, E. *Eur. J. Org. Chem.* **2001**, 735-740.
56. Cho, C. S.; Ren, W. X.; Shim, S. C. *Tetrahedron Lett.* **2007**, *48*, 4665-4667.
57. Wu, Z.; Ede, N. J. *Tetrahedron Lett.* **2001**, *42*, 8115-8118.
58. Xekoukoulotakis, N. P.; Hadjiantoniou-Maroulis, C. P.; Maroulis, A. J. *Tetrahedron Lett.* **2000**, *41*, 10299-10302.
59. McNab, H. *J. Chem. Soc., Chem. Commun.* **1980**, 422-423.
60. Bhosale, R. S.; Sarda, S. R.; Ardhapure, S. S.; Jadhav, W. N.; Bhusare, S. R.; Pawar, R. P. *Tetrahedron Lett.* **2005**, *46*, 7183-7186.

61. More, S. V.; Sastry, M. N. V.; Wang, C. C.; Yao, C. F. *Tetrahedron Lett.* **2005**, *46*, 6345-6348.
62. Darabi, H. R.; Mohandessi, S.; Aghapoor, K.; Mohsenzadeh, F. *Catal. Commun.* **2007**, *8*, 389-392.
63. Kumar, A.; Kumar, S.; Saxena, A.; De, A.; Mozumdar, S. *Catal. Commun.* **2008**, *9*, 778-784.
64. Saxena, A.; Kumar, A.; Mozumdar, S. *Appl. Catal. A: Gen.* **2007**, *317*, 210-215.
65. More, S. V.; Sastry, M. N. V.; Yao, C. F. *Green Chem.* **2006**, *8*, 91-95.
66. Bhatnagar, I.; George, M. V. *J. Org. Chem.* **1968**, *33*, 2407-2411.
67. Robinson, R. S.; Taylor, R. J. K. *Synlett* **2005**, 1003-1005.
68. Schultz, M. J.; Park, C. C.; Sigman, M. S. *Chem. Commun.* **2002**, 3034-3035.
69. Cho, C. S.; Oh, S. G. *Tetrahedron Lett.* **2006**, *47*, 5633-5636.
70. Kotharkar, S. A.; Shinde, D. B. *Bull. Korean Chem. Soc.* **2006**, *27*, 1466-1468.
71. Cho, C. S.; Oh, S. G. *J. Mol. Catal. A: Chem.* **2007**, 205-210.
72. Morgan, D. V.; Howes, M. J. *Solid State Electronic Devices*; Wykeham Publications Ltd: London, 1972.
73. Amemiya, S.: Three Bond technical news; Tokyo, 2004; pp. 1-8.
74. Bahnemann, D.; Cunningham, J.; Fox, M.; Pelizzetti, E.; Pichat, P.; Serpone, N. *Aquatic and Surface Photochemistry*; Lewis Publishers: U.S.A., 1994.
75. Para, S. PhD Thesis, Lausanne, 2001.
76. Childs, L. P.; Ollis, D. *J. Catal.* **1980**, *66*, 383-390.
77. Wold, A. *Chem. Mater.* **1993**, *5*, 280-283.
78. Maruska, H. P.; Gosh, A. K. *Sol. Energy* **1978**, *20*, 443-458.
79. Tryk, D. A.; Fujishima, A.; Honda, K. *Electrochim. Acta* **2000**, *45*, 2363-2376.
80. Phillips, L. G.; Barbano, D. M. *J. Dairy Sci.* **1997**, *80*, 2726-2733.
81. Hewitt, J. *Cosmet. Toiletries* **1999**, *114*, 59.
82. Barrons, K. C.; Watson, A. J. *The Pesticide Manual*, 1983.
83. Naman, S. A.; Khammas, Z. A.-A.; Hussein, F. M. *J. Photochem. Photobiol A: Chem.* **2002**, *153*, 229-236.
84. Abu Tariq, M.; Faisal, M.; Muneer, M. *J. Hazard Mater. B* **2005**, *127*, 172-179.
85. Mahalakshmi, M.; Arabindoo, B.; Palanichamy, M.; Murugesan, V. *J. Hazard Mater.* **2007**, *143*, 240-245.
86. Yu, J. C.; Xie, Y.; Tang, H. Y.; Zhang, L.; Chan, H. C.; Zhao, J. *J. Photochem. Photobiol A: Chem.* **2003**, *156*, 235-241.
87. Fujishima, A.; Honda, K. *Nature* **1972**, *238*, 37-38.
88. Fujishima, A.; Kobayakawa, K.; Honda, K. *J. Electrochem. Soc.* **1975**, *122*, 1487-1489.
89. Fujishima, A.; Rao, T. N.; Tryk, D. A. *J. Photochem. Photobiol C: Photochem. Rev.* **2000**, *1*, 1-21.
90. Caronna, T.; Gambarotti, C.; Palmisano, L.; Punta, C.; Recupero, F. *Chem. Commun.* **2003**, 2350-2351.
91. Citterio, A.; Gentile, A.; Minisci, F.; Serravalle, M.; Ventura, S. *J. Org. Chem.* **1984**, *48*, 3364.
92. Palmisano, G.; Augugliaro, V.; Pagliaro, M.; Palmisano, L. *Chem. Commun.* **2007**, 3425-3437.

93. Yamagata, S.; Nakabayashi, S.; Sancier, K. M.; Fujishima, A. *Bull. Korean Chem. Soc. Jpn.* **1988**, *61*, 3429-3434.
94. Hussein, F. H.; Rudham, R. *J. Chem. Soc., Faraday Trans. 1* **1987**, *83*, 1631-1639.
95. Subba Rao, K. V.; Srinivas, B.; Prasad, A. R.; Subrahmanyam. *Chem. Commun.* **2000**, 1533-1534.
96. Anderson, L. M.; Butler, A. R. *J. Chem. Soc., Perkin Trans. 2* **1994**, 323-326.
97. Raw, S. A.; Wilfred, C. D.; Taylor, R. J. K. *Org. Biomol. Chem* **2004**, *2*, 788-796.
98. Fox, M. A.; Dulay, M. T. *Chem. Rev.* **1993**, *93*, 341-357.
99. Regan, B. O.; Gratzel, M. *Nature* **1991**, *353*, 737-740.
100. Oyama, T.; Aoshima, A.; Horikoshi, S.; Hidaka, H.; Zhao, J.; Serpone, N. *Sol. Energy* **2004**, *77*, 525-532.
101. Gassim, F. A. Z. G.; Alkhateeb, A. N.; Hussein, F. H. *Desalination* **2007**, 342-349.
102. Emeline, A. V.; Frolov, A. V.; Ryabchuk, V. A.; Serpone, N. *J. Phys. Chem. B* **2003**, *107*, 7109-7119.
103. Ishibashi, K.; Fujishima, A.; Watanabe, T.; Hashimoto, K. *J. Photochem. Photobiol. A: Chem.* **2000**, *134*, 139-142.
104. Pichat, P.; Herrmann, J.-M.; Disdier, J.; Courbon, H.; Mozzanega, M.-N. *Nouv. J. Chim.* **1981**, *5*, 627-636.
105. Pichat, P.; Mozzanega, M.-N.; Disdier, J.; Herrmann, J.-M. *Nouv. J. Chim.* **1982**, *6*, 559-564.
106. Prahov, L. T.; Disdier, J.; Herrmann, J.-M.; Pichat, P. *Int. J. Hydrogen Energy* **1984**, *9*, 397-403.
107. Mohamed, O. S.; Gaber, A. E. A. M.; Abdel-Wahab, A. A. *J. Photochem. Photobiol A: Chem.* **2002**, *148*, 205-210.
108. Tang, X.; Li, D. *J. Phys. Chem. C* **2008**, *112*, 5405-5409.
109. Rudham, R.; Hussein, F. H. *J. Chem. Soc., Faraday Trans. 1* **1987**, *83*, 1631-1639.
110. Kim, S. S.; Jung, H. C. *Synthesis* **2003**, 2135-2137.
111. Horikoshi, S.; Hidaka, H.; Serpone, N. *Chem. Phys. Lett.* **2003**, *376*, 475-480.
112. Booske, J. H.; Cooper, R. F.; Dobson, I. *J. Mater. Res.* **1992**, *7*, 495-501.
113. Kim, S. Y.; Park, K. H.; Chung, Y. K. *Chem. Commun.* **2005**, 1321-1323.
114. Moriarty, R. M.; Berglund, B. A.; Penmasta, R. *Tetrahedron Lett.* **1992**, *33*, 6065-6068.
115. Schadt, F.; Bently, T.; Schleyer, P. v. R. *J. Am. Chem. Soc.* **1976**, *98*, 7667.
116. Mohsenzadeh, F.; Aghapoor, K.; Darabi, H. R. *J. Braz. Chem. Soc.* **2007**, *18*, 297-303.
117. Carp, O.; Huisman, C. L.; Reller, A. *Prog. Solid State Chem.* **2004**, *32*, 33-177.
118. Wu, T.; Lin, T.; Zhao, J.; Hidaka, H.; Serpone, N. *Environ. Sci. Technol.* **1999**, *33*, 1379-1387.
119. Wu, T.; Liu, G.; Zhao, J.; Hidaka, H.; Serpone, N. *J. Phys. Chem. B* **1999**, *103*, 4862-2867.
120. Lindgren, T.; Mwabora, J. M.; Avendaño, E.; Jonsson, J.; Hoel, A.; Granqvist, C.-G.; Lindquist, S.-E. *J. Phys. Chem. B* **2003**, *107*, 5709-5716.
121. Che, M.; Naccache, C. *Chem. Phys. Lett.* **1971**, *8*, 45-48.
122. Sato, S. *Chem. Phys. Lett.* **1986**, *123*, 126-128.
123. Chatterjee, D.; Dasgupta, S. *J. Photochem. Photobiol. C: Photochem. Rev.* **2005**, *6*, 186-205.

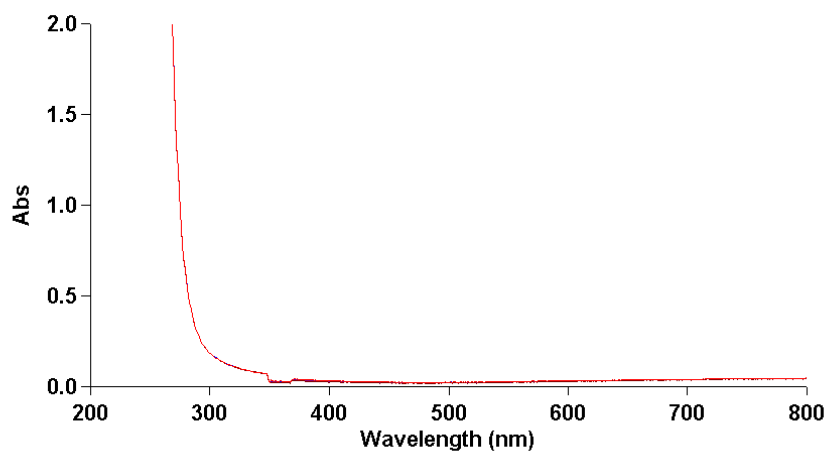
124. Yamashita, H.; Honda, M.; Harada, M.; Ichihashi, Y.; Anpo, M.; Hirao, T.; Itoh, N.; Iwamoto, N. *J. Phys. Chem. B* **1998**, *102*, 10707-10711.
125. Choi, W.; Termin, A.; Hoffmann, M. R. *J. Phys. Chem.* **1994**, *98*, 13669-13679.
126. Zheng, S. K.; Wang, T. M.; Hao, W. C.; Shen, R. *Vacuum* **2002**, *65*, 155-159.
127. Wu, J. C. S.; Chen, C. H. *J. Photochem. Photobiol. A:Chem.* **2004**, *163*, 509-515.
128. Dann, S. E. *Reactions and Characterization of SOLIDS*; Royal Society of Chemistry: Cambridge, 2000.
129. Murphy, A. B. *Solar Energy Mater. Solar Cells* **2007**, *91*, 1326-1337.
130. Wendlandt, W. W.; Hecht, H. G. *Reflectance Spectroscopy*; Wiley Interscience: New York, 1966.
131. Zhang, Z.; Wang, C. C.; Zakaria, R.; Ying, J. Y. *J. Phys. Chem. B* **1998**, *102*, 10871-10878.
132. Wang, C. C.; Zhang, Z.; Ying, J. Y. *Nanostr. Mater.* **1997**, *9*, 583-586.
133. Anpo, M.; Shima, T.; Kodama, S.; Kubokawa, Y. *J. Phys. Chem.* **1987**, *91*, 4305-4310.
134. Maira, A. J.; Yeung, K. L.; Lee, C. Y.; Yue, P. L.; Chan, C. K. *J. Catal.* **2000**, *192*, 185-196.
135. Sahoo, C.; Gupta, A. K.; Pal, A. *Desalination* **2005**, *181*, 91-100.
136. Liu, S. X.; Qu, Z. P.; Han, X. W.; Sun, C. L. *Catal. Today* **2004**, *93-95*, 877-884.
137. Yu, H.-F. *J. Phys. Chem. Solids* **2007**, *68*, 600-607.
138. Wang, J.; Zhu, W.; Zhang, Y.; Liu, S. *J. Phys. Chem. C* **2007**, *111*, 1010-1014.
139. Chen, D.; Yang, D.; Wang, Q.; Jiang, Z. *Ind. Eng. Chem. Res.* **2006**, *45*, 4110-4116.
140. Moon, S. C.; Mametsuka, H.; Tabata, S.; Suzuki, E. *Catal. Today* **2000**, *58*, 125-132.
141. Reddy, K. M.; Baruwati, B.; Jayalakshmi, M.; Rao, M. M.; Manorama, S. V. *J. Solid State Chem.* **2005**, *178*, 3352-3358.
142. Hong, X.; Wang, Z.; Cai, W.; Lu, F.; Zhang, J.; Yang, Y.; Ma, N.; Liu, Y. *Chem. Mater.* **2005**, *17*, 1548-1552.
143. Asahi, R.; Morikawa, T.; Ohwaki, T.; Aoki, K.; Taga, Y. *Science* **2001**, *293*, 269-271.
144. Irie, H.; Watanabe, Y.; Hashimoto, K. *J. Phys. Chem. B* **2005**, *107*, 5483-5486.
145. Ihmels, H.; Maggini, M.; Prato, M.; Scorrano, G. *Tetrahedron Lett.* **1991**, *32*, 6215.
146. Hahn, W. E.; Lesiak, J. *Pol. J. Chem.* **1985**, *59*, 627-629.

## **APPENDIX**

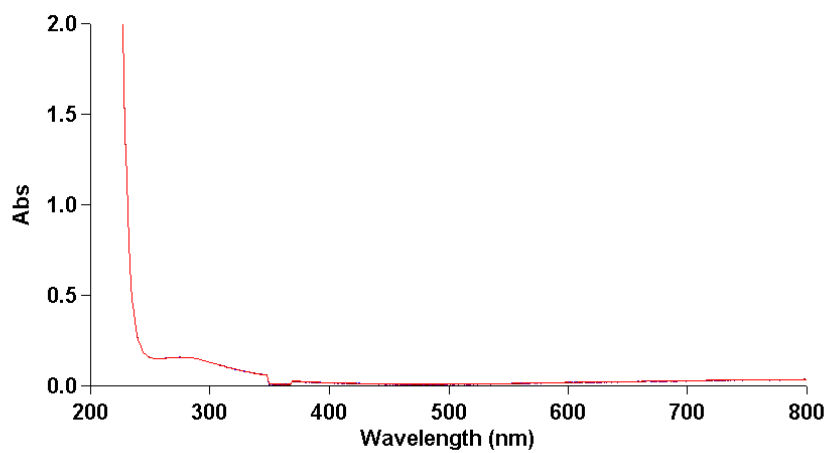


## **APPENDIX A**

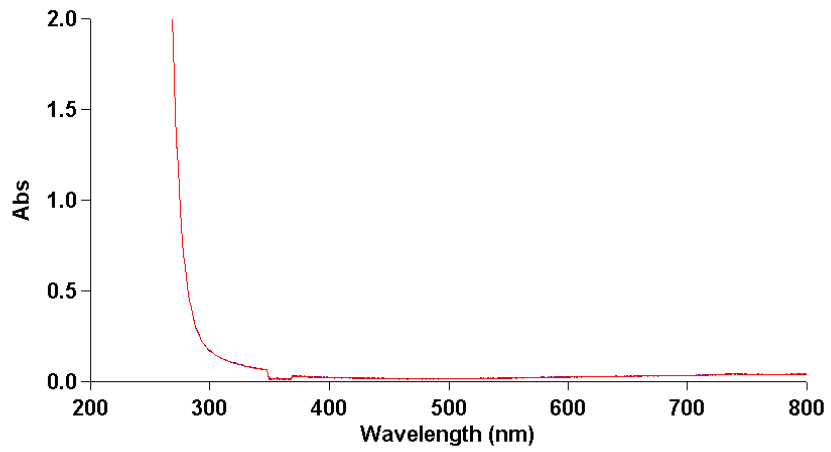
### Solvent 1: Dichloromethane in pyrex glass



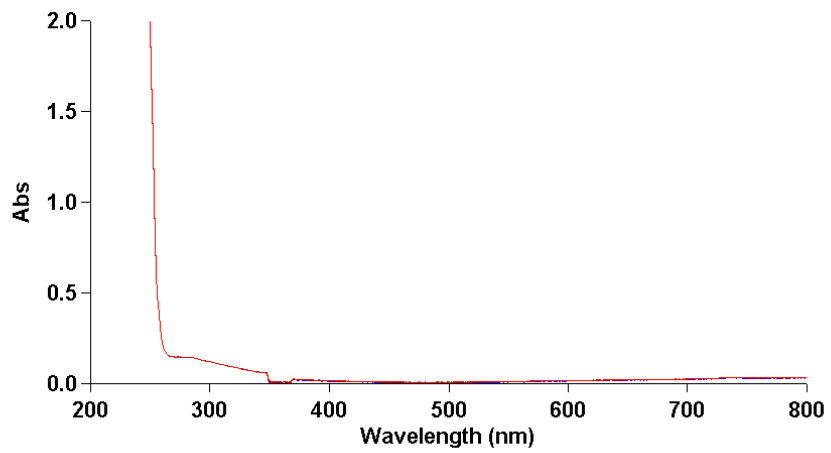
### Dichloromethane in quartz



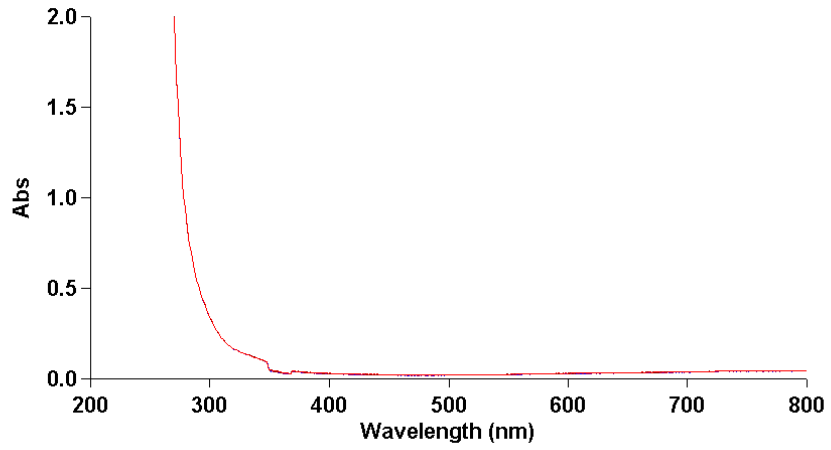
### Solvent 2: Ethyl acetate in pyrex glass



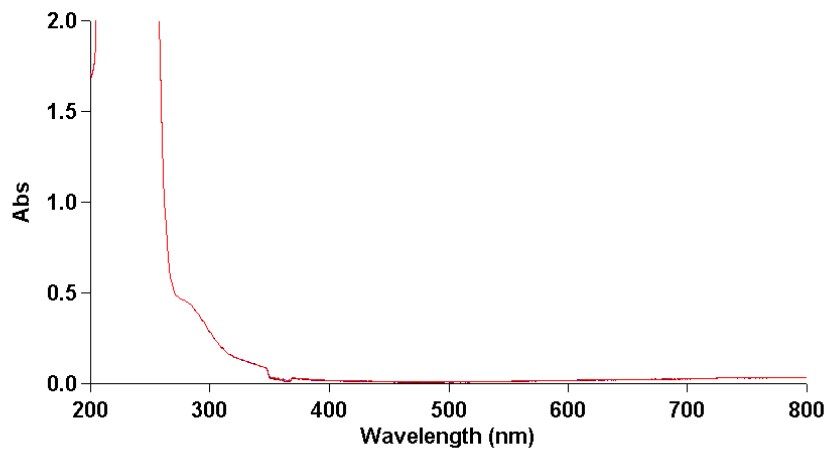
### Ethyl acetate in quartz



### Solvent 3: Acetonitrile in pyrex glass



### Acetonitrile in quartz



## **APPENDIX B**

The afore mentioned publication was submitted to Organic Letters and on the advice of the editors is being drawn up as a full publication, which will be submitted to the journal Beilstein in due course.